University of Alberta

Numerical Solutions for Pipeline Wrinkling

By

Xuejun Song

A thesis submitted to the Faculty of Graduate Studies and Research in partial fulfillment of the requirements for the degree of Master of Science

in

Structural Engineering

Department of Civil & Environmental Engineering

Edmonton, Alberta

Spring 2003

National Library of Canada
Acquisitions and Bibliographic Services
395 Wellington Street
Ottawa ON K1A 0N4
Canada

Bibliothèque nationale du Canada
Acquisitions et services bibliographiques
395, rue Wellington
Ottawa ON K1A 0N4
Canada

Your file Votre référence

Our file Notre référence

The author has granted a non-exclusive licence allowing the National Library of Canada to reproduce, loan, distribute or sell copies of this thesis in microform, paper or electronic formats.

L'auteur a accordé une licence non exclusive permettant à la Bibliothèque nationale du Canada de reproduire, prêter, distribuer ou vendre des copies de cette thèse sous la forme de microfiche/film, de reproduction sur papier ou sur format électronique.

The author retains ownership of the copyright in this thesis. Neither the thesis nor substantial extracts from it may be printed or otherwise reproduced without the author's permission.

L'auteur conserve la propriété du droit d'auteur qui protège cette thèse. Ni la thèse ni des extraits substantiels de celle-ci ne doivent être imprimés ou autrement reproduits sans son autorisation.

0-612-82346-6

Canada

University of Alberta

Library Release Form

Name of Author: Xuejun Song

Title of Thesis: Numerical Solutions for Pipeline Wrinkling

Degree: Master of Science

Year this degree granted: 2003

Permission is hereby granted to the University of Alberta Library to reproduce single copies of this thesis and to lend or sell such copies for private, scholarly or scientific research purposes only.

The author reserves all other publication and other rights in association with the copyright in the thesis, and except as herein before provided, neither the thesis nor any substantial portion thereof my be printed or otherwise reproduced in any material form whatever without the author's prior written permission.

Xuejun Song

201 RH, Michener Park
Edmonton, AB
T6H 4M5
Canada

Date: Jan. 6, 2003

University of Alberta

Faculty of Graduate Studies and Research

The undersigned certify that they have read, and recommend to the Faculty of Graduate Studies and Research for acceptance, a thesis entitled Numerical Solutions for Pipeline Wrinkling submitted by Xuejun Song in partial fulfillment of the requirements for the degree of Master of Science in Structural Engineering.

Dr. D. W. Murray (Supervisor)

Dr. J.J. Roger Cheng (Co-Supervisor)

Dr. Xiaodong Wang (External Examiner)

Date: Jan. 2, 2003

ABSTRACT

There are two computer programs commonly used in the University of Alberta for studying the pipeline behavior, namely, the finite element package ABAQUS, which is used to do local wrinkling analysis, and ABP (ABP stands for Analysis of Buried Pipelines), which is used to do the global upheaval or snaking buckling analysis.

After presenting some validation solutions for the ABP program, numerical analyses are carried out for field failures that occurred in a gas pipeline in Northern Alberta. The validation solutions include the comparison with Hobbs' differential equation solutions for pipeline upheaval buckling, and the comparison with the differential equation solutions for pipe-soil slip mechanisms. The numerical analyses are done using the ABP program, the ABAQUS package, and a spreadsheet for the pipe-soil slip mechanisms, based on the data in hand from the field.

Cyclic loading analysis by using ABAQUS is done and the number of cycles to cause the fracture failure of the pipe is estimated based on a recently finished thesis by Das et al. (2002). This also contributes to the verification of the formula proposed by Das et al. (2002). Conclusions are drawn based on the studies that are presented.

ACKNOWLEDGEMENTS

This study was conducted with the financial assistance of the Natural Sciences and Engineering Research Council of Canada (NSERC) under operating grant No. 5307. The financial support from Civil & Environmental Engineering Department of the University of Alberta in the form of scholarships is also acknowledged.

I would like to thank my supervisor Dr. D. W. Murray for his guidance, assistance and great instructions throughout this study and my co-supervisor Dr. J. J. Roger Cheng for his generous help.

In addition, I wish to thank the following individuals or organizations for their assistance of various type:

- –To Gary Oulette of Canadian Natural Resources Ltd. (CNRL) for permission to access the NPS-8 Gold Creek Pipeline reports and data of StressTech Engibeering inc., Thurber Engineering Ltd., and BJ Pipeline Inspection Services Ltd.
- –To Heiniich Heinz of Thurber Engineering Ltd. for a copy of their report
- –To Jarek Cyzy of BJ Pipeline Inspection Services Ltd. for assistance in accessing the GEOPIG software and data records
- –To Darren Skibinsky of Enbridge Pipeline Inc. for assistance in running the GEOPIG software.

I would like to acknowledge the contribution from previous students who developed FEA models. Specifically, I would like to thank: Dr. Sreekanta Das, Dr. Nader Yoosef-Ghodsi, Dr. Alfred Dorey, Mohammad Behbahanifard and Bino Huns.

I would like to thank my colleagues Anthony Ng, Bino Huns and Clinton Miller for always lending a hand whenever I needed help during my course of studies.

I would like to thank my parents and my parents-in-law for installing in me the confidence to do the research work successfully. To my wife, Geng, and my daughter, Yingxin, for their endless love, support and encouragement. You sheltered me with a place of comfort and inspired me with the will to succeed. Thanks also to my sister-in-law, Sophie Fu Song, for her encouragement and generous help for my graduate study.

I would like to thank all the people who gave me help for my graduate study in the University of Alberta.

TABLE OF CONTENTS

CHAPTER 1 INTRODUCTION 1

1.1 INTRODUCTION 1

1.2 OBJECTIVES 3

1.3 LAYOUT OF THE THESIS 3

CHAPTER 2 LITERATURE REVIEW 5

2.1 GLOBAL BUCKLING 5

2.1.1 CLASSICAL SOLUTIONS 5

2.1.1.1 Analysis of railroad Track by A.D. Kerr (1978), ... 5

2.1.1.2 Analysis by Hobbs (1984) 6

2.1.1.3 Analysis by Ju and Kyriakides (1984) 7

2.1.2 INELASTIC SOLUTIONS 8

2.2 LOCAL BUCKLING 9

2.2.1 CRITICAL BUCKLING STRAIN (Dorey et al, 2001) 9

2.2.2 WRINKLE FORMATION DUE TO BENDING (Anon, 1998) .. 11

2.2.3 WRINKLE FORMATION DUE TO UPHEAVAL BENDING .. 11

2.2.4 WRINKLE FORMATION DUE TO SNAKING BENDING (Yoosef-Ghodsi and Murray, 2000) 12

2.2.5 BENDING WRINKLE FRACTURE FORMATION (Murray and Yoosef-Ghodsi, 2001) 13

2.2.6 WRINKLE FRACTURE FORMATION (Das et al., 2002) 13

CHAPTER 3 VALIDATION SOLUTIONS FOR THE COMPUTER PROGRAM ABP-V2002 23

3.1 GENERAL DISCRIPTION 23

3.2 COMPARISON OF ABP RESULTS WITH HOBBS'S DIFFERENTIAL EQUATION SOLUTIONS 24

3.2.1 Data for the Pipeline 24

3.2.2 Data for the Soil 24

3.2.3 Case Study for the Comparative Solutions 25

3.2.3.1 Differential Equation Solution by Hobbs (1984)..... 25
3.2.3.2 Numerical Analysis by Using the ABP Program..... 30
3.3 COMPARISON OF THE ABP SOLUTIONS WITH THE DESs FOR PIPE-SOIL SLIP MECHANISMS 31
3.3.1 INTRODUCTION 31
3.3.2 BRIED DESCRIPTION OF PIPE-SOIL SLIP 31
3.3.3 AVAILABLE DATA FOR THE HOT OIL PIPELINE 32
3.3.3.1 Material Properties 33
3.3.3.2 Soil Spring Stiffness 32
3.3.4 NUMERICAL ANALYSIS 33
3.3.4.1 Pipe End Displacement without Axial Force 33
3.3.4.2 Pipe End Displacement with Axial Force..... 35
CHAPTER 4 CASE HISTORY OF WASCANA GOLD CREEK LINE AND NUMERICAL SIMULATIONS..... 49
4.1 GENERAL..... 49
4.2 INTRODUCTION 49
4.3 DATA FOR THE PIPE AND THE SOIL 50
4.3.1 Data for the Pipe..... 50
4.3.2 Data for the Soil..... 50
4.3.3 Pipeline Operational Condition 52
4.3.4 Pipe Imperfection Length and Magnitude in Pipe Upheaval Buckling Analysis..... 52
4.3.5 Local wrinkle Analysis for the Critical Segment..... 53
4.4 Numerical Analysis For Site #4..... 53
4.4.1 Numerical Upheaval Analyses for Site #4..... 53
4.4.2 Numerical Wrinkling Analyses for Site #4 55
4.5 Numerical Analyses for the Site #5 55
4.5.1 Numerical Upheaval Analyses for Site #5..... 55
4.5.2 Numerical Wrinkling Analyses for Site #5 56
4.6 Numerical Analyses for the Fracture Site..... 57
4.6.1 Numerical Analyses for Pipe Slip at Fracture Site 57

4.6.2 Numerical Analysis for Pipe Wrinkling at Fracture Site 59
4.7 Numerical Analysis for Fracture Model 60
CHAPTER 5 CONCLUSIONS 99
REFERENCES 101
APPENDIX A Fundamental Solutions for mechanics of Soil-Pipe Slip 103
APPENDIX B FRACTURE MODEL OF PIPELINE UNDER CYCLIC LOAD 108
B1 Fracture Model 109
B2 Application to Axial Pipe Specimen 110
B3 Application to Bending Pipe Specimen 111

LIST OF TABLES

CHAPTER 3

Table 3.1 Properties for Soil Springs 24

Table 3.2 End Displacements For Different Pipeline Lengths Under $\Delta T = 110^{o}F$ and $\tau_y = 0.009\ N/mm^2$ 33

Table 3.3 End Displacements Under Different Soil Yield Strengths And Pipeline Lengths 35

Table 3.4 End Displacements Under Different Axial Forces For Two Pipeline lengths 36

CHAPTER 4

Table 4.1 Nodal Coordinates at Crest and Foot of the Wrinkle for Two configurations 62

LIST OF FIGURES

CHAPTER 2

Figure 2.1 Different Buckling Modes in Railroad Tracks and Pipelines..... 14
Figure 2.2 Vertical Buckling Mode of Pipelines..... 15
Figure 2.3 Typical Temperature vs. Pipe Displacement Relationship 16
Figure 2.4 Temperature vs. Pipe Displacement Curves for Different Imperfections 16
Figure 2.5 Photograph of Experimental Buckling Mode for Plain Pipe with Internal Pressure (Dorey et al., 2001) 17
Figure 2.6 FEA Model Generated Buckling Mode for Plain Pipe with Internal Pressure (Dorey et al., 2001) 17
Figure 2.7 Schematic of "Blister" Type Assumed Initial Imperfection (Dorey et al. 2001)..... 18
Figure 2.8 Schematic of "Offset" Type Assumed Initial Imperfection (Dorey et al. 2001)..... 18
Figure 2.9 Local Wrinkle for KP318 from the Field Dig (Yoosef-Ghodsi et al, 2000)..... 19
Figure 2.10 Wrinkle Formed by FEA Model Imposing Geometric Displacemente (Yoosef-Ghodsi et al, 2000) 19
Figure 2.11 Numerical Model Layout for Brazil Snaking Problem 20
Figure 2.12 Temperature Change vs. Pipe Buckle Amplitude Curve for Brazil Snaking Problem 21
Figure 2.13 Pipe Deformed Shape at Different Temperature Differential for Brazil Snaking Problem 22

CHAPTER 3

Figure 3.1 Details of Pipe Upheaval Buckling Mode..... 38
Figure 3.2 Free-body Diagram for Pipe Segment at Buckled Part 38
Figure 3.3 Compatibility Condition for Buckled Length of Pipeline 39
Figure 3.4 Temperature Change vs. Pipe Vertical Displacement Curve from DESs 40

Figure 3.5 Schematic Model Used in ABP Program 41
Figure 3.6 Temperature Change vs. Pipe Displacement Curve from the ABP Program for Two Different IOS's 42
Figure 3.7 Comparison of Temperature Change vs. Pipe Vertical Displacement Curve from ABP and DESs 43
Figure 3.8 Schematic of Pipe Segment Embedded in Soil 44
Figure 3.9 Field Measurements of Pipe Friction Force vs. Pipe Slip 45
Figure 3.10 Characteristics of End Displacement vs. Pipe Length Curve from ABP and DESs 46
Figure 3.11 Pipe End Displacement vs. Pipe length Curves from ABP and DESs. 47
Figure 3.12 Effect of Axial Force on Pipe End Displacement from ABP and DESs48

CHAPTER 4

Figure 4.1 Thermal Profile along Gold Creek NPS-8 Pipeline 64
Figure 4.2 True Stress vs. True Strain Curve Used for NPS-8 Pipeline Steel..... 65
Figure 4.3 Muskeg Plot along Gold Creek NPS-8 Pipeline 66
Figure 4.4 FEA Mesh and Boundary Conditions Used for ABAQUS 67
Figure 4.5 GEOPIG Plot of Upheaval Site #4 for Wascana NPS-8 Pipeline 68
Figure 4.6 Schematic Model Used in ABP Program for Site #4 69
Figure 4.7 Soil Resistance vs. Pipe Uplift Displacement Curve for Site #4 70
Figure 4.8 Temperature Increase vs. Pipe vertical Displacement Curves from ABP Analyses (Site #4)..... 71
Figure 4.9 Pipe Deformed Configuration at Temperature Increase of 84.4°C from ABP Analyses (Site #4)..... 72
Figure 4.10 Pipe Deformed Configuration at Temperature Increase of 84.4°C from ABP Analyses with Smaller Scale (Site #4)..... 73
Figure 4.11 GEOPIG Plot of Upheaval Site #4 with Smaller Scale for Wascana NPS-8 Pipeline 74
Figure 4.12 Comparison of the Pipe Configuration Between GEOPIG Plot and ABP Result at Site #4..... 75
Figure 4.13 Pipe Deformed Shape at Critical Segment #4 (ABAQUS)..... 76

Figure 4.14 GEOPIG Plot of Upheaval Site #5 for Wascana NPS-8 Pipeline 77
Figure 4.15 Schematic Model Used in ABP Program for Site #5 78
Figure 4.16 Soil Resistance vs. Pipe Uplift Displacement Curve for Site #5 79
Figure 4.17 Temperature Increase vs. Pipe vertical Displacement Curves from ABP Analyses (Site #5) 80
Figure 4.18 Pipe Deformed Configuration at Temperature Increase of 90°C from ABP Analyses (Site #5) 81
Figure 4.19 Pipe Deformed Configuration at Temperature Increase of 90°C from ABP Analyses with Smaller Scale (Site #5) 82
Figure 4.20 GEOPIG Plot of Upheaval Site #5 with Smaller Scale for Wascana NPS-8 Pipeline 83
Figure 4.21 Comparison of the Pipe Configuration Between GEOPIG Plot and ABP Result at Site #5 84
Figure 4.22 Pipe Deformed Shape at Critical Segment #5 (ABAQUS) 85
Figure 4.23 GEOPIG Plot of Fracture Site for Wascana NPS-8 Pipeline 86
Figure 4.24 Computed Anchor Length by Closed Form Solution for Fracture Site 87
Figure 4.25 Axial Load vs. Axial Displacement Curve from Closed Form Solution88
Figure 4.26 Expansion Interaction of Anchor Length and FE Model Segment 89
Figure 4.27 Axial Load vs. Axial Displacement Curves for Different Rotation Values of a 6D Segment from ABAQUS 90
Figure 4.28 Axial Load vs. Axial Displacement Curve from DES and ABAQUS . 91
Figure 4.29 Axial Load vs. Axial Displacement Curves from Closed Form Solution and ABAQUS 92
Figure 4.30 Pipe Deformed Shape for NPS-8 Pipeline at Fracture Site 93
Figure 4.31 Comparison of the Wrinkles from the Field and ABAQUS 94
Figure 4.32 Axial Load vs. Axial Displacement Curve for Unloading with 10mm End Movement 95
Figure 4.33 Axial Load vs. Axial Displacement Curve for Unloading with 20mm End Movement 96
Figure 4.34 Pipe Deformed Configuration at Maximum Tension 97
Figure 4.35 Pipe Deformed Configuration at Maximum Compression 98

APPENDIX A

Figure A1 Model for Differential Equation Solution of Pipe – Slip Interactive Slip Problem.....107

APPENDIX B

Figure B1 Single Load Hysteresis Cycle for a Strip Specimen 115
Figure B2 Model for the Axial Loaded Pipe Specimen 115
Figure B3 Bending Pipe Specimen and Its Detail 'R' 116
Figure B4 Model for Deformed Shape of a Bending Pipe Specimen.....116

LIST OF SYMBOLS

Latin Characters

a	Magnitude of the imperfection
A	Cross sectional area of the pipeline
amp_{max}	Maximum amplitude of an initial local imperfection
c	A coefficient substituting nL/2
D	Outside diameter of the pipeline
D/t	Diameter-to-thickness ratio of pipe
E	Modulus of elasticity of the pipeline material
F_y	Yield strength of the soil for every unit length along the pipeline
F_{yL}	Longitudinal soil spring yield strength
F_{yu}	Uplift soil spring yield strength
I	Moment of inertia
imp	Imperfection expressed as a percent of the wall thickness
k_L	Longitudinal soil spring stiffness
k_u	Vertical soil spring stiffness
L	the buckled length between the lift-off points
L_{LI}	Length of the initial local imperfection
L_{imp}	half of the length of the imperfection
L_{min}	Minimum buckled length
L_s	Length of slipping pipe adjacent to buckle
ΔL	Pipe slip
M_{ext}	External moment acting on the cut section of buckled part of pipeline
M_{int}	Internal moment
m	A coefficient substituting P/EI
n	A coefficient substituting w/EI
p	Internal pressure
p_y	Internal pressure that causes yielding in the hoop direction
P	Axial force in buckled pipe
P_0	Axial force due to thermal effect

P_0'	Axial force due to thermal and Poisson's ratio effect
Q	A coefficient substituting $\phi wL/2$
q	A coefficient substituting ϕw
r	Actual radius of the imperfect pipe
r_0	Radius of the "perfect" pipe
t	Wall thickness of the pipeline
ΔT	the temperature differential
ΔT_{cr}	the limiting temperature rise (critical temperature)
ΔT_1	the temperature rise required to cause first uplift
ΔT_m	the local minimum temperature rise
w	pipe self-weight
y_{max}	Maximum buckled magnitude

Greek Characters

α	Coefficient of thermal expansion of the pipeline material
Δ	Axial displacement of the pipeline (pipe slip)
ϕ	Coefficient of friction between the pipe and the subgrade
$\sigma_{\Delta T}$	Thermal stress of the pipe
σ_θ	Circumferential hoop stress of the pipe
μ	Poisson's Ratio
τ_y	Pipe-soil interface yield strength

SYMBOLS IN APPENDIX

APPENDIX A

Latin Characters

A	Cross sectional area of the pipeline
E	Modulus of elasticity of the pipeline material
F_y	Frictional yield force
k	Pipe-soil interface stiffness
L	Computed anchor length

N	the axial force in the pipe
P	Axial force exerted by adjacent pipe component
ΔT	the temperature differential
u	Pipe slip relative to the soil

Greek Characters

α	Coefficient of thermal expansion of the pipeline material
β	A coefficient substituting $(P+F_yL)/(AE)-\varepsilon_0$
δ_y	Pipe slip corresponding to soil yield point
ε_0	Effective thermal strain
γ	A coefficient substituting $\varepsilon_0-P/(AE)$
λ	A coefficient substituting $k/(AE)$
ν	Poisson's ratio
ρ	A coefficient substituting $F_y/(AE)$
σ	Axial tensile stress
σ_θ	Circumferential hoop stress of the pipe

APPENDIX B

Latin Characters

A	A coefficient that depend on the thickness of strip specimens
a	Distance of NA from the extreme compression edge of pipe cross section
b	width of straight strip cut from a pipe specimen (57mm)
D_c	Diameter at the centerline of the pipe cross section
d	Arm-length of a strip specimen or a pipe wrinkle
L_t	The distance between foot of wrinkle and the nearest end point of a bending pipe specimen
M_u	Ultimate moment capacity of a strip specimen or a 57 mm wide pipe slice
N_s	Numbers of cycles to fracture a wrinkled pipe specimen

S_{ar}	Stroke at any arbitrary time during cyclic loading, due to rotational or bending component in a bending pipe specimen
S_{as}	Stroke at any arbitrary time during cyclic loading, due to axisymmetric axial deformation in a bending or axial pipe specimen
S_{at}	Total stroke at any arbitrary time, during cyclic loading of a bending pipe specimen
S_r	Absolute value of stroke range for a strip specimen or a 57 mm wide slice of a pipe wrinkle
t	Wall thickness of the pipeline
U_0	HLE of a 57 mm wide strip specimen or a 57 mm wide pipe wrinkle slice
U_{0c}	HLE absorbed at the crest of a 57 mm wide wrinkle slice of a pipe specimen
U_{0cr}	HLE absorbed at crest of a 57 mm wide wrinkle slice, due to change in end rotation of a bending pipe specimen
U_{0f}	HLE absorbed at each foot of a 57 mm wide wrinkle slice of a pipe specimen
U_{0fr}	HLE absorbed at each foot of a 57 mm wide wrinkle slice, due to change in end rotation of a bending pipe specimen
$2W_c$	Wrinkle wave-length due to maximum compressive stroke, during load cycling
$2W_t$	Wrinkle wave-length due to maximum tensile stroke, during load cycling
Z	Plastic sectional modulus of a 57 mm wide strip or slice of pipe

Greek Characters

α_a	Rotation applied at top end of a bending pipe specimen at any arbitrary time, during cyclic loading
β	Angle change at each foot of wrinkle in a bending pipe specimen, due to rotation change in one cycle

β_a	Change in angle at top foot relative to its initial (monotonic) value at any arbitrary time, during cyclic loading of a bending pipe specimen
ϕ	Change in internal angle at the crest of the strip wrinkle, due to stroke change (S) in one cycle
$(\phi)_r$	Angle change at the crest of wrinkle in a bending pipe specimen, due to rotation change in one cycle
κ_a	Change in angle at top end relative to its initial (monotonic) value at any arbitrary time, during cyclic loading of a bending pipe specimen
$2\theta_0$	Initial (monotonic) internal bend angle at the crest of a strip specimen
$2\theta_a$	Internal bend angle at the crest of a strip specimen or pipe wrinkle due to an arbitrary stroke (S_a) on it, during cyclic loading
$2\theta_c$	Internal bend angle at the crest of a strip specimen or a pipe wrinkle due to maximum compressive stroke on it, during cyclic loading
$2\theta_t$	Internal bend angle at the crest of a strip specimen or a pipe wrinkle due to maximum tensile stroke on it, during cyclic loading
σ_u	Ultimate yield strength of pipe material
τ_a	Change in half-internal bend angle at the crest relative to its initial (monotonic) value at any arbitrary time, during cyclic loading of a bending pipe specimen and this is same as $\phi_a/2$ of an axial pipe specimen and a strip specimen

CHAPTER 1 INTRODUCTION

1.1 INTRODUCTION

With the popularization and the powerfulness of the computer, the computer becomes an indispensable tool for our daily work. The computer makes it possible for engineers to solve field problems by doing numerical analysis providing that sufficient field data can be obtained.

A numerical analysis program called ABP (ABP stands for Analysis of Buried Pipelines) was developed by the researchers in the University of Alberta (Zhou and Murray, 1993). The most recent version of the ABP program uses two-dimensional, elastic-plastic, isoparametric C^1 pipe beam elements, each of which has 3 nodes, and each node of which has 4 degrees of freedom. Also, elastic-plastic material properties and nonlinear constitutive relationships for the soil springs are adopted in the ABP program, so it is capable of modeling large displacement and finite strains and the numerical model of the ABP program can handle irregular pipe and ground profiles (Yoosef-Ghodsi and Murray, 2002). In particular, it can be used to analyze thermal buckling phenomena of pipelines such as "upheaval" (vertical) buckling (where the pipe segment moves in the vertical plane) and "snaking" (lateral) buckling (where the pipe segment moves in the horizontal plane). These thermal buckling phenomena of the pipelines are becoming common failure modes in the pipe industry.

As the two buckling phenomena above involve an overall behavior of the pipe segment and span at least several pipe diameters along their length, they are called Global Buckling modes of pipelines. Consequently, any imperfections that trigger these two kinds of buckling behavior are called Global Imperfections.

As the beam element used in the ABP program has only 12 degrees of freedom, only global (overall) behavior of the pipe segment can be captured. But

some of the pipeline field failures start with global behavior and then become localized into a local bulge somewhere in the critical segment. As this kind of wrinkle happens in a very short length, usually confined within a pipe diameter in length, they are called Local Wrinkles. Also, sometimes a local wrinkle forms in the pipeline without any global behavior involved. Localized pipe behavior has been studied in the University of Alberta for a decade. The numerical analytical tool presently used in the U of A is the commercial Finite Element Package ABAQUS, which was upgraded to Version 6.2 recently. The reasons for selecting the ABAQUS finite element package are as follows: (a) it can deal with large non-linear deformation, (b) it has an automated increment size control feature, (c) elastic-plastic hardening material properties and internal pressure can be applied to the finite element model, and (d) ABAQUS allows for both load and displacement control (Dorey et al., 2001).

Among the element library of ABAQUS, the three-dimensional "Shell Element" S4R is used in modeling the pipe segment as if the pipe is a kind of thin wall shell structure. The 'Shell Element' is a 4 node, double curved element with hourglass control intended for both thick and thin shell application, that accounts for finite membrane strains and allows for transverse shear stress (Dorey et al., 2001). Each shell element has 4 nodes and each node has 6 degrees of freedom. So by using shell elements to model the pipe segment, localized pipe behavior can be captured.

A standard model length (six times diameter (6D)) is commonly used at the U of A in creating the finite element (FE) model for ABAQUS to study the local behavior of the pipe. The length of the FE model is selected such that its end effects can be avoided. Small imperfections are also used in the ABAQUS model in order to trigger local wrinkles. As the imperfections used in ABAQUS model are confined within one pipe diameter in length, they are called Local Imperfections. Some results of previous studies in the University of Alberta will be reviewed in

next chapter. It will be seen that many analytical results are close to the laboratory test results and field data.

1.2 OBJECTIVES

The main objective of this research project is to further validate the capability of the ABP program by comparing the ABP numerical solutions with differential equation solutions and available field problems, which have documented in pipelines in Northern Alberta. The field failures in the pipeline, including not only a local fracture but also several examples of upheaval buckling phenomena, were selected to be studied based on the field data in hand, through the ABP program, the ABAQUS package and a solution technique for soil-pipe slip mechanisms. Cyclic loading analysis by using ABAQUS is done and the number of cycles to cause the fracture failure of the pipe is estimated based on a recently finished structural engineering report by Das et al. (2002). This also serves to verify the formula proposed by Das et al. (2002), as no field applications were available in that study. Conclusions are drawn based on the studies hereafter.

1.3 LAYOUT OF THE THESIS

This thesis consists of five Chapters and Appendices A and B. The main subjects of each of the following Chapters are summarized as follows.

Chapter 2 contains the review of the literature regarding the classical solutions of the global buckling of not only pipelines, but also railroad tracks, which were studied for a long time and are the basis of much of the research on the global buckling phenomenon of pipelines. In addition, different kinds of pipeline field failures and their analytical results done in the University of Alberta are reviewed.

Chapter 3 describes, in detail, some validation solutions of the capacity of the ABP program. The comparisons between the ABP solutions and Hobbs' classical solutions for the pipeline global buckling, and the comparison between the

ABP solutions and the differential equation solutions for the 'soil-slip' mechanism developed in the U of A will be presented.

Chapter 4 presents the case history failures of the Gold Creek NPS-8 Pipeline formerly operated by Wascana Energy Ltd. and the numerical simulation of the events. It is the core part of this research project. Two recently finished structural engineering reports, namely, "Fracture of Wrinkled Energy Pipelines" (Das et al., 2002) and "Analysis of Buried Pipelines with Thermal Application" (Yoosef-Ghodsi and Murray, 2002) will be used to test the capability of the numerical methods to simulate the field problems.

Chapter 5 presents conclusions based on the study in Chapters 3 and 4.

CHAPTER 2 LITERATURE REVIEW

2.1 GLOBAL BUCKLING

2.1.1 CLASSICAL SOLUTIONS

The thermal buckling of railroad tracks as well as pipelines has been studied for decades. Field observations and test results indicate that track buckling often occurs in the horizontal plane. Pipeline buckling does also if the pipeline is untrenched.

Among a series of factors which can induce axial load to the pipeline, two major causes can be identified. These arise from the restraint of the strains associated with thermal loadings and internal pressure loadings.

The buckling analyses for railroad tracks and pipelines are discussed in the following subsection, where the work of Kerr (1978), Hobbs (1984), and Ju and Kyriakides (1987) is reviewed.

2.1.1.1 Analysis of railroad track by A. D. Kerr (1978)

A. D. Kerr (1978) studied the lateral buckling behavior of continuously welded track to determine the safe temperature increase. In his analysis, 4 different buckling modes, as shown in Figure 2.1, were studied through the principle of virtual displacement and nonlinear theory of elasticity. A series of assumptions were made by Kerr in order to simplify the analysis. They are:

1. The "rail-tie" structure is replaced by an equivalent beam, i.e., "track beam". Kerr also assumed that the beam is subjected to a uniform temperature change.

2. The vertical deflection of the rail-tie structure, prior to and during lateral buckling, is negligible.

3. The lateral resistance per unit length of track axis is assumed constant. .

4. The axial resistance per unit length of track axis in the adjoining region is constant and is negligibly small in the buckled zone.

5. Prior to and during buckling, the response of the rail-tie structure is elastic.

Kerr stated that an analysis based on the mode 2 deformation shape may be sufficient for engineering purposes for the determination of the safe temperature increase based on the comparison of the results for mode shapes 1 to 4. Also, he pointed out that the assumptions 3 and 4 are only valid for monotonically increasing deformation and that modifications to his solutions are needed to study the behavior of track buckling with small geometric imperfections.

2.1.1.2 Analysis by Hobbs (1984)

Based on the related work on railroad tracks, Hobbs (1984) studied the vertical and lateral buckling modes of pipelines. These two buckling modes both involve an overall column-type response without gross distortion of the pipeline cross-section. A fully elastic modulus of the pipe for resisting bending is assumed in the analysis. The pipe is modeled as a beam-column under uniform lateral load equal to the pipe selfweight.

For the vertical mode as shown in Figure 2.2, Hobbs assumed that the bending moment at the lift-off point is zero because the curvature in the contact region is assumed to be zero. Small slope assumptions for the column are also used. For the lateral mode, Hobbs assumed that an initially perfect pipe would buckle into an indefinite series of half waves and that the lateral frictional force is fully mobilized everywhere.

Hobbs showed that horizontal snaking modes occur at a lower axial load than the vertical mode, and a horizontal mode is therefore dominant unless lateral restraint is provided by trenching the pipe. The analyses of lateral modes 2, 3 and 4 (as shown in Figure 2.1) can be recommended for lower bound design use. Hobbs recommended that further work on the effects of initial imperfections would be valuable.

As part of the study of the verification of the capability of the ABP program, the analytical results from the ABP program will be compared with Hobbs's differential equation solutions for the global buckling of pipelines. The details of the comparison are shown in Chapter 3.

2.1.1.3 Analysis by Ju and Kyriakides (1988)

Ju and Kyriakides (1988) also studied the upheaval buckling behavior of offshore pipelines. The pipeline was modeled as a long beam resting on a rigid foundation. The surrounding soil was modeled using Coulomb friction. The study was concerned with the effect of localized, small initial geometric imperfection on the response and the stability of the structure. Two main types of imperfection were adopted: (1) the pipe is supported at a hard point. This might represent a rock or the crossing of another pipe; (2) the pipe is supported continuously over a short length. This represents a locally elevated sea-floor relief. The effects of the magnitude of the initial imperfection and the pipe material inelastic characteristics are also studied. The beam deflections and small rotations were assumed in the study.

Ju and Kyriakides stated that in the presence of a relatively "small" fully contacting imperfection, the temperature rise vs. deformation response of the structure was found to be characterized by three critical temperatures. These are (see Figure 2.3):

(1) the temperature rise required to cause first uplift (ΔT_i)

(2) the limiting temperature rise (ΔT_{cr}) (first peak temperature value) beyond which the structure is unstable (i.e.: snap through behavior occurs); and

(3) the local minimum temperature rise (ΔT_m) (minimum temperature during snap through behavior) which occurs after the limiting temperature rise.

The first two of the above temperature increments were found to be strongly influenced by the initial amplitude, wavelength and the shape of the imperfection. The critical values for the initially straight pipes were substantially higher than those with an initial geometry matching that of the imperfect foundation. They were relatively insensitive to frictional effects. The quantity of ΔT_m was relatively unaffected by "small" imperfections, but strongly dependent on the value of the friction coefficient used.

For smaller values of imperfection, the temperature increment rises to a limiting temperature (ΔT_{cr}), it then decays to a minimum value (ΔT_m) and rises again. When the critical temperature ΔT_{cr} is reached, the pipe would snap dynamically to a static equilibrium configuration on the stable branch horizontally. For "larger" values of the imperfection, the response was monotonically increasing, but with severely reduced resistance to deformation. The responses stated above are shown in Figures 2.3 and 2.4 and produce the typical temperature vs. pipe displacement plot. Inelastic material behavior leads to more localized deformations and can result in local shell buckling.

2.1.2 INELASTIC SOLUTIONS

It can be seen, from the Section 2.1.1, that the classical solutions are based on the assumptions that the material properties fall into elastic range and the rotations are small. Since the pipeline is required to deform into elastic-plastic range in order to form a wrinkle, inelastic material properties and large displacements must be considered in order to obtain a better understanding of behavior of the pipeline. The most recent version of the ABP program, namely,

ABP-Version2002 (ABP-V2002 hereafter) was coded such that inelastic material properties and large displacements are incorporated into to the model and therefore inelastic global behavior of the pipe segment can be captured. Using ABP-V2002, Yoosef-Ghodsi and Murray (2002) did "upheaval" and "snaking" buckling analysis to test the capability of the program by comparing with alternate solutions and the field data available. It will be shown, in Section 2.2, that good agreement can be obtained between the analytical results of ABP-V2002 and the field data.

2.2 LOCAL BUCKLING

Localized pipe behavior has been studied in the University of Alberta since 1988. New equations to identify the localized critical buckling strain were developed by A. B. Dorey, et al. (2001). Also, different numerical analytical solutions for different pipe failure modes that were observed in the field were obtained in the University of Alberta. They will be reviewed in the following subsections.

2.2.1 CRITICAL BUCKLING STRAIN (Dorey et al., 2001)

Dorey et al. (2001) conducted a total of 15 full-scale experimental tests on NPS30 line pipe with a D/t ratio of approximately 92. The test specimens were subjected to load cases that are representative of 'typical' load cases the pipe may experience in the field under normal operational conditions, i.e., a combination of axial load, internal pressure and monotonically increasing curvature. Dorey also carried out a series of numerical analyses by using ABAQUS Version 5.7-1 to compare his analytical results with not only his own test results but also some typical results from the database of the line pipe established by others in the University of Alberta. Good agreement between the test results and analytical results were reached, as shown in Figures 2.5 and 2.6. Four important parameters, which influence the development of load capacity and the critical buckling strain of the pipe segment, are identified. They are: Diameter-to-thickness (D/t) ratio, internal pressure (p/p_y) ratio, material properties and initial imperfections.

Based on the test and analytical results, Dorey drew the conclusions as follows:

1. Initial imperfections are an extremely important feature in the buckling response of segments of line pipe. Inclusion of an appropriate initial imperfection pattern in an FEA model is crucial in predicting experimental behavior.

2. Using an assumed 'blister-type' initial imperfection pattern, as shown in Figure 2.7, provides excellent correlation with the experimental data for the plain pipe specimens. Using an assumed 'offset-type' initial imperfection pattern, as shown in Figure 2.8, provides excellent correlation for the girth-welded specimens

3. The results of the experimental phase of this project show that there are two dominant characteristic buckling modes for segments of line pipe subjected to combined loads. These two modes are dependent on the level of internal pressure in the test specimen. For the unpressurized specimens, the wrinkle develops into a 'diamond-shape' buckle. For the specimens with an internal pressure equal to or greater than that required to produce a circumferential stress of 20% SMYS, the wrinkle develops into a 'bulge' buckle.

4. The local and global response of a test specimen is highly dependent on the grade of the material. For specimen groups in which the only variable was the material strength, an increase in material strength resulted in an increase in peak moment capacity and a reduction in the critical buckling strain.

5. The global and local behaviors of segments of line pipe subjected to combined load cases can be accurately predicted using FEA modeling techniques provided accurate initial imperfection, material property and boundary condition criteria are incorporated into the model.

2.2.2 WRINKLE FORMATION DUE TO BENDING (Anon, 1998)

Interprovincial Pipe Line (NW) Ltd. (IPL) has run an inertial geometry tool (GEOPIG) on Norman Wells–Zama Pipeline from Norman Wells to Wrigley Station on an annual basis with the purpose of detecting pipe movement associated with slope stability and thaw settlement. The terrain conditions of the majority of the pipeline route in that region are characterized by discontinuous permafrost in silty clayey soils with moderate to high ice contents. Consequently, the company has been running the GEOPIG once a year to monitor the pipe movement in that region since the line was first put into operation. It was noted that, at Slope 92 (KP318), the 1997 vertical strain increased significantly in comparison with the 1995 GEOPIG data. As part of the further investigative work, the PipeTech Group in the University of Alberta was asked to do numerical analysis to see if a wrinkle could be predicted as the result of the imposed geometric displacements that occurred in the field.

Numerical analysis done by ABAQUS Version 5.5 was conducted in the University of Alberta. Based on the predicted behavior of the line pipe and the GEOPIG record, it was concluded that a wrinkle would exist on Slope 92 and it was decided that an investigative dig should be conducted to verify the existence the wrinkle. The Slope 92 wrinkle after the field dig is shown in Figure 2.9. The numerical analytical result by ABAQUS is shown Figure 2.10. The shape of the wrinkle in Figure 2.9 is surprisingly close to that in Figure 2.10. Since the wrinkled configuration involves only localized pipe behavior due to settlement involved, the local wrinkle at Slope 92 is identified as a "*l*ocal *b*ending *w*rinkle".

2.2.3 WRINKLE FORMATION DUE TO UPHEAVAL BENDING

The formation of the wrinkle in Slope 92 has severe distortions only in the vicinity of the wrinkle. Consequently, it is said to have developed a 'local buckle' and no global buckling behavior is involved. But some of the field failure modes start with global behavior, i.e., part of the pipe segment moves vertically or laterally, and then the behavior becomes localized and eventually a local wrinkle forms at the

critical location of this segment. Typical of these kinds of failure modes are the upheavals that occured in the Gold Creek Pipeline of Wascana Energy Ltd.. The details of the formation of these Gold Creek upheavals will be the core part of this project and will be discussed in Chapter 4.

2.2.4 WRINKLE FORMATION DUE TO SNAKING BENDING (Yoosef-Ghodsi and Murray, 2000)

In January 2000, a failure happened on an oil pipeline in a canal close to Guanabera Bay in Brazil. After measuring the final configuration of the pipeline in the field, it was concluded that the pipeline buckled horizontally (snaking buckling) with an amplitude of about 4m. It formed a wrinkle and fractured in the critical location. As part of the study of the behavior of that pipeline, some thermal analyses were carried out using the ABP program in order to simulate the snaking phenomenon that the pipe experienced prior to the formation of the fracture. The operational temperature for that pipeline was around 75°C. An ABP analysis for this problem was carried out by Yoosef-Ghodsi in November 2000.

The layout of the numerical model used in the ABP program by Yoosef-Ghodsi and Murray (2000) is shown in Figure 2.11. The initial out-of-straightness (IOS) is chosen such that the S-shape buckling model, similar to that observed for the actual pipe, is triggered. Figure 2.12 shows the temperature change vs. buckle amplitude for the ABP solution. The pipe deformed shapes at different temperature differentials are shown in Figure 2.13. It is noted, from Figure 2.10, that an acceptable global buckling solution has been obtained using the ABP program. Since ABP is not presently capable of analyzing for local buckling, it can not simulate the wrinkling that occurred in the field situation. A solution technique that may be capable of simulating the wrinkling triggered by global snap-through buckling is to apply the displacement arising from the global buckling solution to the ends of an ABAQUS model of the segment at the crest of the snaking configuration.

2.2.5 BENDING WRINKLE FRACTURE FORMATION (Murray and Yoosef-Ghodsi, 2001)

In the year 2000, Murray and Cheng Ltd. had the opportunity to investigate a wrinkle and a fracture, which occurred within the wrinkle, for a pipeline supplying fuel oil to a thermal power plant in the Eastern United States. The wrinkle occurred in a cold bend in the horizontal plane. There is no global behavior involved for this wrinkle. Based on this problem, a pipe–soil slip mechanism and its solutions were developed in the University of Alberta. This differential equation solution (DESs) technique for the pipe-soil slip mechanism is shown in Appendix A. As part of the validation solution for the ABP program, the solutions between the DESs and ABP solutions will be compared and will be described in Chapter 3.

2.2.6 WRINKLE FRACTURE FORMATION (Das et al., 2002)

In order to understand the load conditions that are able to produce a fracture at a wrinkle as a result of cyclic loading, Das et al. (2002) conducted 12 full-scale pipe tests. A FEA model was developed to simulate the behavior of these cyclic pipe specimens. The global behavior and deformed shapes correlated well with the experimental results. In addition, Das carried out strip tests in order to develop a fracture failure criterion based on the energy absorption behavior of the strip specimen. Applying the fracture model to pipe test specimens showed that it works reasonably well and predicts conservative result for the residual life of the wrinkles. The detailed description of Das's test and the proposed formula are discussed in Appendix B.

In addition, as part of this project, the equations proposed by Das et al. (2002) will be applied to the fracture failure of Gold Creek NPS-8 Pipeline (see Appendix B for the equations).

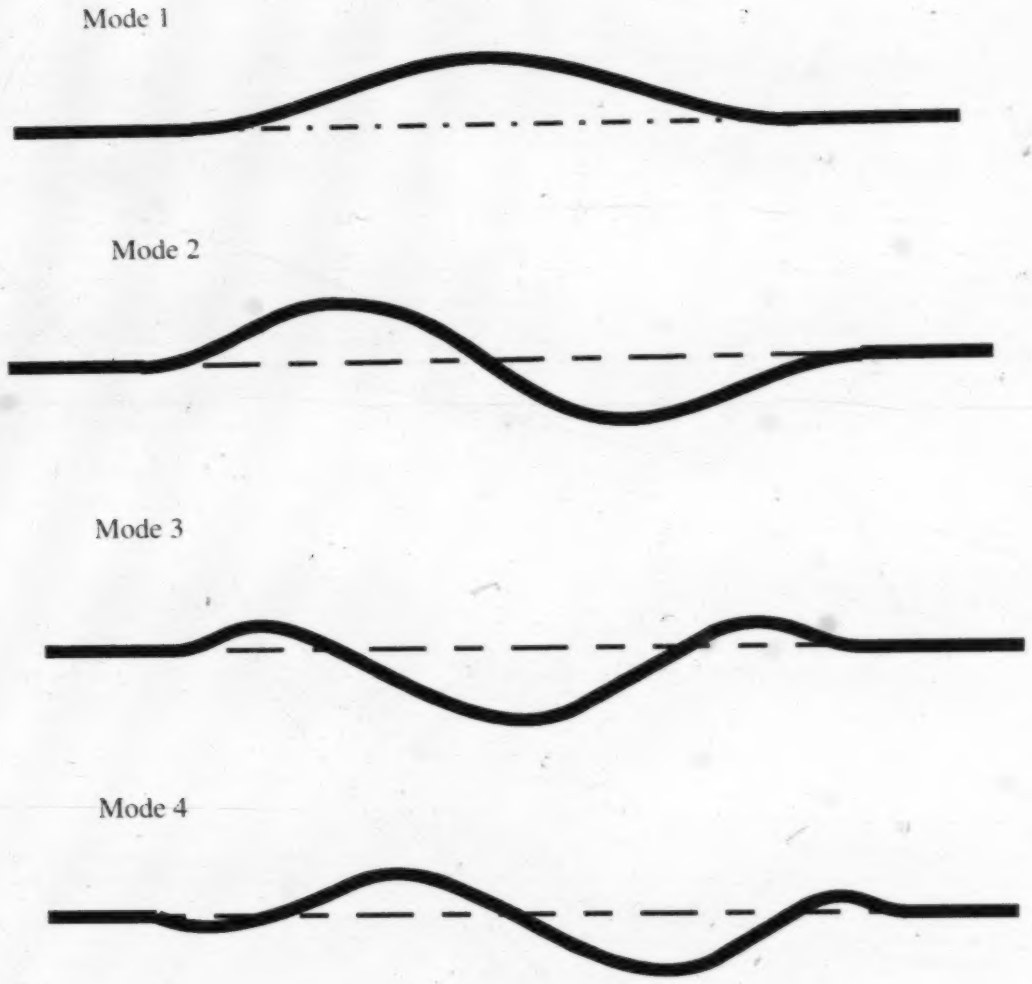

Figure 2.1 Different Buckling Modes in Railroad Tracks and Pipelines

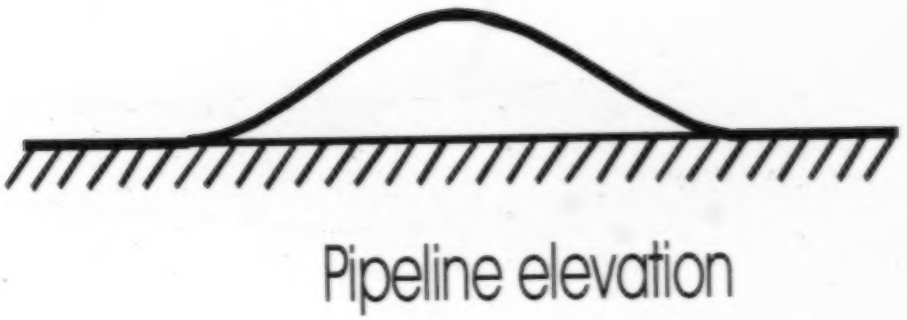

Figure 2.2 Vertical Buckling Mode of Pipelines

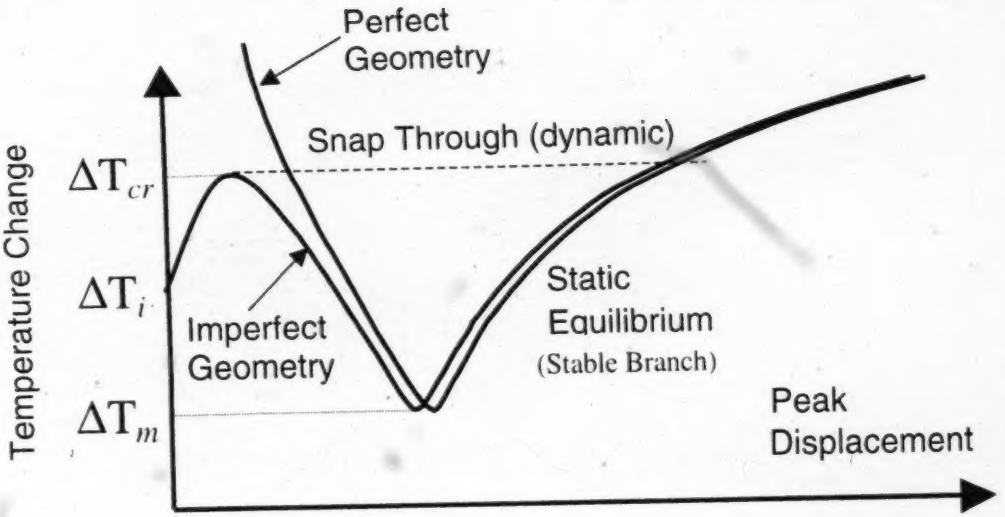

Figure 2.3 Typical Temperature vs. Pipe Displacement Relationship

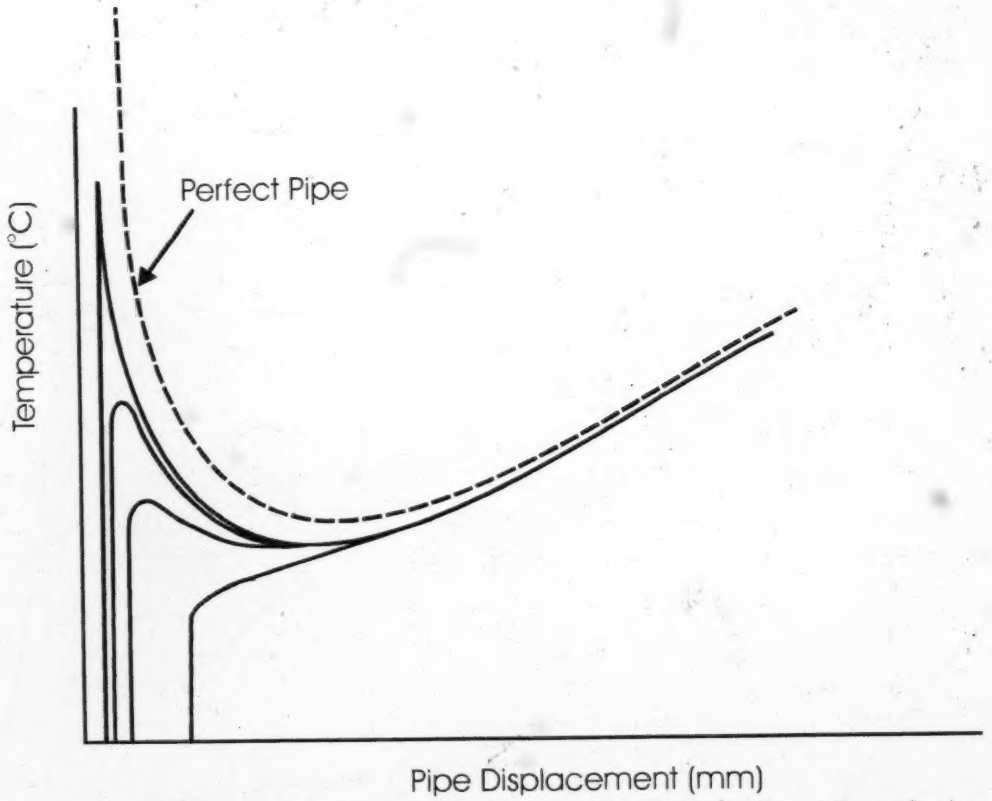

Figure 2.4 Temperature vs. Pipe Displacement Curves for Different Imperfections

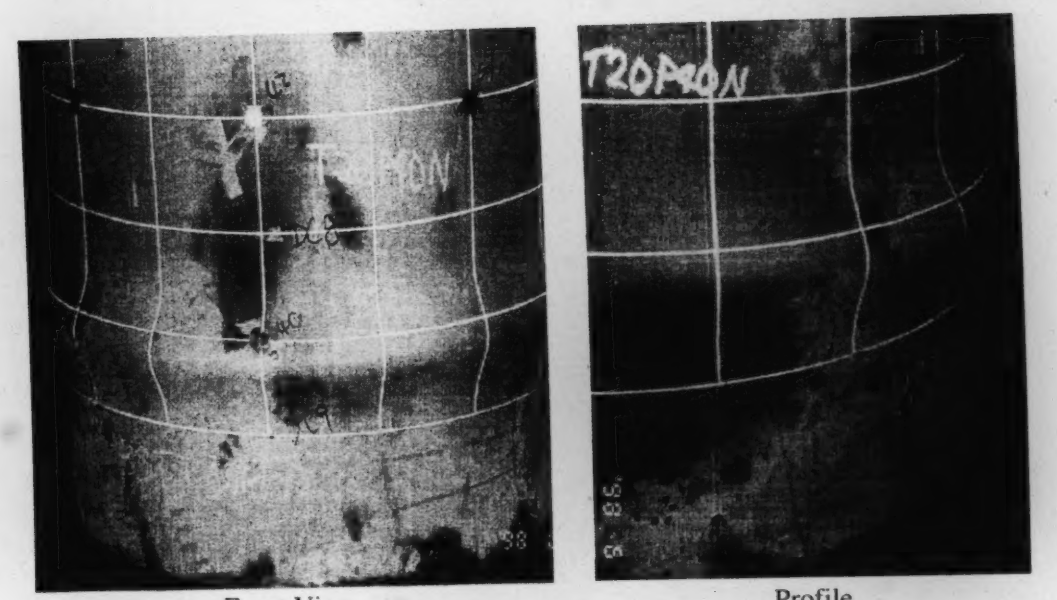

Front View Profile

Figure 2.5 Photograph of Experimental Buckling Mode for Plain Pipe with Internal Pressure (Dorey et al. 2001)

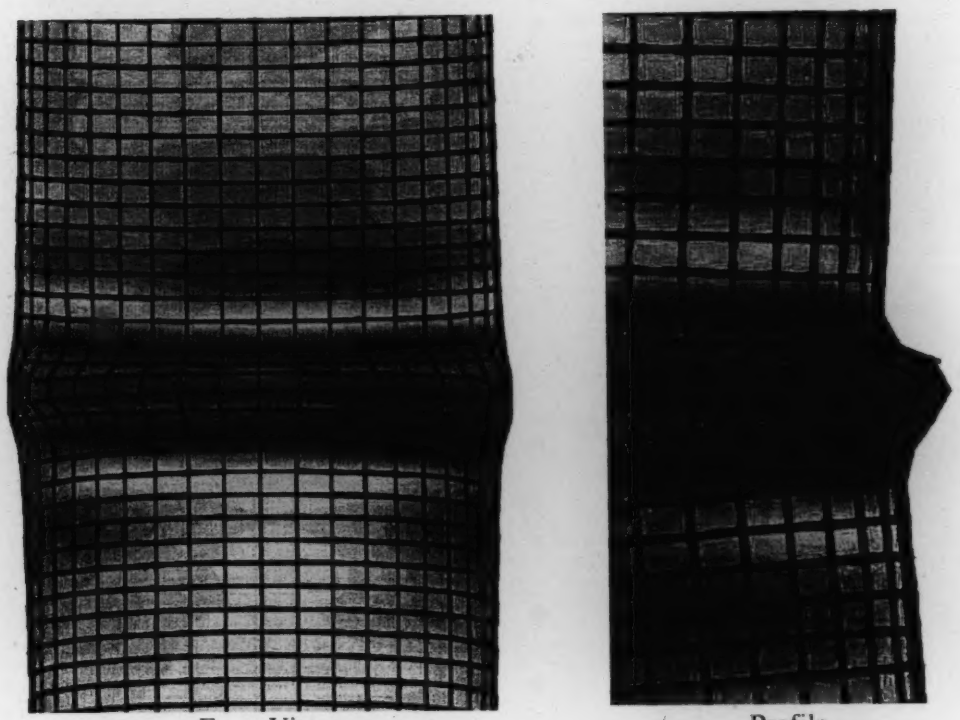

Front View Profile

Figure 2.6 FEA Model Generated Buckling Mode for Plain Pipe with Internal Pressure (Dorey et al. 2001)

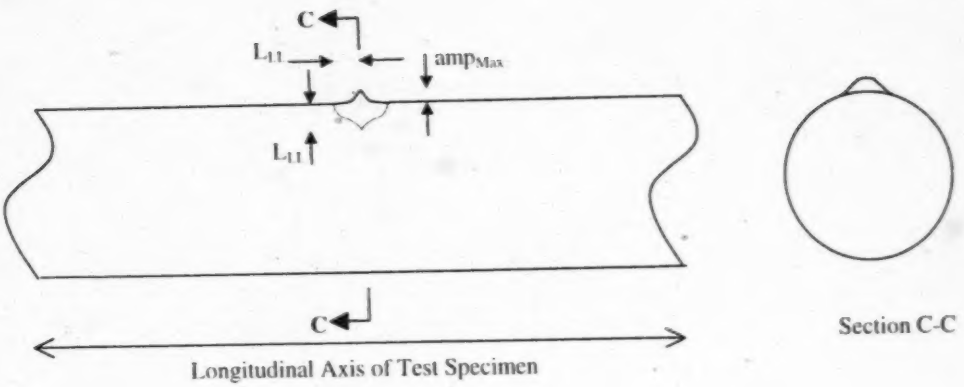

Figure 2.7 Schematic of "Blister" Type Assumed Initial Imperfection (Dorey et al. 2001)

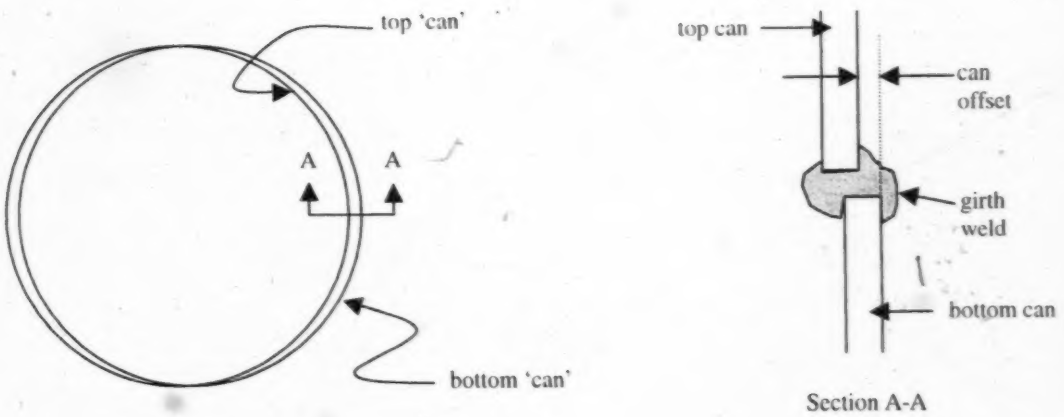

Figure 2.8 Schematic of "Offset" Type Assumed Initial Imperfection (Dorey et al. 2001)

Figure 2.9 Local Wrinkle for KP318 from the Field Dig (Yoosef-Ghodsi et al, 2000)

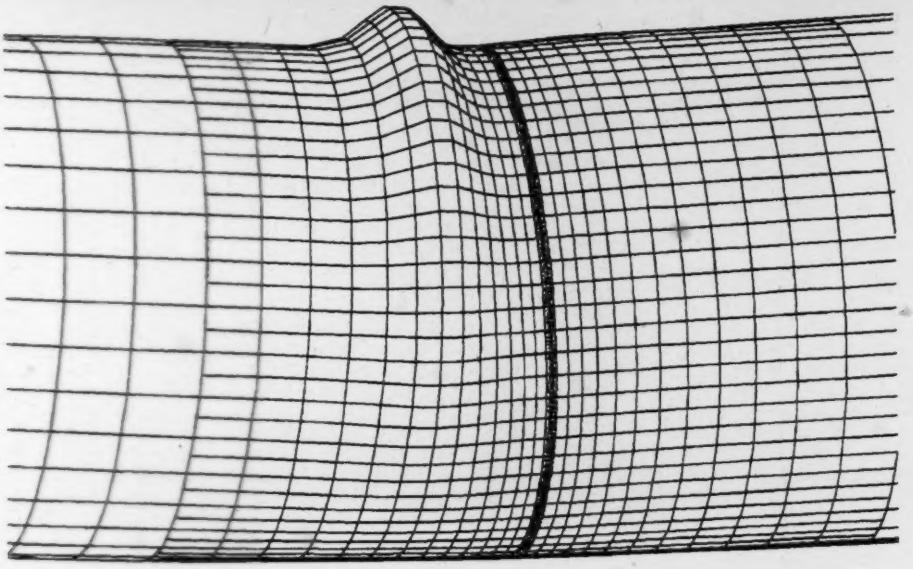

Figure 2.10 Wrinkle Formed by FEA Model Imposing Geometric Displacement (Yoosef-Ghodsi et al, 2000)

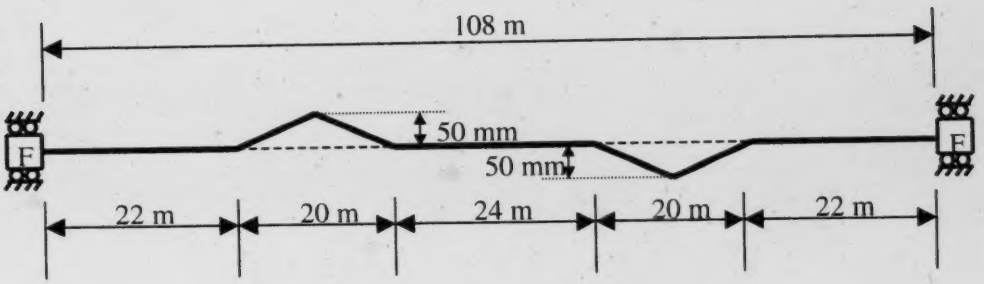

Figure 2.11 Numerical Model Layout for Brazil Snaking Problem

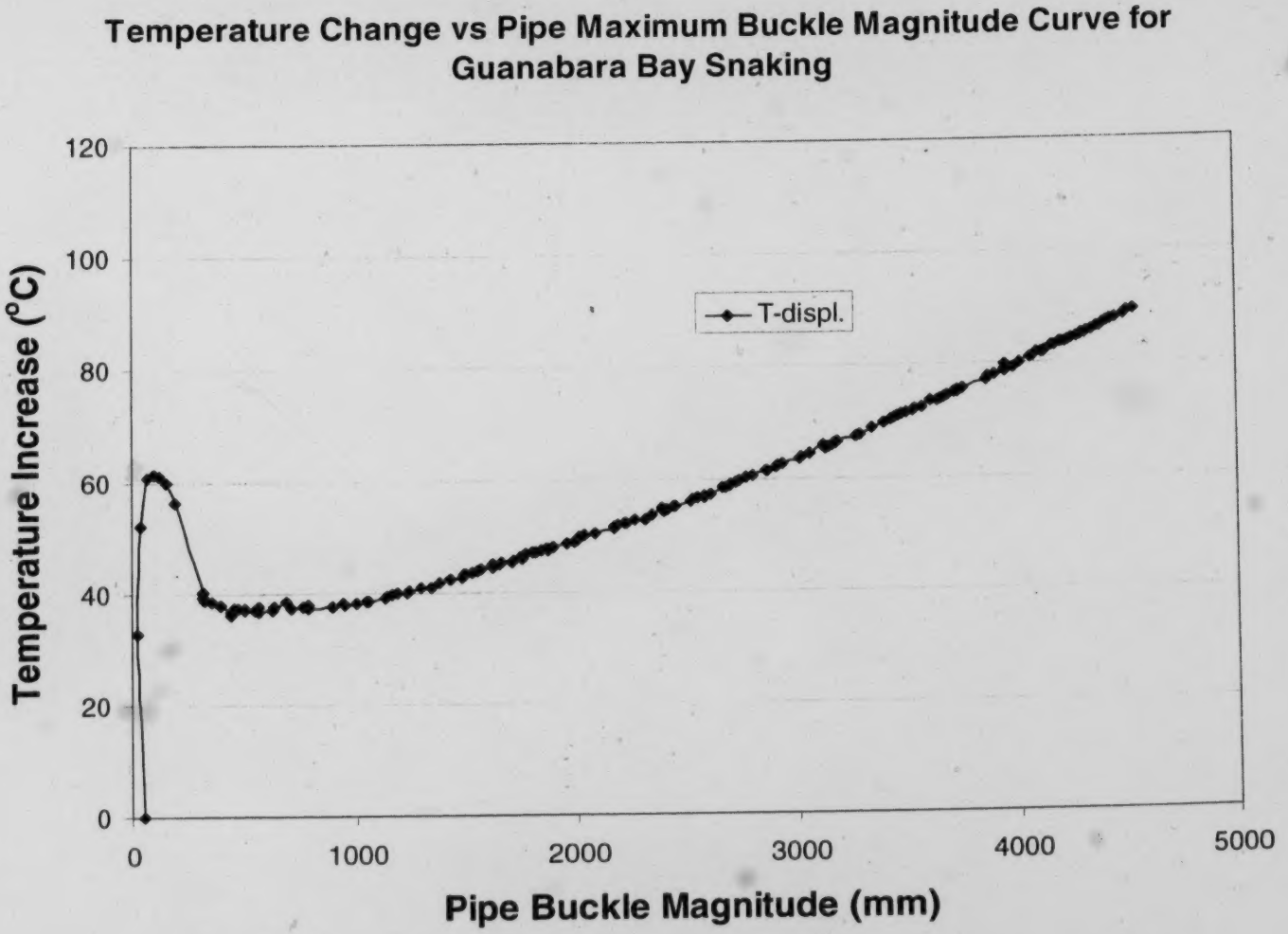

Figure 2.12 Temperature Change vs. Pipe Buckle Amplitude Curve for Brazil Snaking Problem

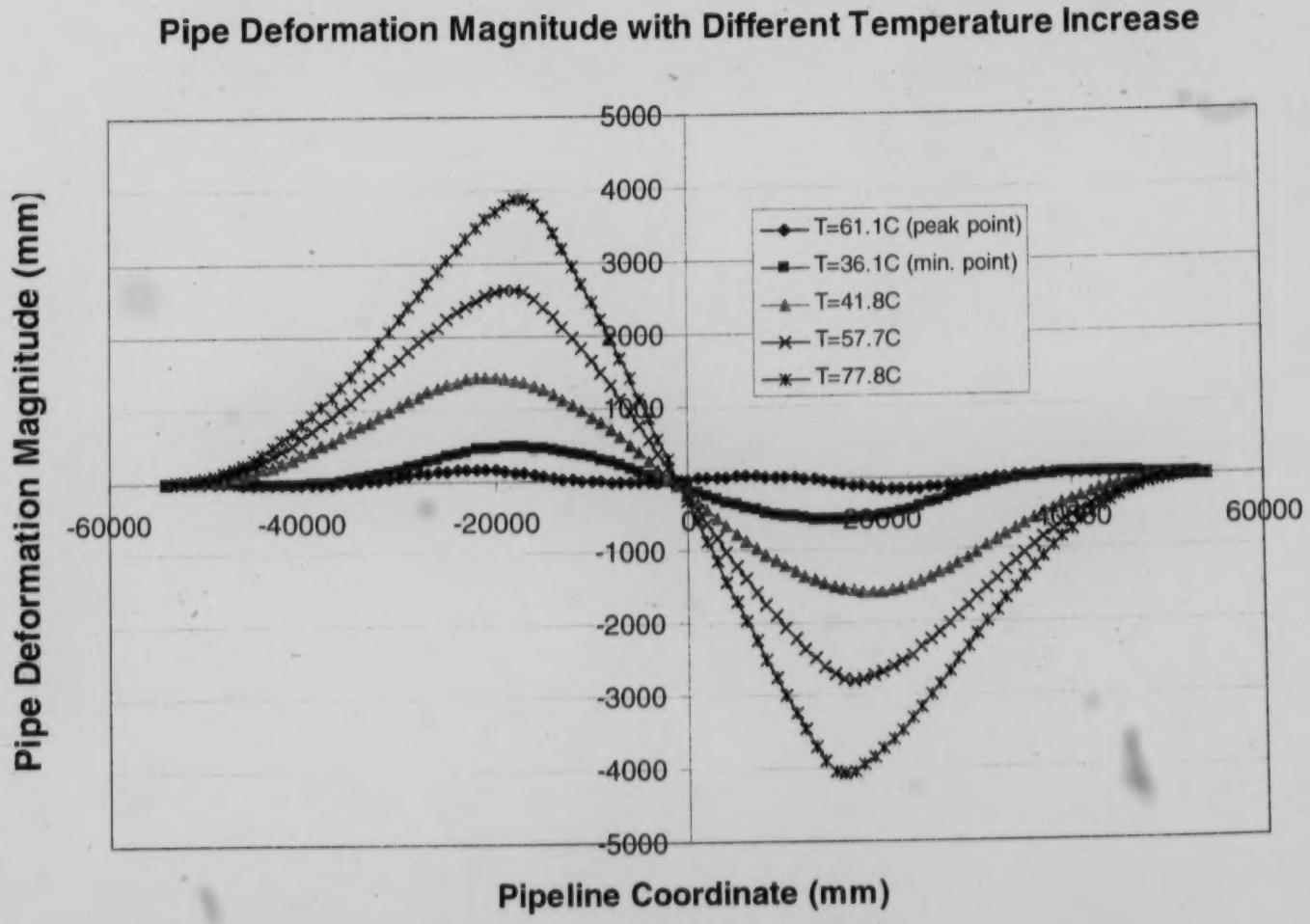

Figure 2.13 Pipe Deformed Shape at Different Temperature Differential for Brazil Snaking Problem

CHAPTER 3 VALIDATION SOLUTIONS FOR THE COMPUTER PROGRAM ABP-V2002

3.1 GENERAL DESCRIPTION

Numerical and experimental behavior of line pipe has been studied for 15 years in the University of Alberta. Numerical analyses were done not only for the experimental tests but also for field problems and good agreement has been reached between them. However, it is difficult to find well documented field results.

The computer program ABP-V2002, based on the one that was initially developed several years ago (Zhou and Murray, 1993), was further improved. In particular, it can be used to deal with thermal buckling analysis of pipelines.

In Chapter 4 of this document, a number of field examples of thermal buckling will be examined where attempts will be made to predict the buckling by analytical means and to compare the predictions using numerical solution techniques with the filed observations. In order to make such predictions, it is necessary to consider the slip between the soil and the pipe arising from thermal expansion. For the numerical modeling of the slip, ABP will be used. As part of the project, some further validation solutions for the ABP were carried out to demonstrate that ABP is capable of simulating the "classical" solutions of Hobbs (1984) and some more recent solutions of pipe-soil interaction using a combination of pipe-soil slip differential equation solutions and ABAQUS solutions (Murray and Yoosef-Ghodsi, 2001). This chapter describes the details of the validation solutions. These validation solutions include the comparison between the ABP solutions and Hobbs' DESs for pipeline global buckling and comparison between ABP solutions and the DESs for pipe-soil slip mechanisms, which was developed by researchers in U of A and is described in Appendix A.

3.2 COMPARISON OF ABP RESULTS WITH HOBBS'S DIFFERENTIAL EQUATION SOLUTION

As stated in Section 2.1.1.2 of Chapter 2, Hobbs studied the behavior of the pipeline based on the related work on railroad tracks. Although elastic material properties and small slope assumptions are used in the differential equation solutions (DESs), general guidelines can be obtained from them. Consequently, as part of the verification of the capability of the ABP program, the numerical results from the ABP-V2002 are compared with Hobbs's DESs. Upheaval buckling analysis is used here, which corresponds to the vertical mode in the DESs. The data is from an offshore pipeline.

3.2.1 Data for the Pipeline

The data used for the comparative solutions are as follows: the pipe outside diameter, OD = 12.75 in (323.85 mm). The pipe wall thickness, t = 0.75 in (19.05mm). The internal pressure for the offshore pipeline is 10.4 MPa. The steel grade used for the pipeline is API X-65. Since DESs are valid only for elastic material properties, elastic material properties were also used in the ABP-V2002 program for comparison purposes.

3.2.2 Data for the Soil

Typical soil data from the experience of previous studies are used in the numerical analysis of the ABP program as listed in Table 3.1.

Table 3.1 Properties for Soil Springs

Bearing Spring	Stiffness (N/mm/mm)	0.26
	Yield strength (N/mm)	19.0
Longitudinal Spring	Stiffness (N/mm/mm)	0.35
	Yield strength (N/mm)	9.0
Uplift Spring	Stiffness (N/mm/mm)	0.00001
	Yield strength (N/mm)	0.9

In order to get convergence during the ABP run, very small soil spring values were used for the uplift soil spring properties, as shown in Table 3.1. As zero soil-cover height above the pipe segment was used, the error induced should be small.

3.2.3 Case Study for the Comparative Solutions

3.2.3.1 Differential Equation Solution by Hobbs (1984)

According to Hobbs (1984), two major causes of the compressive force in the pipeline can be identified. These arise from the restraint of the longitudinal strain associated with thermal loadings and internal pressure loadings. The force P_0 created by full restraint of thermal expansion is

$$P_0 = EA\alpha\Delta T \qquad (3.1)$$

where E is the modulus of elasticity, A is the pipe cross sectional area, α is the coefficient of thermal expansion and ΔT is the temperature differential.

For the vertical buckling mode, the buckled part of the pipeline is treated as a beam-column under uniform lateral load equal to the pipe self-weight. It is assumed that the bending moment at the lift-off point is zero and the slope is small so that linear equations related to column buckling are appropriate. Referring to Figure 3.1 for the vertical buckling mode, a free-body diagram of a segment from the buckled part at the right lift-off point, as shown in Figure 3.2, is obtained. The external moment acting on the cut section is:

$$\begin{aligned} M_{ext} &= Py + w(L/2 - x)\,(L/2 - x)/2 - wL(L/2 - x)/2 \\ &= Py + w(L^2/4 - x^2)/2 \end{aligned} \qquad (3.2)$$

and the internal moment is:

$$M_{int} = -EIy'' \qquad (3.3)$$

For equilibrium, $M_{ext} = M_{int}$. Substituting Equation 3.3 into Equation 3.2, the following relationship can be obtained:

$$y'' + n^2 y + (m/8)(4x^2 - L^2) = 0 \qquad (3.4)$$

in which a prime denotes differentiation of y with respect to the longitudinal coordinate x, the pipe self-weight is w (force per unit length), and the moment of inertia is I, $m = w/EI$, $n^2 = P/EI$, and the buckled length between the lift-off points is L.

The solution of Equation 3.4 is given by (Marek and Daniels, 1971)

$$y = \frac{m}{n^4}\left[A\cos(nx) + B\sin(nx) - \frac{1}{2}n^2x^2 + \frac{1}{8}n^2L^2 + 1\right] \qquad (3.5)$$

in which A and B are unknown constants of integration and can be solved from the boundary conditions.

Using the boundary conditions that $y'|_{x=0} = 0$, $y|_{x=\pm(L/2)} = 0$ and $y'|_{x=\pm(L/2)} = 0$, the solution for Equation 3.5 becomes:

$$y = (m/n^4)\,[-\cos(nx)/\cos(nL/2) - n^2x^2/2 + n^2L^2/8 + 1) \qquad (3.6)$$

Considering the displacement boundary conditions that the slope at the ends of the buckle should be zero (as shown in Figure 3.1), the unknown buckled length, L, can be determined from

$$y' = \tan(nL/2) - nL/2 = 0 \text{ (at } x = L/2) \qquad (3.7)$$

or

$$\tan(nL/2) = nL/2 \qquad (3.8)$$

Which has the lowest non-trivial root

$$nL = 8.9868 \tag{3.9}$$

From Equation 3.8, and substituting for n, the following expression can be obtained:

$$c = nL/2 = [PL^2/(4EI)]^{1/2} \tag{3.10}$$

Combining Equations. 3.6 and 3.10, the deflected shape for the pipe segment becomes (Marek and Daniels, 1971):

$$y = m/n^4[(c^2 + 1)^{1/2}\cos(nx) - n^2x^2/2 + c^2/2 + 1] \tag{3.11}$$

Figure 3.3 shows the compatibility conditions (Marek and Daniels, 1971) for the buckled segment of an infinitely long pipeline. In the figure, points A, B, C, D, and E locate the position of the pipeline just prior to buckling. After buckling, points B, C, and D move to B′, C′ and D′, respectively. Points A and E do not displace during buckling. However, all points between A and B′ and between D′ and E are assumed to undergo axial displacement only. As shown in Figure 3.3, ΔL represents the axial displacement BB′ or DD′ which occurs during buckling.

Referring to Figure 3.1b for the axial force distribution and setting $q = \phi w$ and $Q = \phi Lw/2 = qL/2$ (where ϕ is the coefficient of friction between the pipe and the subgrade) in order to simplify the expression, the following relationship can be obtained:

$$P = P_0 - qL_s - Q \tag{3.12}$$

It can be shown that the displacement, ΔL, is given by:

$$\Delta L = \frac{1}{2}\frac{q}{EA}L\xi^2 = \frac{q}{2EA}\left(\frac{P_0 - P - Q}{q}\right)^2 = \frac{(P_0 - P - Q)^2}{2AEq} \qquad (3.13)$$

Referring to Figure 3.3, the curved length B′C′D′ will be larger than the length BCD as there will be a decrease in axial force from P_0 to P upon buckling.

Therefore

$$\overline{B'C'D'} = (L + 2\Delta L)[1 + (P_0 - P)(AE)] \qquad (3.14)$$

in which $L + 2\Delta L = L + (P_0 - P - Q)^2/(AEq)$ (3.15)

also $\overline{B'C'D'} = L + \frac{1}{2}\int_{-L/2}^{L/2}(y')^2 dx$ (3.16)

From Equations 3.14, 3.15 and 3.16, the following relationship can be set up:

$$L + \frac{1}{2}\int_{-L/2}^{L/2}(y')^2 dx = [L + (P_0 - P - Q)^2/(AEq)][1 + (P_0 - P)(AE)] \qquad (3.17)$$

Considering that the product $[(P_0 - P - Q)^2/(AEq)][(P_0 - P)(AE)]$ as negligible, Equation 3.17 reduces to

$$(P_0 - P - Q)^2 + (P_0 - P)qL - AEq\,\frac{1}{2}\int_{-L/2}^{L/2}(y')^2 dx = 0 \qquad (3.18)$$

Using Equation 3.11 to obtain y′ and substituting for Q = qL/2, Equation 3.18 reduces to:

$$[P_0 - (P + \frac{qL}{2})]^2 + [P_0 - (P + \frac{qL}{2})]qL + \frac{1}{2}(qL)^2 - 0.4167c^2AE(\frac{m}{n^3})^2 qL = 0 \qquad (3.19)$$

from which

$$P_0 = P + [0.4167c^2EA(m/n^3)^2qL - (qL/2)^2]^{1/2} \quad (3.20)$$

After substituting for m and n into Equation 3.20, the following results are obtained

$$P = 80.76EI/L^2 \quad (3.21)$$

$$P_0 = P + \{wL[1.597 \times 10^{-5}EA\phi wL^5 - 0.25(\phi EI)^2]^{1/2}\}/(EI) \quad (3.22)$$

The maximum amplitude of the buckle

$$y_{max} = 2.408 \times 10^{-3}wL^4/(EI) \quad (3.23)$$

For very large coefficient of friction, i.e., $L_s = 0$, a minimum buckle length can be obtained as

$$L_{min} = [1.6856 \times 10^6(EI)^3/(w^2AE)]^{0.125} \quad (3.24)$$

Based on the equations above, for a given buckle length L, the corresponding axial force or temperature change can be determined. The procedure is as follows:

(a) Compute L_{min} using Equation 3.24.

(b) For $\phi = 0.5$ (the average value of ϕ), and for 20 values of L between $0.1L_{min}$ and $3L_{min}$, compute P_0 using Equation 3.22, ΔT using Equation 3.1, and the buckled amplitude y_{max} using Equation 3.23.

The calculated temperature change vs. pipe buckled magnitude curve for ϕ=0.5, as shown in Figure 3.4, can be determined from a spreadsheet.

The following limitations of the analyses presented by Hobbs should be borne in mind:

1. Only perfect systems have been examined. No account was taken of the initial out-of straightness. The classical column (Fourier) analysis of initial out-of-straightness is inappropriate because the buckled length changes progressively as the load increases.

2. Perfect elasticity and small slopes have been assumed. The analyses presented assume that the full elastic modulus of the pipe is available to resist bending. Once plasticity occurs the analysis loses its validity.

3.2.3.2 Numerical Analysis by Using the ABP Program

As computed by Equation 3.24, the minimum buckle length for the data in Sections 3.2.1 and 3.2.2 is about 40 m. Based upon previous experience, a length of pipe segment of 840 m with Initial Out of Straightness (IOS) spanning over 40 m was assumed to be reasonable as the finite element model for the ABP program in order to simulate an infinitely long pipe. Two different IOS's were used for comparison purpose, i.e., 50 mm and 20 mm. The whole ABP pipe model is shown in Figure 3.5 and consists of 120 elements and 241 nodes. It is assumed that no soil cover exists above the pipeline. But small values were given to the uplift spring properties just for convergence purposes in the numerical analysis. The temperature change vs. pipe vertical displacement, obtained from the numerical analysis of the ABP program for the IOS's of 50mm and 20mm, are shown in Figure 3.6.

The comparison of the Hobbs DES solutions and the numerical ABP analytical results is shown in Figure 3.7. Figure 3.7 indicates that the buckling behaviors from these two solution types are similar.

It is shown, in Figure 3.7, that there are some differences between the ABP plots and DES plot in the post-buckling region. It is believed that the reason for this

is that the DESs can only handle small displacement problems but the ABP program includes vertical soil springs and the formulation to handle large displacement problems.

3.3 COMPARISON OF THE ABP SOLUTIONS WITH THE DESs FOR PIPE-SOIL SLIP MECHANISMS

3.3.1 INTRODUCTION

As described Section 2.2.5 and Appendix A, a solution technique for pipe-soil slip was developed in the University of Alberta. Good agreement between this solution technique and field measurement was obtained and the differential equation approach appears to produce a good result for predicting the creation of the local wrinkle in the field (Murray and Yoosef-Ghodsi, 2001). As part of the validation of the ABP program, the numerical results from the ABP program will be compared with that of the DESs for the pipe slip example that occurred in a hot oil pipeline in the Eastern United States.

3.3.2. BRIEF DESCRIPTION OF PIPE-SOIL SLIP

A schematic of a pipe-soil interactive slip assemblage is shown in Figure 3.8. It is assumed that there are points in the pipeline, remote from wrinkle, that do not move relative to the soil. The first point that one encounters when traversing along the pipeline away from the wrinkle will be called a 'soil anchor point' as represented schematically by the fixed end D in Figure 3.8. It is also assumed that End C is a free end at which the wrinkle forms. As a thermal change occurs, the pipe expands away from the anchor point D and produces a relative displacement with the soil causing the pipe to protrude a distance of Δ from the soil at end C. A force P in Figure 3.8 is assumed to be exerted by the adjacent pipe component as the pipe expands toward the weakest location (end C). Consequently, the pipe-soil slip mechanism can be used to determine the compatible displacement and driving force at the junction of the anchorage section and the wrinkle segment, which represents the wrinkle for the ABAQUS model.

As upheaval behavior is another failure mode of the pipeline and also occurs in the weakest location in the line, the pipe-soil slip mechanism can be used in creating the ABP model for upheaval buckling analysis. This will be described in Chapter 4.

3.3.3. AVAILABLE DATA FOR THE HOT OIL PIPELINE

3.3.3.1. Material Properties

For this example, the outside diameter of the pipe, OD, is 12.75 in (323.85 mm), the pipe wall thickness, WT, is 0.203 in (5.156 mm), and the operational temperature is 110°F.

Since the differential equation approach is valid only for elastic material properties, elastic material properties are also used in the ABP program for verification purposes.

3.3.3.2. Soil Spring Stiffness

The field test data for the soil in the field for this pipeline is shown in Figure 3.9. The pipe-soil interface yield strength, τ_y, from the plots in Figure 3.9, is important for both the differential equation approach and the ABP program. In the ABP program, the soil is represented by three different kinds of springs along the pipeline, namely longitudinal, uplift, and bearing springs. In the DESs, the longitudinal spring properties (i.e. axial soil-pipe interface stiffness properties obtained by field test) are the most important among those of the three springs because there is no vertical pipeline settlement to be concerned with in this example.

From Figure 3.9, the longitudinal soil spring stiffness can be calculated as follows. First, the soil shear yield strength is estimated as 0.009 N/mm^2 as shown by the heavy line. Figure 3.9 indicates that this value is reasonably representative of the in-situ measurement. The diameter of pipe is OD = 12.75 in, and there is a one-inch thick insulation layer around the outside of the pipe wall. So the yield strength, for every unit length along the pipe can be calculated as:

$$F_y = 0.009 \times (12.75+1+1) \times 25.4 \times \pi = 10.46 \text{ N/mm} = 0.0598 \text{ kips/in} \quad (3.25)$$

According to Figure 3.9, at the yield point, the pipe slip δ is equal to 3 mm. So, the longitudinal soil spring stiffness is

$$k_L = 10.46/3 = 3.487 \text{N/mm}^2 = 0.506 \text{ kips/in/in} \quad (3.26)$$

Based on the data above, the pipe slip corresponding to different lengths of pipe can be calculated by evaluating the equations in Appendix A and are shown in Table 3.2.

For the field example, the estimated length between the fixed end and the wrinkle location is 36.6 m (1440 in), and since an element length of 60 in is used in creating the ABP model, the total number of elements is 1440/60 = 24 and the total number of nodes is 49. Similarly, a different number of element and nodal numbers corresponding to different pipeline lengths for the ABP model can be obtained as shown in Table 3.2.

3.3.4. NUMERICAL ANALYSIS

3.3.4.1 Pipe End Displacement without Axial Force

After creating input files according to the data of Table 3.2 and analyzing by using the ABP program, the slip results are shown in the second last row of Table 3.2 where they are compared with those from the closed form differential equation solution in the last row as stated in Murray and Yoosef-Ghodsi (2001). Using the results in Table 3.2, the displacement vs. pipe length curves are plotted as shown in Figure 3.10 for $\tau_y = 0.009$ N/mm^2. Figure 3.10 indicates that the results from the differential equation approach and the ABP program show a very good agreement.

Also, according to Figure 3.9, it is known that the field test data for the soil-slip yield strength spans a range of approximately a factor of 4. If three other typical values for soil yield strength, namely, $\tau_y = 0.006$ N/mm^2, 0.012 N/mm^2 and

Table 3.2 End Displacements For Different Pipeline Lengths Under $\Delta T = 110^{o}F$ and $\tau_y = 0.009$ N/mm^2

Pipe length (m)		9.15	18.3	30.5	36.6	50.3	61.0	80.8	100.6	150.9	199.7	300.3
Yield strength(N/mm)		10.46	10.46	10.46	10.46	10.46	10.46	10.46	10.46	10.46	10.46	10.46
# of Element		12	24	30	24	33	40	53	66	99	131	197
# of Node		25	49	61	49	67	81	107	133	199	263	395
Pipe slip (mm)	ABP	6.1632	11.4706	17.2621	19.6083	23.5973	25.5132	26.9370	27.2095	27.238	27.238	27.238
	DESs	6.1649	11.4822	17.3004	19.6682	23.6962	25.6621	27.1758	27.4330	27.465	27.465	27.465

0.02 N/mm^2, and a corresponding pipe end slip of 3 mm are used, following the procedure above, the corresponding end displacement along the pipeline under different soil yield strengths can be obtained as shown in Table 3.3. Using the results in Table 3.3, the curves of end displacements vs. pipe anchorage length for the four different soil yield shear strengths under the conditions of: (1) zero internal pressure; (2) temperature increase of 110°F; and, (3) zero externally applied axial force (i.e. P = 0), are shown in Figure 3.11. It is indicated from Figure 3.11 that, for four different soil yield strengths, the comparison from the differential equation and the ABP program shows excellent agreement.

3.3.4.2 End Displacement with Axial Force

Considering the in-situ condition, if the end anchorages expand toward the free end (or wrinkle end), they will exert a compressive force that "squashes" the wrinkle segment. The wrinkle segment will resist this action and the axial force developed will suppress some of the slip movement occurring in the anchor section at the junction with the wrinkle segment. This effect must be assessed in order to get an estimate of the magnitude of the force and imposed displacement to which the wrinkle segment is subjected.

Since the temperature increase is $\Delta T = 110°F$, the uniform thermal stress for a straight pipe without slip will be

$$\sigma_{\Delta T} = -E\alpha\Delta T = -29.6\times6.5\times10^{-6}\times110 = -21.16 \text{ ksi} \quad (3.27)$$

Therefore, the axial force in the constrained pipeline arising from the uniform temperature differential of 110°F is

$$P_0=A\sigma_{\Delta T}=-(\pi/4)\times[12.75^2-(12.75-2\times0.203)^2]\times21.16=-169.3 \text{ kips}=-753 \text{ kN} \quad (3.28)$$

Table 3.3 End Displacements Under Different Soil Yield Strengths And Pipeline Lengths

Pipe length (m)		9.15	18.3	30.5	36.6	50.3	61.0	80.8	100.6	150.9	199.7	300.3
τ_y= 0.006 N/mm^2	ABP	6.2891	12.0056	18.7662	21.7775	27.6593	31.3807	36.3433	38.967	40.089	40.102	40.102
	DESs	6.2892	12.0117	18.7891	21.8129	27.7198	31.4858	36.5272	39.2283	40.4325	40.4325	40.432
τ_y= 0.009 N/mm^2	ABP	6.1632	11.4706	17.2621	19.6083	23.5973	25.5132	26.9370	27.2095	27.238	27.238	27.238
	DESs	6.1649	11.4822	17.3004	19.6682	23.6962	25.6621	27.1758	27.4330	27.465	27.465	27.465
τ_y= 0.012 N/mm^2	ABP	6.0388	10.9431	15.7900	17.5111	19.8284	20.5058	20.7705	20.7986	20.800	20.800	20.800
	DESs	6.0421	10.9594	15.8408	17.5819	19.9480	20.6646	20.9495	20.972	20.972	20.972	20.972
τ_y= 0.02 N/mm^2	ABP	5.7173	9.5880	12.222	12.7293	13.045	13.0762	13.0820	13.082	13.082	13.082	13.082
	DESs	5.7233	9.6163	12.2923	12.8154	13.1450	13.1781	13.1843	13.184	13.184	13.184	13.184

Using the ABP program and applying different axial forces as concentrated end nodal forces, the end displacement for two different embedded anchor lengths of pipe (36.6 m and 100 m) under varying axial force and 110°F temperature increase are shown in Table 3.4.

Table 3.4 End Displacements Under Different Axial Forces For Two Pipeline lengths

Axial Force (kN)		753	600	550	500	400	300	200	100	0.0
Displ.(mm) L=36.6 m	ABP	0.00	2.453	3.263	4.219	6.658	9.601	12.83	16.19	19.61
	DESs	0.00	2.58	3.362	4.339	6.791	9.732	12.94	16.28	19.67
Displ.(mm) L=100 m	ABP	0.00	2.527	3.373	4.408	7.157	10.82	15.38	20.83	27.21
	DESs	0.00	2.649	3.480	4.536	7.323	11.01	15.59	21.07	27.43

Plotting the data in Table 3.4, the four curves of end displacement for the two lengths of pipe under varying axial force, and 110°F temperature increase, are shown in Figure 3.12. It is apparent that there is close agreement between the DESs and ABP solutions.

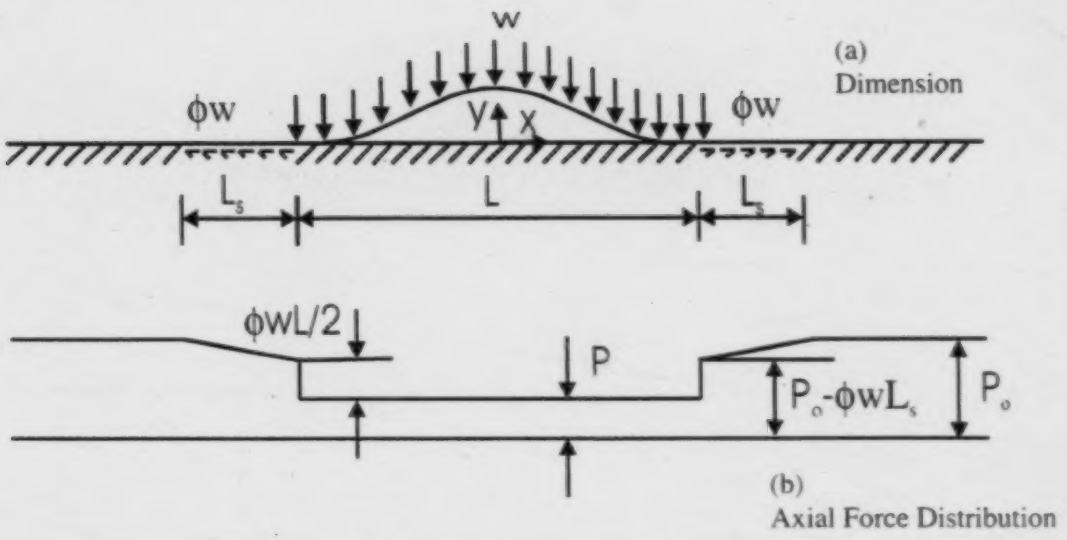

Figure 3.1 Details of Pipe Upheaval Buckling Mode

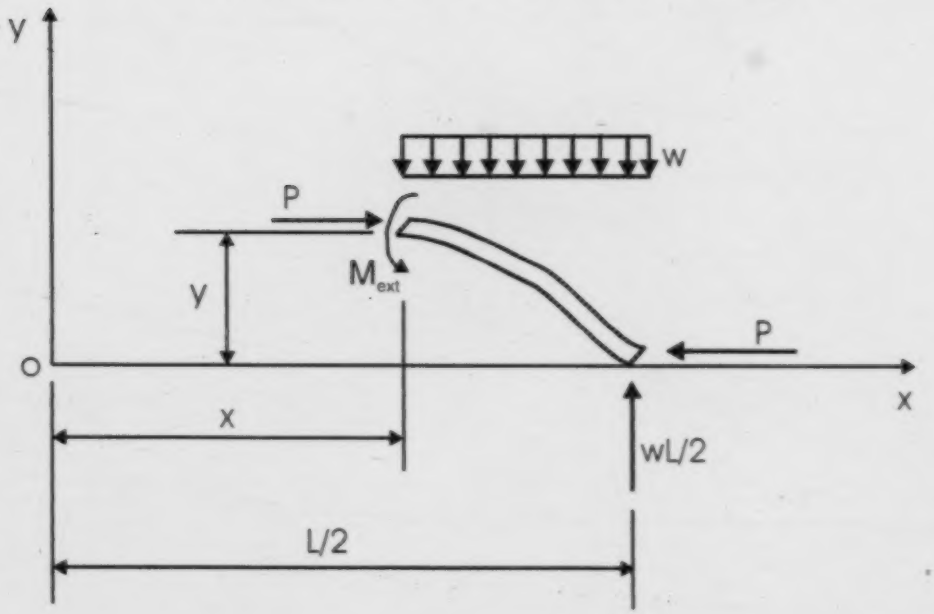

Figure 3.2 Free-body Diagram for Pipe Segment at Buckled Part

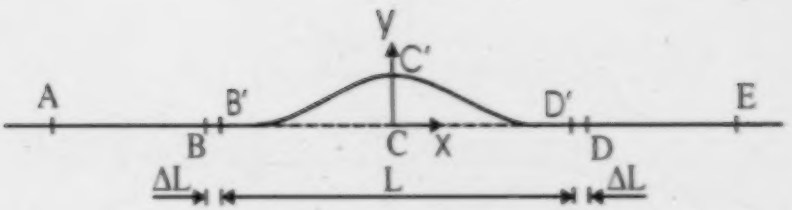

Figure 3.3 Compatibility Condition for Buckled Length of Pipeline

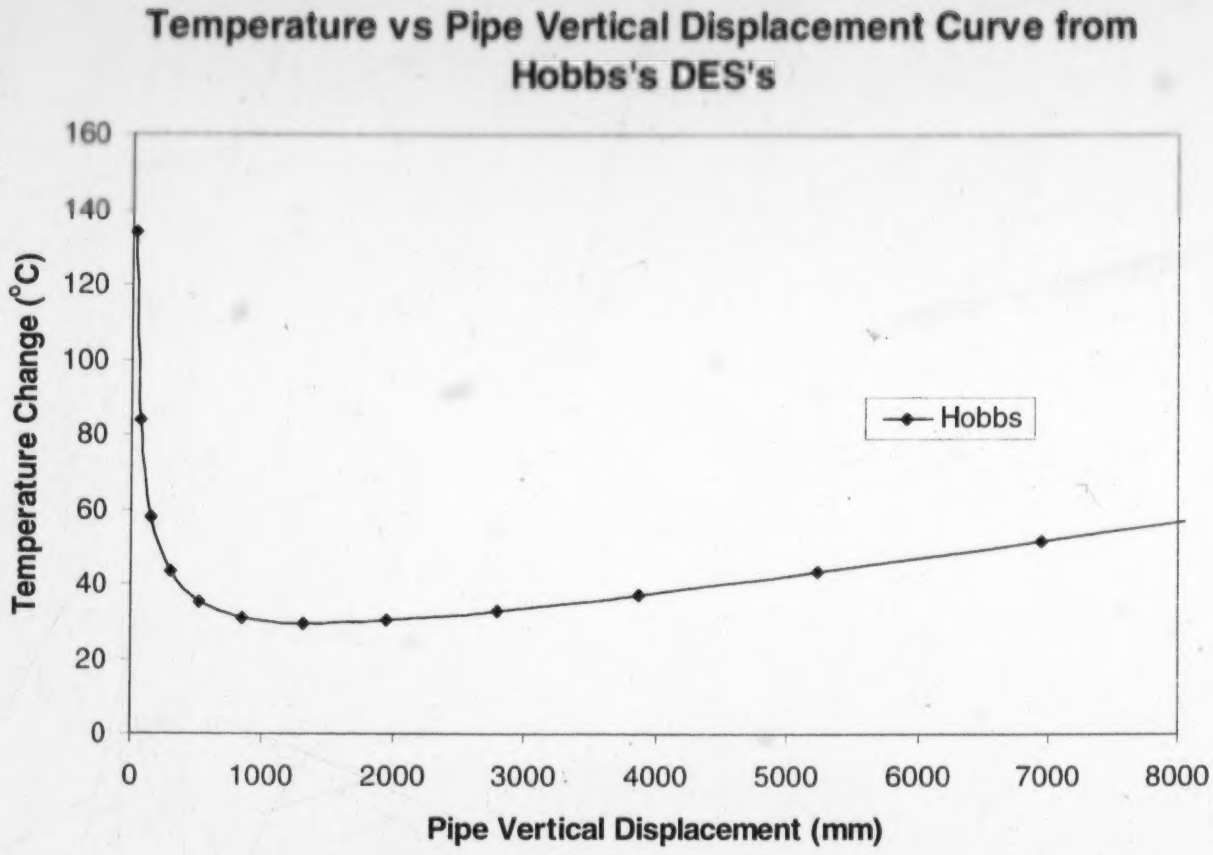

Figure 3.4 Temperature Change vs. Pipe Vertical Displacement Curve from DESs

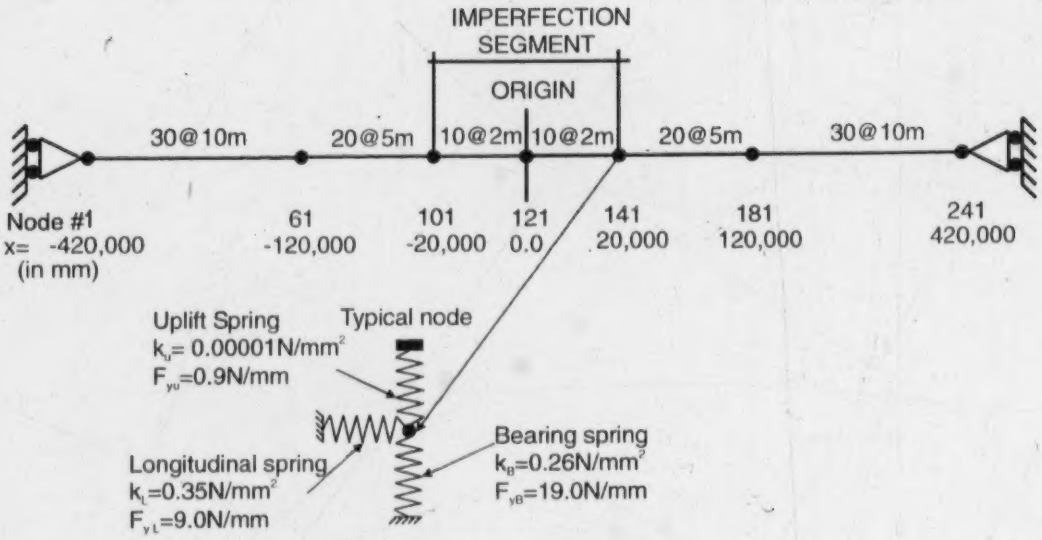

Figure 3.5 Schematic Model Used in ABP Program

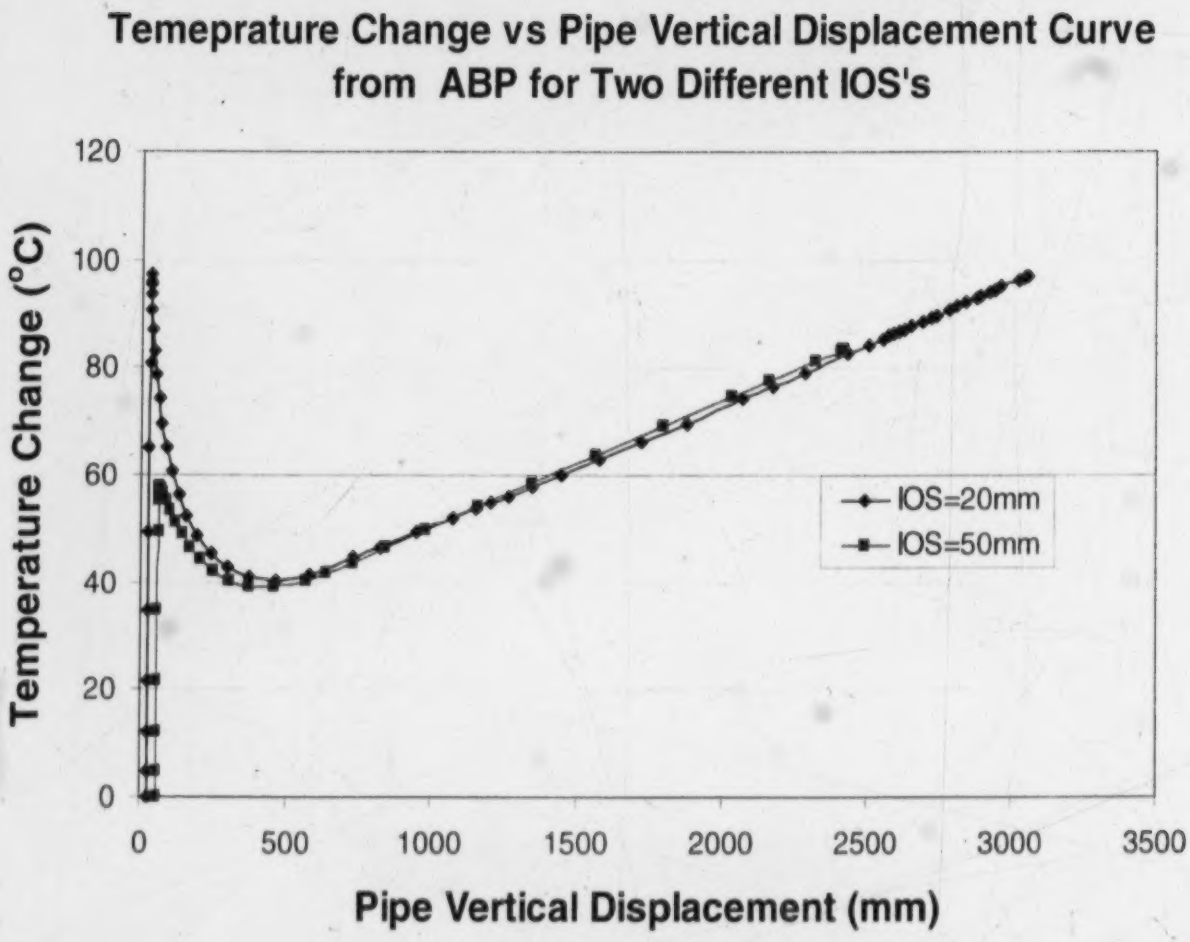

Figure 3.6 Temperature Change vs. Pipe Displacement Curve from the ABP Program for Two Different IOS's

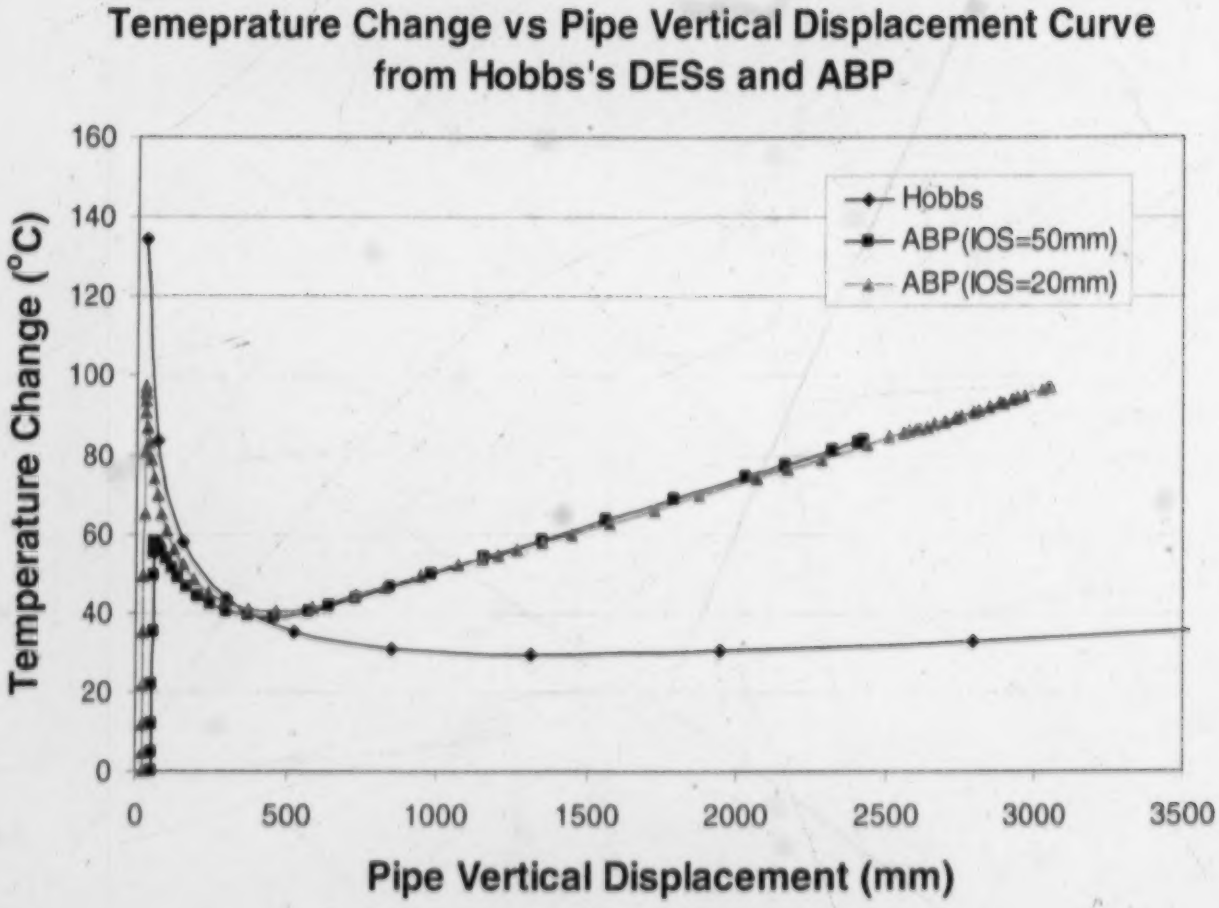

Figure 3.7 Comparison of Temperature Change vs. Pipe Vertical Displacement Curve from ABP and DESs

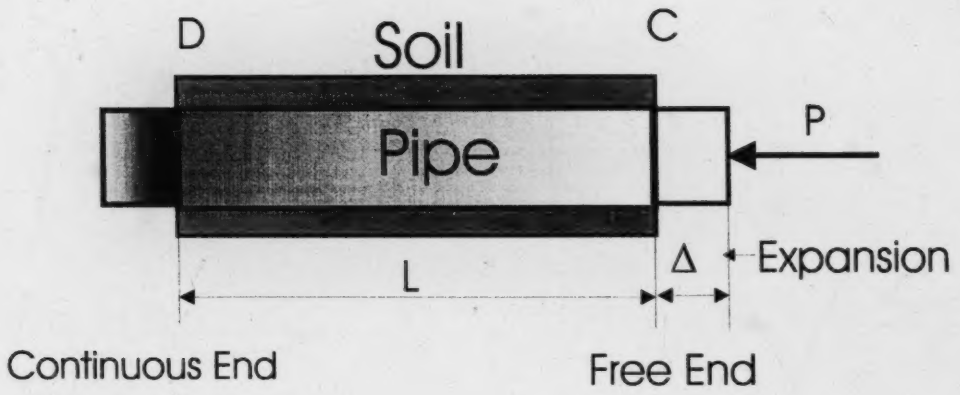

Figure 3.8 Schematic of Pipe Segment Embedded in Soil

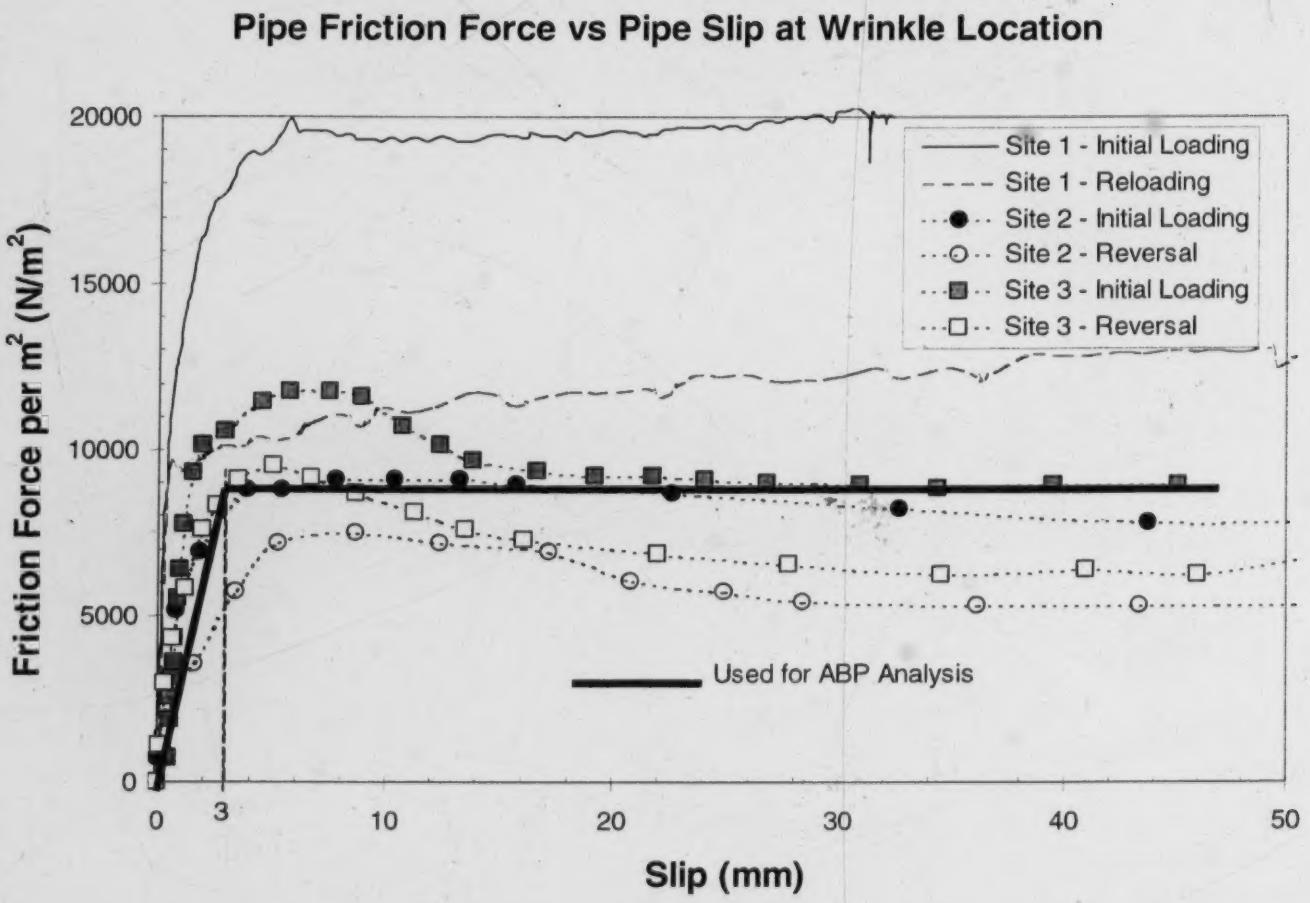

Figure 3.9 Field Measurements of Pipe Friction Force vs. Pipe Slip

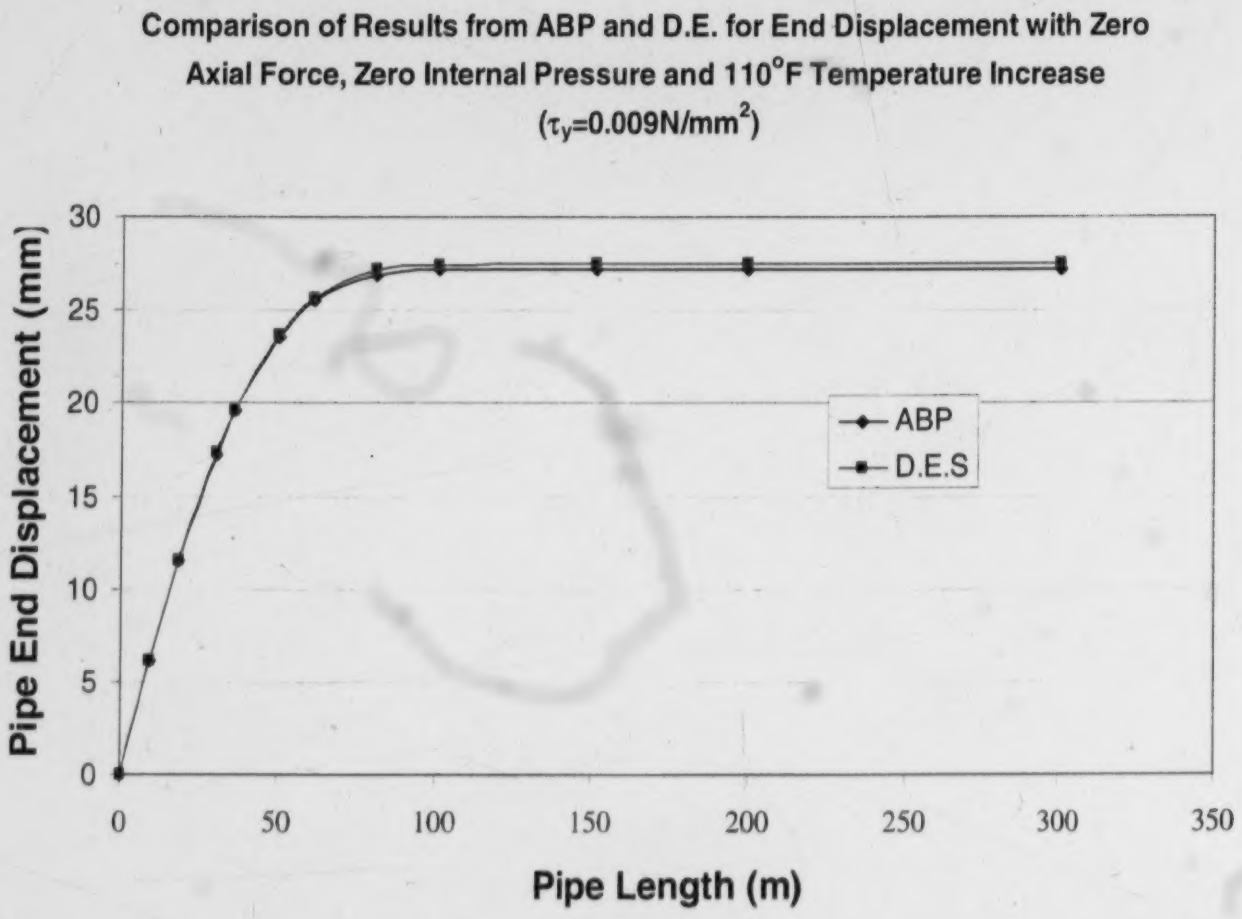

Figure 3.10 Characteristics of End Displacement vs. Pipe Length Curve from ABP and DESs

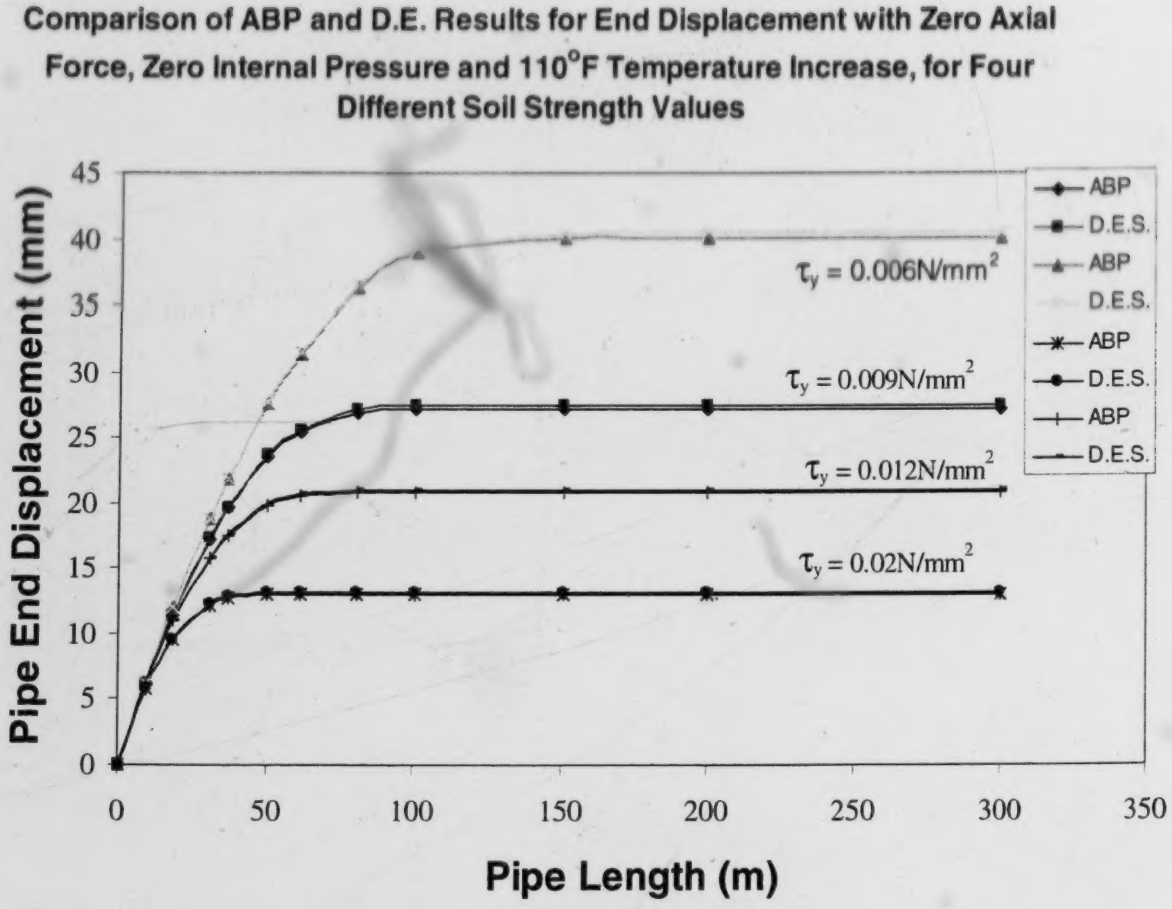

Figure 3.11 Pipe End Displacement vs. Pipe length Curves from ABP and DESs

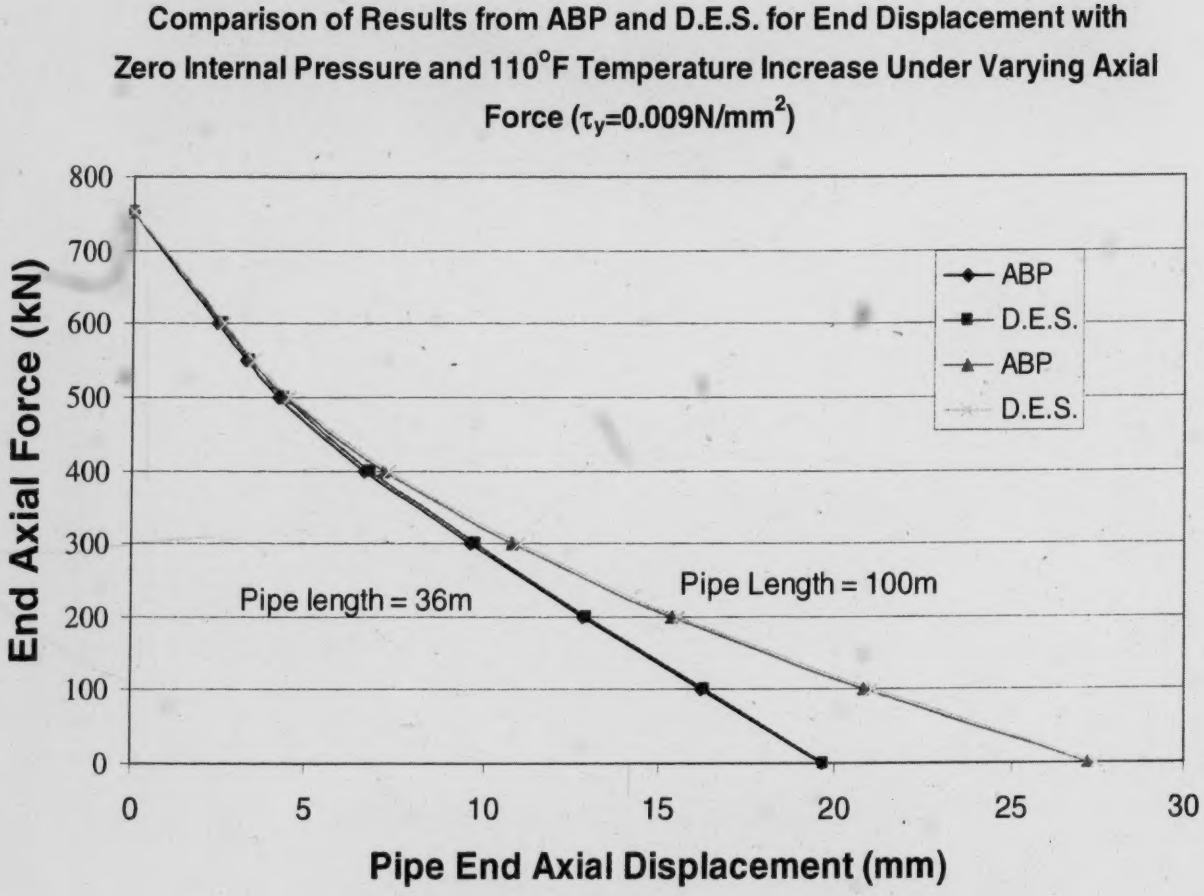

Figure 3.12 Effect of Axial Force on Pipe End Displacement from ABP and DESs

CHAPTER 4 CASE HISTORY OF WASCANA GOLD CREEK LINE AND NUMERICAL SIMULATIONS

4.1 GENERAL

As the core part of this project, field pipeline failures that occurred in the Wascana Gold Creek NPS-8 Pipeline were studied. This chapter presents the details of the study.

4.2. INTRODUCTION

The Wascana Energy Ltd. Company's NPS-8 Gold Creek Pipeline, which was constructed at the end of 1996 and put into operation on February 28, 1997, carried sour natural gas from the 10-34 facility to Petro-Canada's gas plant. This pipeline is located south of Grande Prairie, Alberta and its total length is 25.4 km. In April 1997, a leak was detected 650 m south of the 10-34 facility. A fracture of the pipe was discovered at the crest of a wrinkle in the line.

From June 18 to 20, 1997, a GEOPIG was run for the whole length of the pipeline by BJ Pipeline Inspection Services and ten upheaval sites with bending strain greater than 0.3% were found. There are two line-heaters along the pipeline, one at 10-34 and one at 7-20. The facility at 7-20 is located 15.2 km south of 10-34. The computed thermal profile along the NPS-8 Pipeline is shown in Figure 4.1 based on the data provided by Nixon Geotech Ltd., who did the thermal profile analyses (Dyck, 1998). All pipeline upheavals occurred within 7 km from a heat source, i.e., within 7 km of the facility at 10-34 or within 7 km of the facility at 7-20.

In July of 2002, the present studies were initiated to analyze the upheaval phenomena and rupture that occured in this pipeline. This chapter describes the numerical analyses done in the University of Alberta using the ABP program developed in the University of Alberta (Yoosef-Ghodsi and Murray, 2002). It also

describes analyses carried out with the commercial finite element package ABAQUS Version 6.2 (Hibbit et al., 2000). These analyses are based on the data documented by Dyck (1998) and BJ Pipeline Inspection Services, who carried out the GEOPIG run, and by Thurber Engineering Ltd., who did the field soil tests (Dyck, 1998).

4.3. DATA FOR THE PIPE AND THE SOIL

4.3.1 Data for the Pipe

The specifications of the NPS-8 Gold Creek Pipeline are as follows: outside diameter OD = 8.625 in (219.1 mm); pipe wall thickness t = 0.22 in (5.58 mm); steel grade= API X-52 (SMYS =359MPa) with 1in thick layer of insulation.

There is no coupon test data available for the stress-strain curve of the pipe steel. A hypothetical true stress-true strain curve is adopted for analytical purposes. The data points for this material are listed below and are plotted in Figure 4.2 (Mohareb et al., 1994).

stress (MPa)	strain (mm/mm)
0.0	0.0
289.0	0.00141
319.0	0.00242
349.0	0.00407
379.0	0.00783
409.0	0.01609
439.0	0.03341
469.0	0.06809

4.3.2 Data for the Soil

The soil data was provided by Thurber Engineering Ltd. (Dyck, 1998). According to the report, there are several muskeg zones along the NPS-8 Gold Creek pipeline as shown in Figure 4.3. Thurber Engineering Ltd. also measured the

length and the depth of the muskeg zones (Dyck, 1998). Combining the reports by BJ Pipeline Inspection Services and Thurber Engineering Ltd., it can be seen that most of the pipeline upheavals are located in the transition zone near the end of muskeg zones. The pipe rupture site and one of the upheaval sites with a local wrinkle, identified in Dyck (1998) as site #4 (see Figure 4.1), are located adjacent to road crossings. The short length of very stiff soil at these road crossings prevented the pipe from bending into a smooth curve as it expanded in the weak muskeg zone. It should be also noted that, at the rupture site (650 m south of the 10-34 facility), the pipeline was installed with a vertical curvature in order to rise to a high elevation as it passed through the road. This pipe profile will be shown subsequently.

Thurber Engineering Ltd. did a series of tests regarding the strength of the soil along the pipeline. Based on their data for the muskeg and adjacent clay, the following approximate characteristic soil data has been derived by Thurber Engineering Ltd. (Crawford, 1997) and is used in our numerical analyses.

– the longitudinal soil spring strength F_{yL} = 155 lbs/ft (2.307 N/mm), and the longitudinal soil stiffness k_L = 0.045 N/mm/mm.

– the uplift soil spring strength (above the pipe) F_{yu} = 250 lbs/ft (3.717 N/mm), and the vertical soil stiffness k_u = 0.0122 N/mm/mm.

It should be noted that the data used in the numerical analysis by the ABP program has been adjusted within the range of measured values at different upheaval sites as specified in association with the specific subsequent examples. Also, in order to simulate the soil response during the pipe upward movement, a soil resistance vs. pipe uplift displacement curve is used instead of a constant value in the upheaval buckling analysis. In addition, reasonably large values for the soil properties for the base spring beneath the pipe are used in order to make sure that the pipe will move upward if it buckles.

4.3.3 Pipeline Operational Condition

Although there are several cases of operational conditions listed in Dyck (1998), the most critical one with the maximum flow conditions is analyzed, and it is applicable during the early operation of the pipeline. The operational condition is: gas flowrate of 10 MMSCFD (million standard cubic feet per day) with condensate of 50 bbl/MMSCFD and water of 35 bbl/MMSCFD, with temperature of 80°C maximum at the outlet of the 10-34 facility and the outlet of 7-20 heater facility. The internal pressure p_i = 1350 psi (9.308 MPa).

Since the pipeline was constructed during winter time, this effect should be considered in the temperature calculation for the numerical analysis. According to Dyck (1998), the pipeline was installed during the period of December 1996 to February 1997. Although the air temperature was much colder, the trench was not left open over night and the temperature in the pipeline trench was believed to be near zero degrees centigrade. Thus, the installation temperature of the pipeline was probably between 0°C and −15°C. Consequently, the maximum temperature differential for the most critical condition, i.e., operational condition above, would range from 80°C to 95°C.

4.3.4 Pipe Imperfection Length and Imperfection Magnitude for Pipe Upheaval Buckling Analysis

A cosine shape global imperfection of the ABP pipe model is used in order to encourage an upheaval buckle in the line. The imperfection length is adopted as the length measured from the plot of the GEOPIG run by the BJ Pipeline Inspection Services. In order to check the effect of the imperfection magnitude on the pipe buckling behavior, a series of global pipe imperfection magnitudes is used in the upheaval buckling analysis as will be shown subsequently.

The numerical upheaval buckling analyses are carried out for the typical upheaval sites #4 and #5 of Figures 4.1 and 4.3, both of which are sites at which local wrinkles formed in the crest of the upheaval buckles.

4.3.5 Local Wrinkle Analysis for the Critical Segment

As the ABP program can only process the global behavior of the pipeline, in order to capture the local behavior of the pipe at the critical segment, an ABAQUS finite element analysis is used to predict the wrinkle.

In order to trigger the wrinkle local buckle in the FEA model, a perturbation of geometry is introduced at the center of the pipe model segment. The shape of the pipe in this area is modified so that the radius of the pipe is increased to.

$$r = r_0 + 0.5 \times a\,[1 + \cos(\pi x / L_{imp})] \qquad (4.1)$$

in which r_0 is the radius of the "perfect pipe", "a" is the magnitude of the imperfection and "L_{imp}" is half of the length of the local imperfection. The mesh and the boundary conditions for the FEA model used in ABAQUS are shown in Figure 4.4. A 6D long pipe segment is usually used as the FEA model. The length of the model is selected such that the end effects can be avoided.

4.4. Numerical Analysis For Site #4

4.4.1 Numerical Upheaval Analysis for Site #4

This site is located at 1616.4 m south of 10-34 facility (see Figure 4.1). The post-buckling GEOPIG plot for this site is shown in Figure 4.5. As shown in Figure 4.5, the pipeline deformed with an upheaval length of 15 m and height of about 1050 mm. Also according to the report by Thurber Engineering Ltd., this upheaval is adjacent to a road crossing.

Based on the post-buckling GEOPIG pipe geometry of Figure 4.5 and the soil data of Section 4.3.2, the "anchor length" is computed in order to determine the length of the pipe model used in the ABP program. The anchor length means, that beyond this length the pipe will not slip (displace) any more. The calculation of the anchor length is shown in Appendix A by using Equations A10 and A11. The calculation of the anchor length is an iterative procedure. By iteration, one can find

the root (x_1) of Equation A10. Substituting x_1 into Equation A11, one can obtain the u(L), slip values. When the u(L) value reaches a constant, the corresponding x_1 value is the anchor length. The calculated anchor length is about 400m. Consequently, a total length of 425 m is modeled. This upheaval model is composed of 129 nodes and 64 elements with imperfection spanning a 15 m length as shown in Figure 4.6. This numerical model is asymmetric in that it has 400 m long Straight Segment (SS) on one side of the imperfection section and 10m long SS on the other side.

The 10 m long SS is used to simulate the road crossing section. Two vertical rollers as shown in Figure 4.6 are used at the ends as the boundary conditions in order to provide displacement restraint in the X direction. One feature of the ABP program is that different soil properties can be applied to different elements. This feature is used here as totally different soil properties exist on the two sides of the pipe upheaval location. Soil data from Thurber Engineering Ltd. is applied to the 400 m long straight segment on the left of the origin with nodes from 1 to 101 and the 15 m long imperfection section with nodes from 101 to 119 as these pipe segments are located inside the muskeg zone as shown in Figure 4.3.

The soil resistance vs. pipe uplift displacement curve used for the ABP program is shown in Figure 4.7. Greater soil stiffness and strength are applied to the 10 m long straight segment from node 119 to 129 to simulate the road crossing segment (see Figure 4.6). The uplift soil spring properties used for the road are: F_{yu} = 440.6 N/mm and the stiffness k_u = 1.4 N/mm/mm. Thermal profile analyses along the NPS-8 pipeline based on the operational condition were computed by Nixon Geotech Ltd. (Dyck, 1998) and are shown in Figure 4.1. According to the analyses based on the operational condition in Section 4.3.3, the maximum temperature of the pipe at this site is 72.7°C. Considering the construction condition as stated in Section 4.3.3, the maximum temperature differentials at this site should be around 72.7+15 = 87°C. This value is assumed in the following numerical analysis.

The analytical results for arbitrary temperature increases vs. pipe vertical displacement curves for different Initial Out-of Straightness (IOS), as predicted by the ABP program analyses are shown in Figure 4.8. The pipeline upheaval configuration corresponding to temperature increase of 84.4°C is shown in Figure 4.9. Figure 4.10 shows the same pipe configuration plotted to a smaller scale. The GEOPIG plot with a smaller scale is shown in Figure 4.11. Figure 4.12 shows the comparison between the GEOPIG plot and the numerical results from ABP upheaval analysis. This comparison is considered to be excellent considering the possible variations in the parameter that are required for analysis.

4.4.2 Numerical Wrinkling Analysis for Site #4

A 6D long pipe segment at the peak location of the upheaval is extracted to do the local wrinkle analysis. The length of the FE wrinkling model is selected such that its end effects can be avoided. Creating a finite element model for ABAQUS and imposing the displacement data directly from the analytical results of the ABP program, the deformed shape of the pipe critical segment is shown in Figure 4.13. The data used in the numerical analysis by ABAQUS is taken directly from the ABP output at the critical segment. It is indicated from Figure 4.13 that a local wrinkle has been created with a height of 9.2 mm and is surprising close to the wrinkle magnitude as shown in Figure 4.11. The formation of the local wrinkle apparent in Figure 4.13 indicates that the segment has passed through its limit point on its moment-rotation curve.

4.5 Numerical Analyses for Site #5

4.5.1 Numerical Upheaval Analysis for Site #5

This site is located at 903.6 m south of 10-34 facility as shown in Figures 4.1 and 4.3. The GEOPIG plot for this site is shown in Figure 4.14. It is shown from Figure 4.14 that the pipeline deformed with an upheaval length of 12 m and height of about 690 mm. Also, from the report by Dyck (1998), this upheaval is located inside the muskeg zone as shown in Figure 4.3.

The anchor length is computed based on the equations A10 and A11 in Appendix A, the same procedure as that for site #4. A total length of 812 m long pipe segment is modeled for the ABP program with a 12m long imperfection section in the midspan and 400 m SS at each side of the imperfection section. A schematic of the pipeline model in this location is shown in Figure 4.15. A parametric study of solutions for several imperfection heights is shown in Figure 4.17. The pipe model is composed of 213 nodes and 106 elements. The soil data for soil spring properties at this upheaval location were adjusted within the range of measured values in order to get a higher post-buckling temperature.

The data for the longitudinal soil spring used here is F_{yL} = 4.50665 N/mm and k_L = 0.5545 N/mm/mm. The soil resistance vs. pipe uplift displacement curve used in this location is shown in Figure 4.16. According to the thermal profile analyses by Nixon Geotech Ltd. (Dyck, 1998) and the operational condition in Section 4.3.3, the maximum temperatures of the pipe at this site is 75.6°C. Considering the construction condition as stated in Section 4.3.3, the maximum temperature differentials at this site should be around 75.6+15 = 90°C. This value for the pipe temperature is assumed in the following numerical analysis.

Using the data stated above, the analytical results for the temperature vs. pipe vertical displacement curves for different IOS by using the ABP program are shown in Figure 4.17. The pipe segment deformed configuration corresponding to a temperature increase of 90°C is shown in Figure 4.18. Figure 4.19 is the plot of Figure 4.18 at a smaller scale. The GEOPIG plot for this site with a larger scale is shown in Figure 4.20. Figure 4.21 shows the comparison between the GEOPIG plot and the numerical results from the ABP program. They exhibit what is considered to be good agreement.

4.5.2 Numerical Wrinkling Analysis for Site #5

A 6D long pipe segment at the peak location of the upheaval is picked to do the local wrinkle analysis. Creating a finite element model for ABAQUS and

imposing the data directly from the analytical results of the ABP program, the deformed shape of the pipe critical segment is shown in Figure 4.22. It is indicated from Figure 4.22 that a compatible local wrinkle has been created with a height of 18.1 mm and is surprisingly close to the wrinkle magnitude as shown in Figure 4.14.

4.6 Numerical Analyses for the Fracture Site

4.6.1 Numerical Analysis for Pipe Slip at Fracture site

The third site to be analyzed for wrinkling is the "fracture site". The fracture site (or rupture site) is located 650 m south of the 10-34 facility (see Figures 4.1 and 4.3). The post-buckling measured deformed configuration of this segment is shown in Figure 4.23 (BJ Pipeline Inspection Service (Dyck, 1998)). The pipe rises up about 4 m through 2 manufactured bends as it passes beneath the road crossing. The fracture location is just beside the bend at the lower elevation immediately to the left of the elevated pipe section. According to the report by the BJ Pipeline Inspection Services (Dyck, 1998), the lower elevation of the pipeline is located inside the muskeg zone (see Figure 4.3). It is apparent that when the pipeline is heated up, a compressive force due to the temperature increase is induced in the pipeline. The pipeline has a tendency to expand toward the road crossing site because of its anchorage at the 10-34 facility and the small resistance of the muskeg. But the stiff soil in the road crossing and the two curved bends at the road crossing restrain the expansion of the pipe. As a result the pipe behaves like a beam-column under a compressive force due to the thermal load and a lateral load due to the pipe self-weight. It is believed that the pipe segment underwent bending behavior first, and then the pipe slipped into the weakest point along the pipe segment, namely, the wrinkle location. A localized wrinkle was created in the pipe segment under the combined load condition. It can be seen from Figure 4.23 that there is no upheaval buckling behavior involved in this location, pipe-soil slip mechanism is decided to use for this location to do the numerical analysis.

Assuming there is no soil movement, the maximum compressive axial load, P_0', that the pipeline can develop from thermal action is the force due to the temperature reduced by the Poisson's ratio effect based on the internal pressure.

$$P_0' = (E\alpha\Delta T - \mu\sigma_\theta)A = (200000 \times 11.7 \times 10^{-6} \times 95 - 0.3 \times 173) \times 3748 = 660\text{kN} \quad (4.2)$$

When the pipe tries to slip, the surrounding soil will try to hold the pipe to its original position because of the development of a frictional force between the pipe and the soil. Referring to Murray and Yoosef-Ghodsi (2001), the pipe-soil slip mechanism is discussed below.

For a straight undamaged buried pipe, thermal expansion as a result of temperature change will not occur because the constraint of the soil and adjacent pipe sections will not permit its length to change. A wrinkle is, however, a location at which the pipe cannot sustain the pre-wrinkling stress. As a result, the pipe yields and buckles. This process allows adjacent pipe to slide into the wrinkle location. Consequently, if a wrinkle forms, the pipe moves relative to the soil in the vicinity of the wrinkle (i.e., the pipe slips in the soil). Referring to Figure A1a in Appendix A, it is assumed that End C is a free end at which the wrinkle forms and End D is the 'soil anchor point' in the sense that any point to the left of D will not move. The force P is exerted by the adjacent components of pipe segments during the expansion of the free end. This force will suppress some of the pipe slip movement. Appendix A has anticipated this need by including the effect of the interactive end axial force P in the derivations. Consequently, the effect of the end axial force on the pipe slip can be evaluated.

Based on the equations in Appendix A, for a pipe with a free end, the curves of end axial displacement vs. pipe segment length are shown in Figure 4.24 for three different temperatures. The curves of axial load at the free end vs. axial end displacement are shown in Figure 4.25.

4.6.2 Numerical Analysis for Pipe Wrinkling at Fracture Site

Figure 4.25 shows the axial force vs. pipe slip curve for the anchor length segment. For geometric compatibility, the expansion of the anchor length should be the same as the relative shortening that occurs between the ends of the wrinkle in the ABAQUS FEA model, because the FEA model represents the critical segment (at free end). The imposed expansion displacement between the ends of the FEA model is considered to be the driving force for developing the changes in the FEA model geometry. The geometric compatibility conditions described above are shown in Figure 4.26.

A 6D long pipe segment from the critical wrinkle location is extracted to do the numerical analysis by using the finite element method. The pipe segment is initially assumed straight. The loading sequence applied to the segment is: (1) apply the internal pressure, (2) bend the pipe and (3) move the end. Different rotation values are assumed to check the axial capacity of the pipe segment after initial bending. The axial load vs. axial displacement curves for the pipe segment with different initial rotation values are shown in Figure 4.27.

Figure 4.27 displays a series of characteristic wrinkle response curves in which the resisting force of the wrinkle segment passes through a limit point at its peak resistance, and then loses its resisting capacity as the wrinkle develops. On the other hand, Figure 4.25 shows the variation of the end forces delivered by the anchor length as the pipe expands due to the temperature change. Recognizing that, according to Figure A1, the end forces in Figure 4.25 are equal and opposite to the end forces forming the wrinkle in Figure 4.27, one can combine the two sets of plots, to solve for the force level at which the wrinkle segment displacement is compatible with the anchor length expansions.

The superimposed load vs. pipe deformation curves, one from the Closed Form Solution in Appendix A and the other from the numerical results by ABAQUS, are shown in Figure 4.28. As shown in Figure 4.28, only the

combination of the highest temperature expansion and the greatest initial rotation FE solution have an intersection point beyond the limit point for the wrinkle segment. The intersection point of the two plots from the two different types of action shown in Figure 4.29 gives the compatible equilibrium point for the wrinkled configuration. The pipe deformed shape, corresponding to the intersection point in the Figure 4.29, is shown in Figure 4.30. A local wrinkle with a height of 31.76 mm has been created. Figure 4.31 shows the blowup of the local wrinkle from ABAQUS and the picture taken for the field fracture. The surprisingly similar shapes from the field dig of the pipeline and the numerical analytical results indicate a good agreement between them.

4.7 Numerical Analysis for Fracture Model

A structural engineering report about the fracture of pipelines by Das et al. (2002) in the University of Alberta deals with cyclic fracture in wrinkled pipe. According to Das et al. (2002), pipe test specimens are highly ductile and do not fail in fracture when they are subjected to monotonically increasing axisymmetric compressive strain. But if the pipe is subjected to strain reversals because of loading and unloading of primary loads, the fracture can occur in the wrinkle region in a few cycles, due to low cycle fatigue. It is believed that operational procedures produced thermal cyclic loads of the Gold Creek Pipeline due to shut down and reheating in the Gold Creek NPS-8 Pipeline. Consequently, cyclic loading analysis using the finite element package ABAQUS was carried out after the analysis of wrinkle formation described in Section 4.6.

It is assumed that when the NPS-8 Pipeline was shut down, the temperature of the pipeline dropped to 0°C. Consequently, the maximum axial force induced in the pipeline, due to the temperature change and the internal pressure is

$$P_0' = (E\alpha\Delta T - \mu\sigma_\theta)A = (200000 \times 11.7 \times 10^{-6} \times 80 - 0.3 \times 173) \times 3748 = 625\text{kN} \quad (4.3)$$

It is also assumed that the soil response to the pipe movement during the unloading period is the same as that of during the loading period. Based on the assumption above, the numerical analysis for the cyclic loading condition has been carried out by using the finite element package ABAQUS. The unloading point starts from the intersection point in Figure 4.29. Considering that the wrinkle can not recover completely due to the plastic deformation, two unloading displacements are used (i.e., 10 mm and 20 mm), to check the capacity of the pipe and to compare the number of cycles to fracture the pipe segment under different strain reversal.

The loading sequence used in the cyclic loading analysis is: (1) apply the internal pressure, (2) bend the pipe, (3) move the end (compressive direction) for about 30 mm, (4) move the end in the opposite direction (tensile direction, i.e., unloading starts) for about 10 mm, (5) move the end at the compressive direction again, until reaching 30 mm axial movement. The axial load vs. axial displacement curve for the cyclic loading analysis defined above for one cycle of cyclic loading is shown in Figure 4.32. In order to check the capacity of the pipe under cyclic loading for an unloading condition with 20 mm displacement, the axial load vs. axial displacement curve for this cycle of loading analysis is shown in Figure 4.33.

Based on the strip test results and energy absorption behavior of the test specimens, Das et al. (2002) developed equations to predict the residual life of the wrinkled pipe as shown in Appendix B. Based on these equations in Appendix B, the number of cycles to cause the fracture is estimated. This is also a good opportunity to verify the capability of the equations by applying them to the field problem.

The computation of the number of the cycles for 10 mm unloading displacement goes as follows. From the ABAQUS Viewer, the pipe deformed configurations at the maximum tension and compression can be obtained as shown in Figures 4.34 and 4.35. Also, the corresponding coordinates of the nodes on the crest (point B) and at the foot (points A and C) of the wrinkle, for these two

configurations, can be read as shown in Table 4.1. Based on the data in Table 4.1, the values of θ and 'd', as shown in Figures 4.34 and 4.35, can be calculated.

Table 4.1 Nodal Coordinates at Crest and Foot of the Wrinkle for Two configurations

Configuration	Node Position	X Coordinate	Y Coordinate
Maximum Tension	Crest (B)	−20	45.5366
	Foot (A)	33	15.5593
Maximum Compression	Crest (B)	−25	36.2759
	Foot (A)	24.3716	1.6192

It should be noted that the value of $0.8D_c$ for 'a', the distance from the extreme compression edge of pipe cross section to the NA, is used in the calculations in which D_c = 219.1 mm. In addition, the value for 'L_t', the distance between the foot of the wrinkle and the nearest end point of a bending pipe specimen (see Figure B4) is 559 mm, which is from the ABAQUS FEA model. Consequently, the values of θ_a can be obtained for the two configurations by Equation B15 and the values of $(\phi)_r$ can be obtained by Equation B10. As β is the maximum angle change at each foot due to the applied end rotations and the end rotations can be obtained from the ABAQUS, the value of β can be obtained. The plastic section modulus, Z, is calculated by Equation B9 as the pipe wall thickness, t, is known. By Equation B8, the ultimate moment capacity, M_u, is computed based on σ_u = 359 MPa. The energy due to rotation part can be calculated by using Equations B17 and B18.

For the calculation of the energy due to the axial movement, the values of φ can be computed by using Equation B10 as the values of θ has already obtained. Consequently, the energy due to axial movement can be calculated by using Equations B6 and B7 and the total energy U_0 can be computed thereafter. The calculated numbers of cycles, by using Equation B4 in Appendix B, to fracture the

pipe is 35 for 10 mm unloading displacements. Exactly the same procedure applied to 20 mm unloading displacement, the calculated numbers of cycles, to fracture the pipe is 3.

According to Dyck (1998), the fracture was detected about 6 weeks after the pipeline was put into service. If the shut down frequency were once per day, the total cycles to fracture is around 40. If the shut down frequency were once per week, the total cycles to fracture is 6. As indicated from above assumption that reasonable agreement is obtained with the prediction.

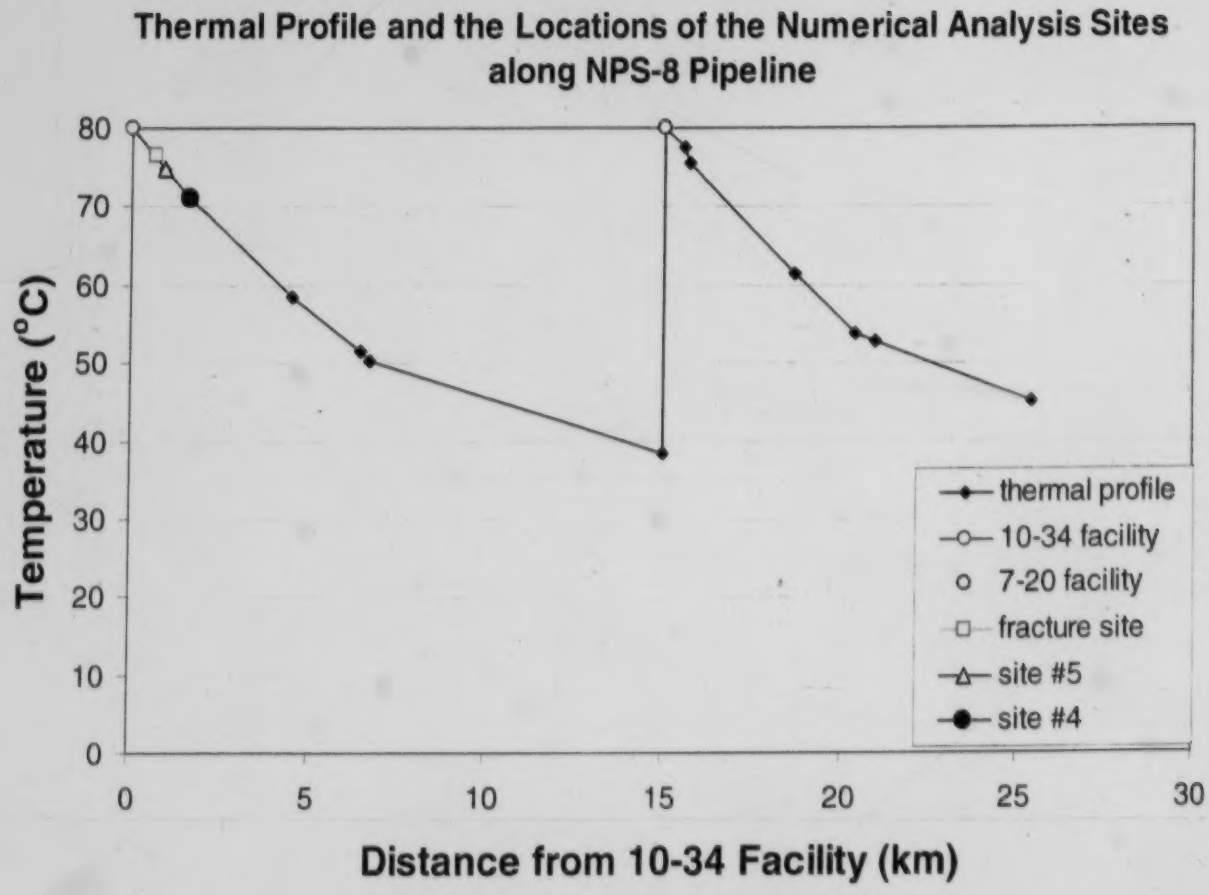

Figure 4.1 Thermal Profile along Gold Creek NPS-8 Pipeline

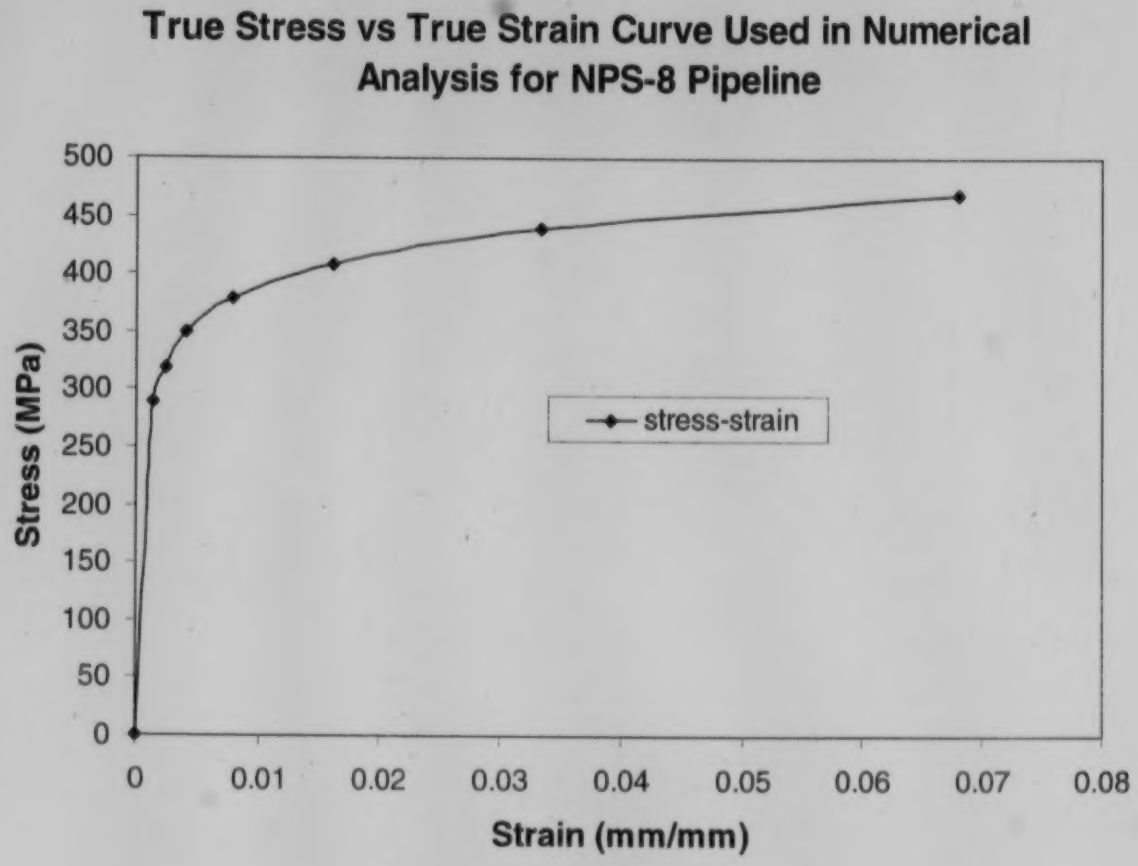

Figure 4.2 True Stress vs. True Strain Curve Used for NPS-8 Pipeline Steel

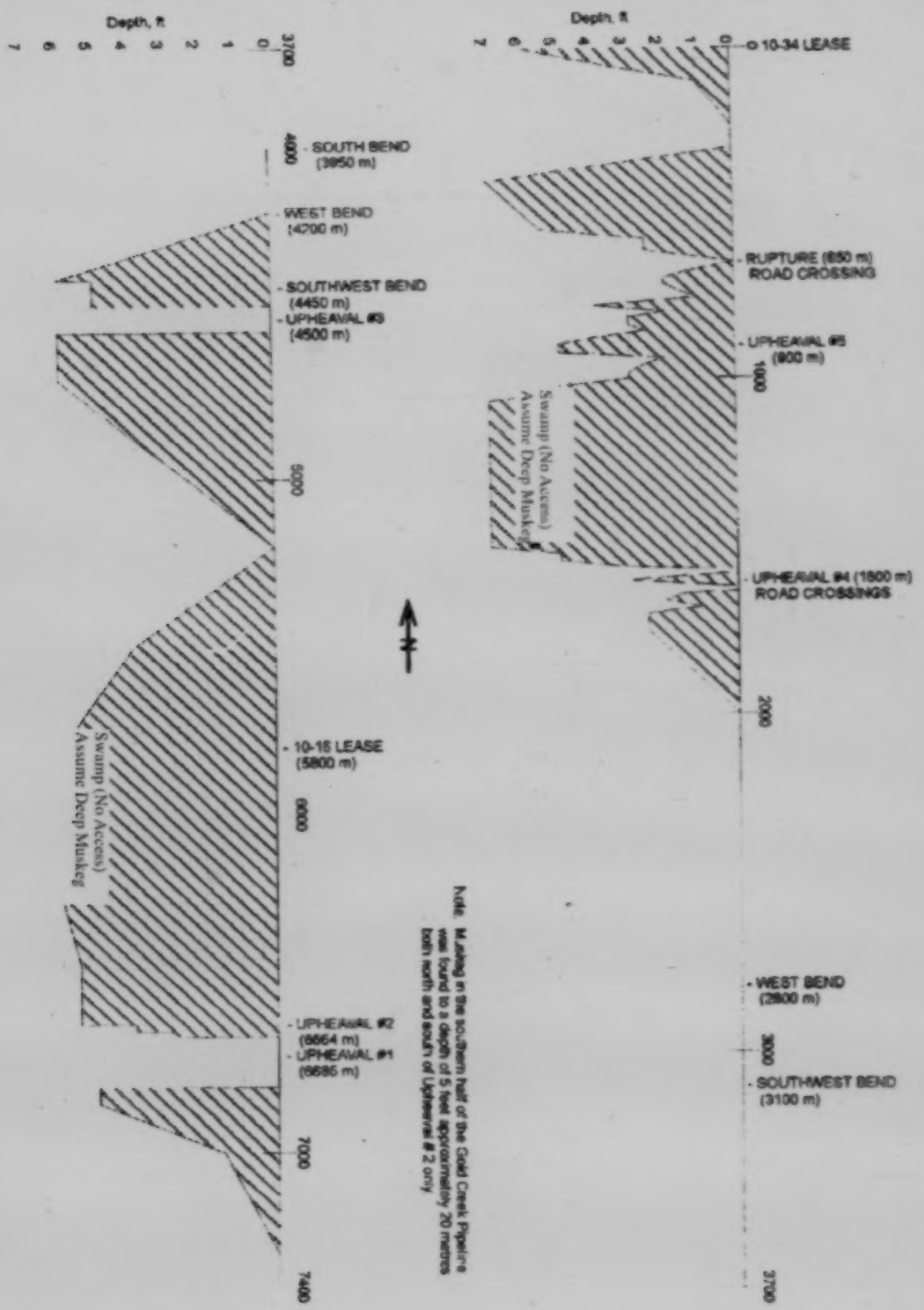

Figure 4.3 Muskeg Plot along Gold Creek NPS-8 Pipeline

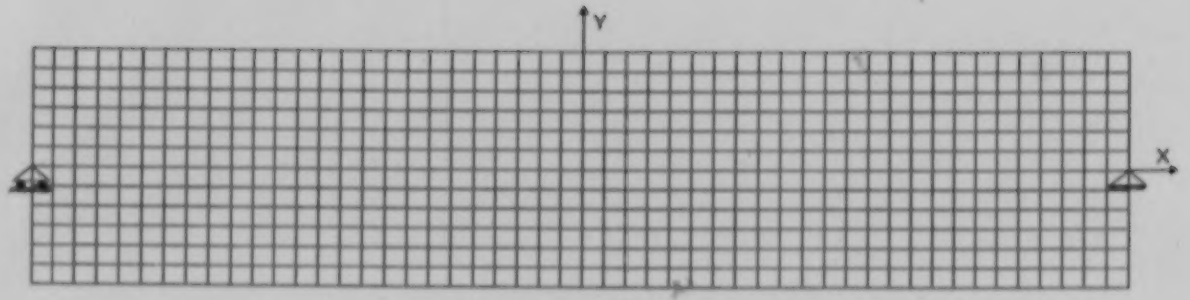

Figure 4.4 FEA Mesh and Boundary Conditions Used for ABAQUS

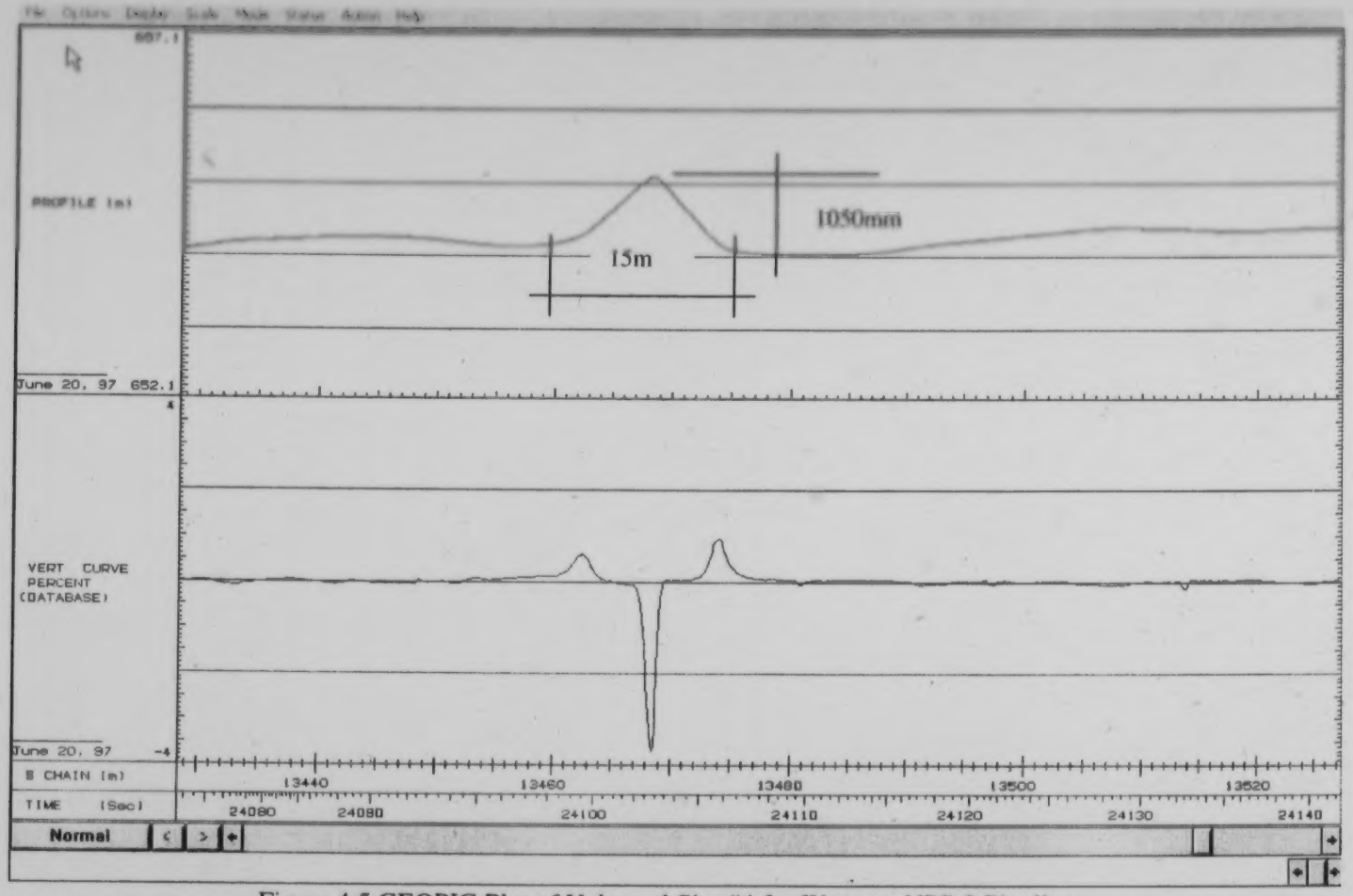

Figure 4.5 GEOPIG Plot of Upheaval Site #4 for Wascana NPS-8 Pipeline

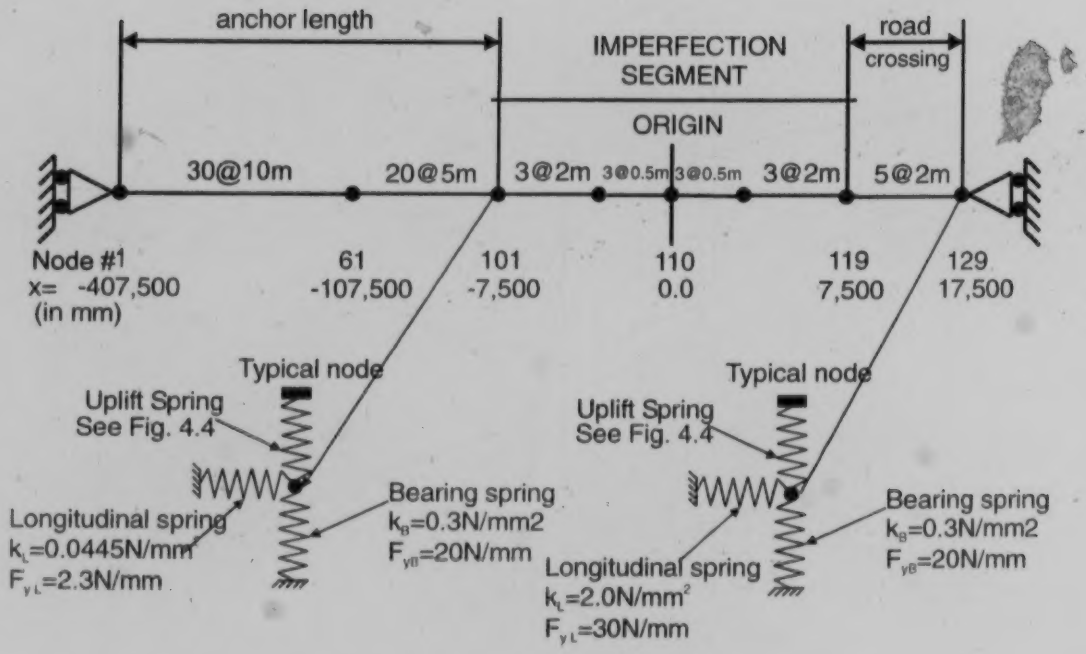

Figure 4.6 Schematic Model Used in ABP Program for Site #4

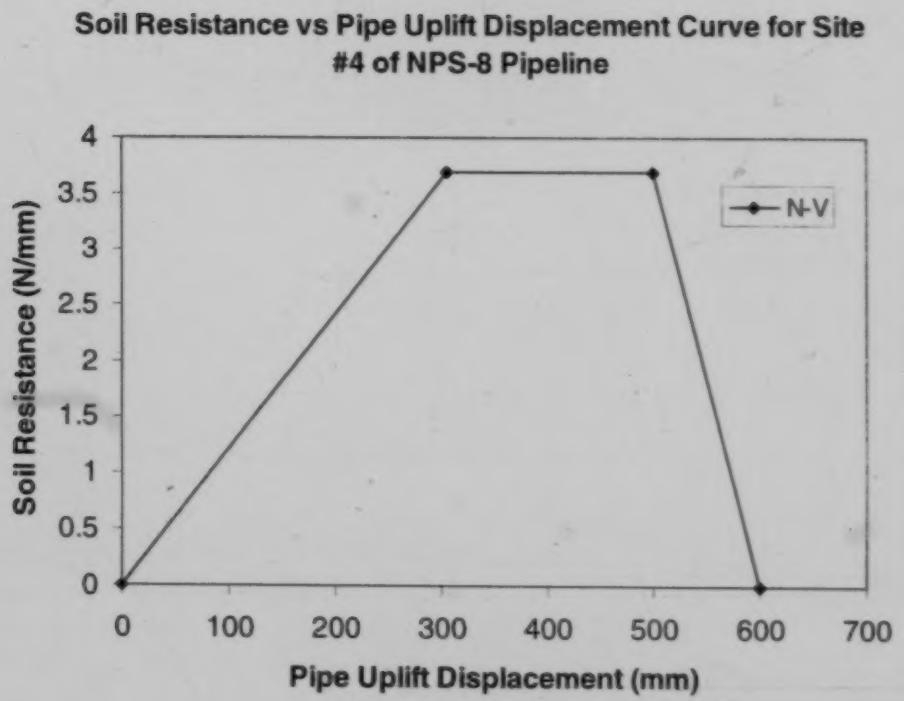

Figure 4.7 Soil Resistance vs. Pipe Uplift Displacement Curve for Site #4

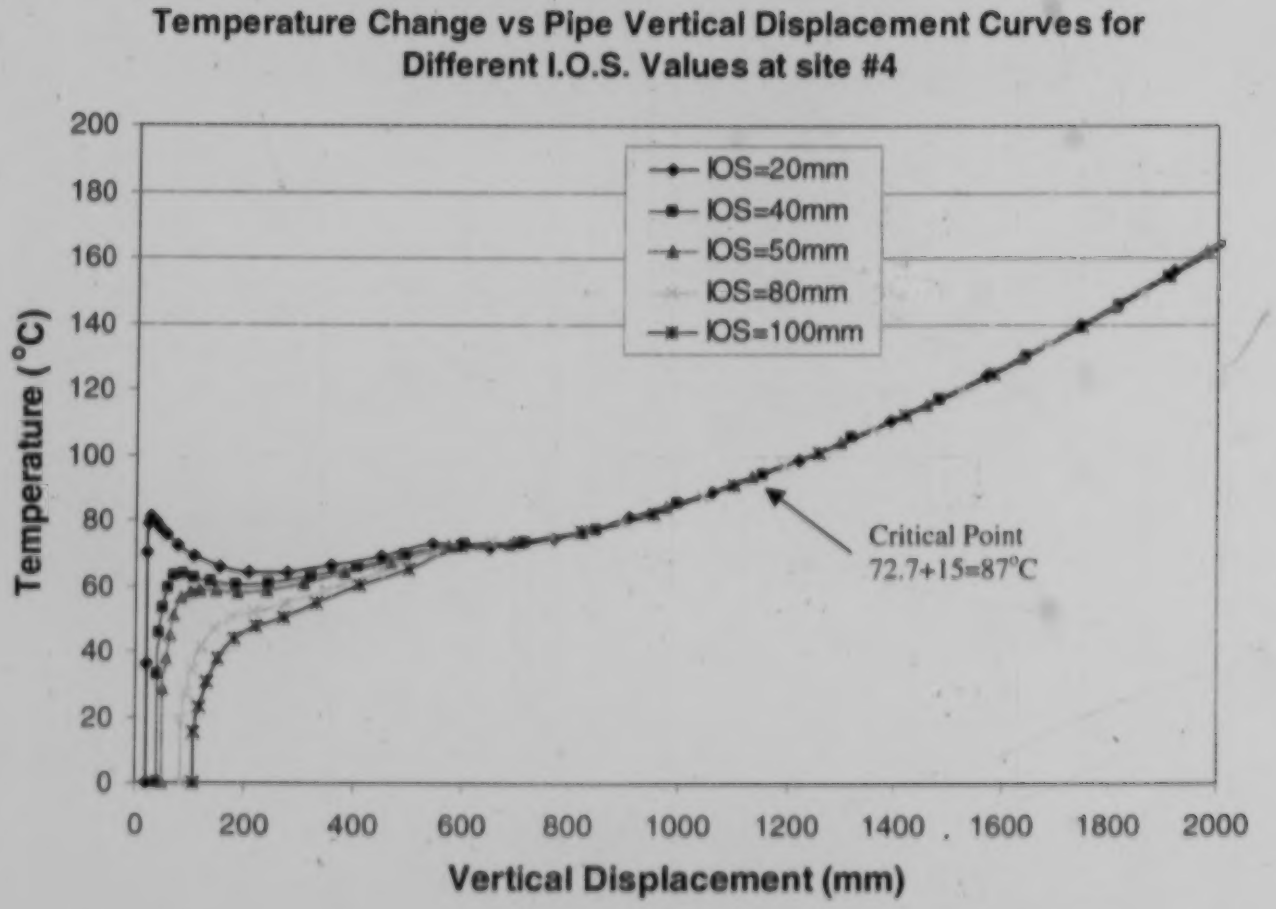

Figure 4.8 Temperature Increase vs. Pipe vertical Displacement Curves from ABP Analyses (Site #4)

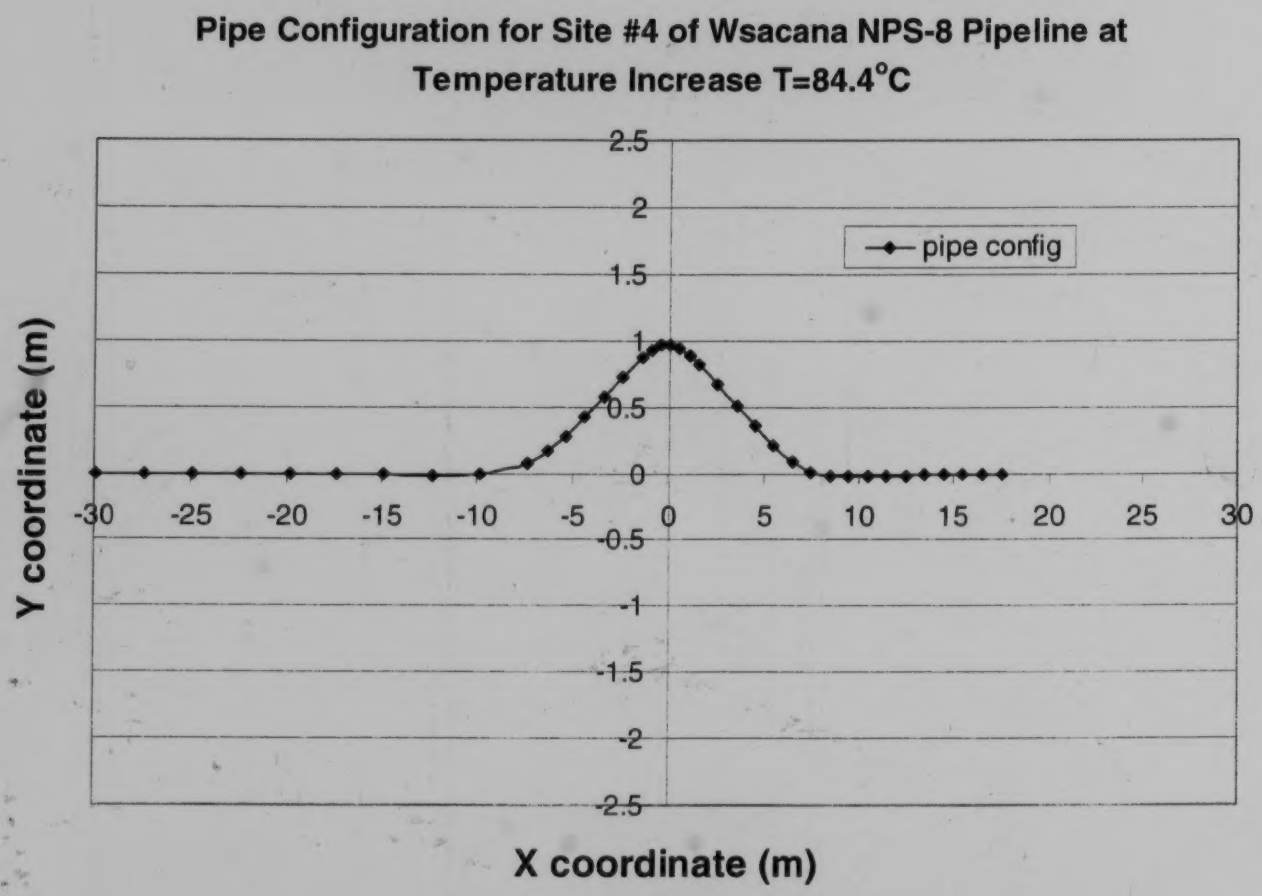

Figure 4.9 Pipe Deformed Configuration at Temperature Increase of 84.4°C from ABP Analyses (Site #4)

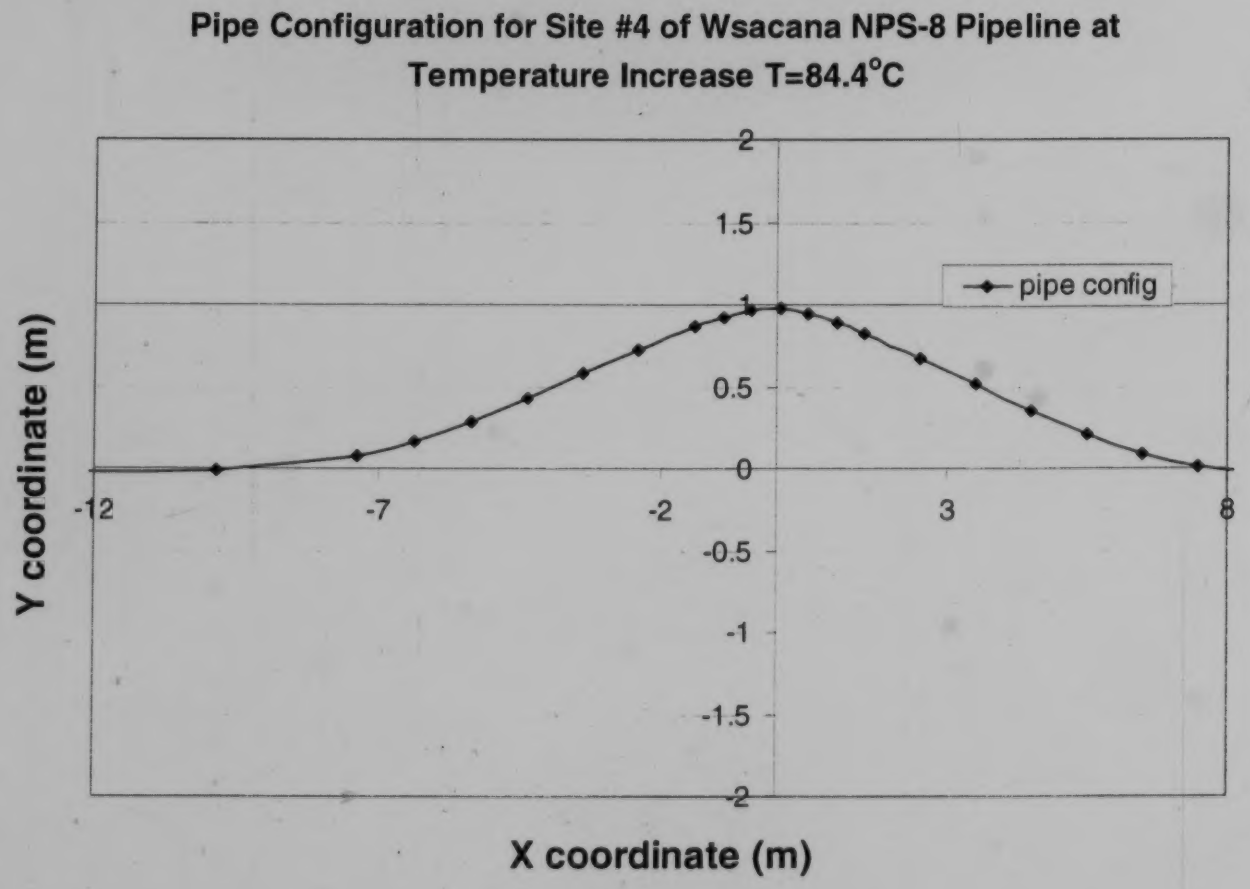

Figure 4.10 Pipe Deformed Configuration at Temperature Increase of 84.4°C from ABP Analyses with smaller Scale (Site #4)

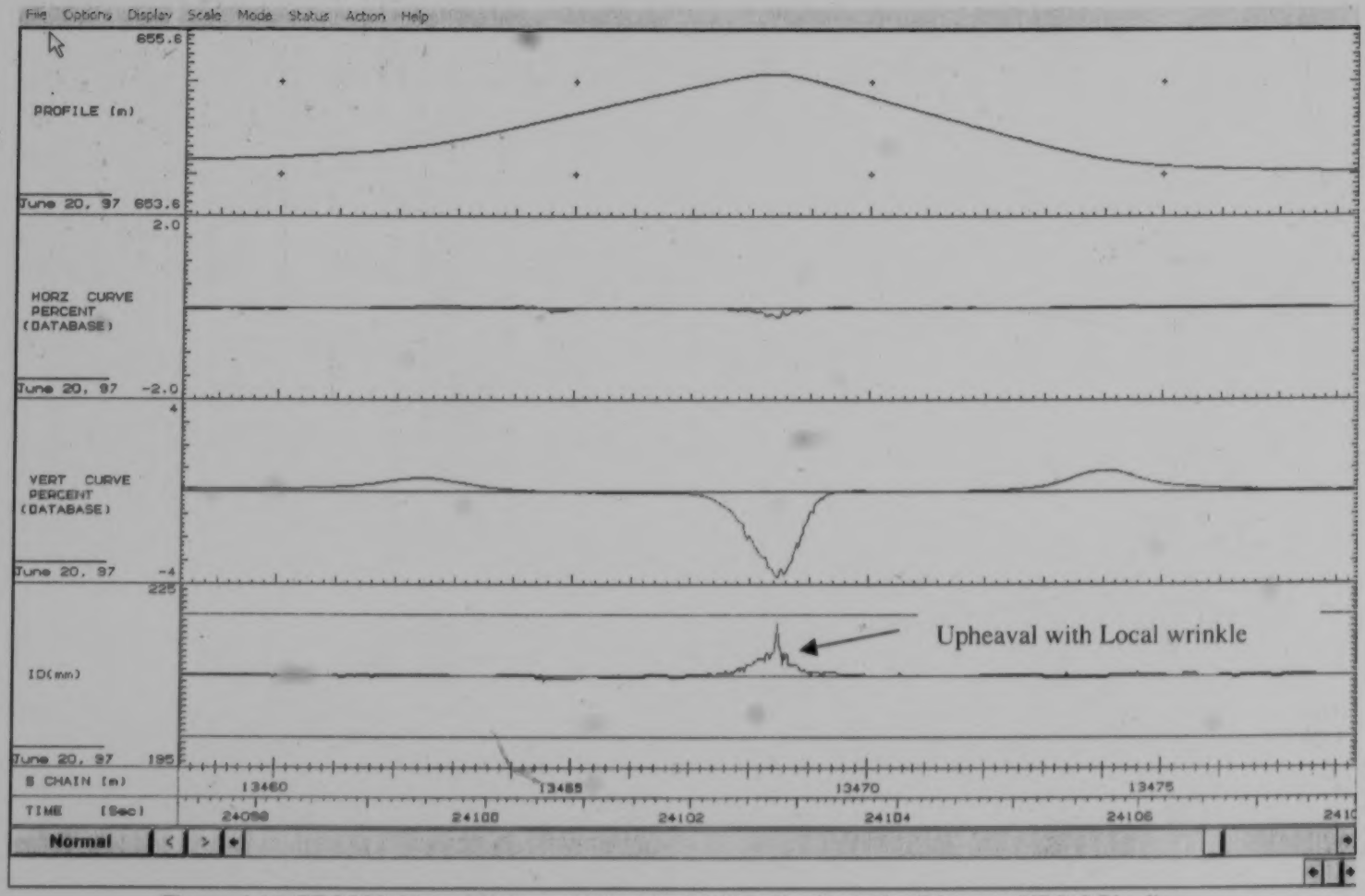

Figure 4.11 GEOPIG Plot of Upheaval Site #4 with Smaller Scale for Wascana NPS-8 Pipeline

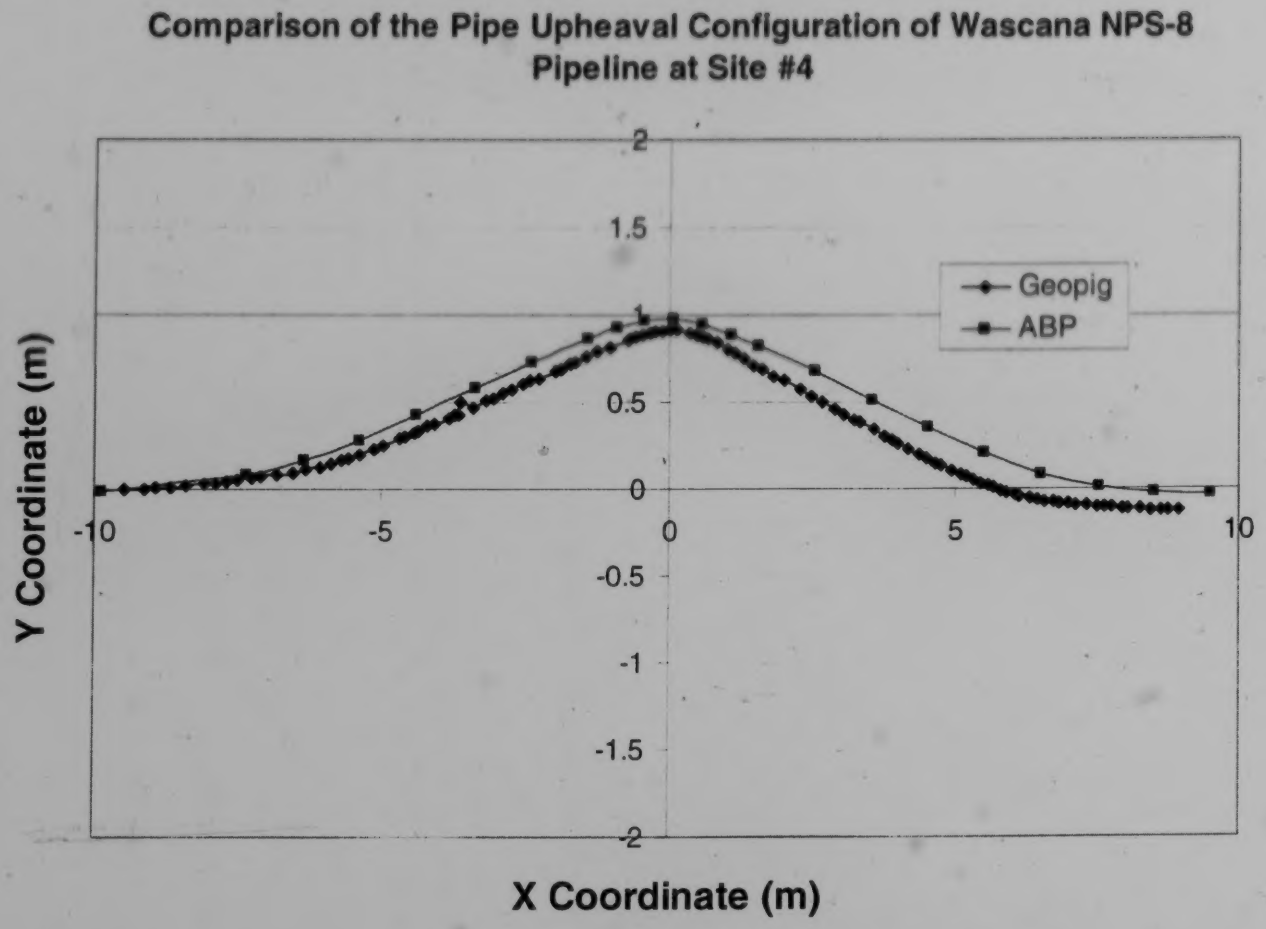

Figure 4.12 Comparison of the Pipe Configuration Between GEOPIG Plot and ABP Result at Site #4

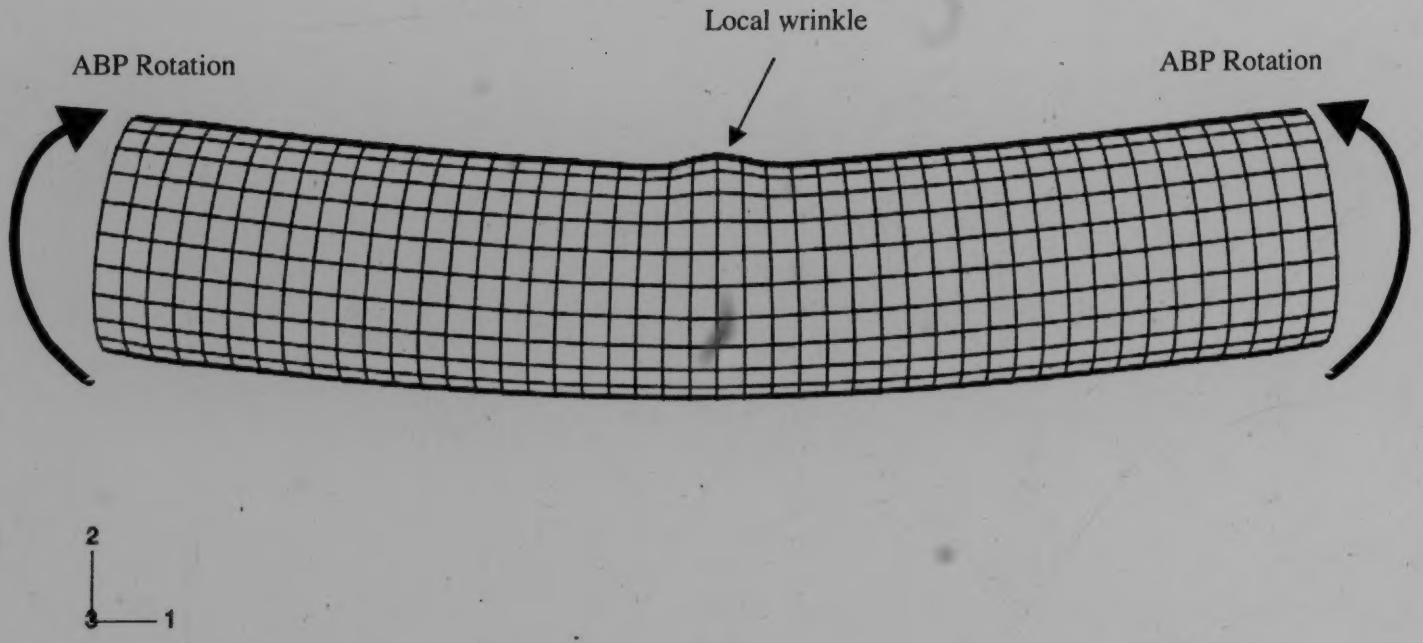

Figure 4.13 Pipe Deformed Shape for Critical Segment at Site #4 (ABAQUS)

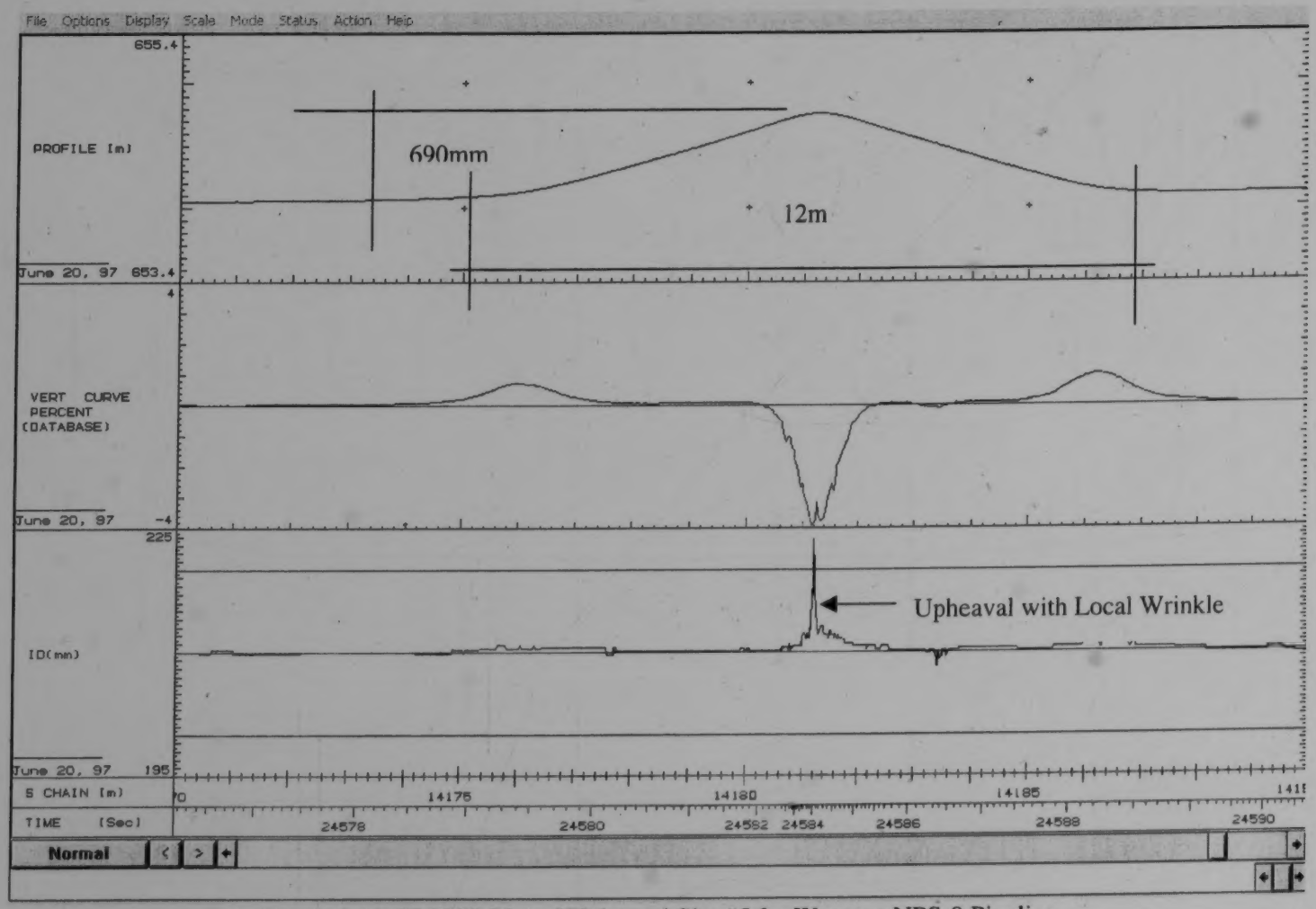

Figure 4.14 GEOPIG Plot of Upheaval Site #5 for Wascana NPS-8 Pipeline

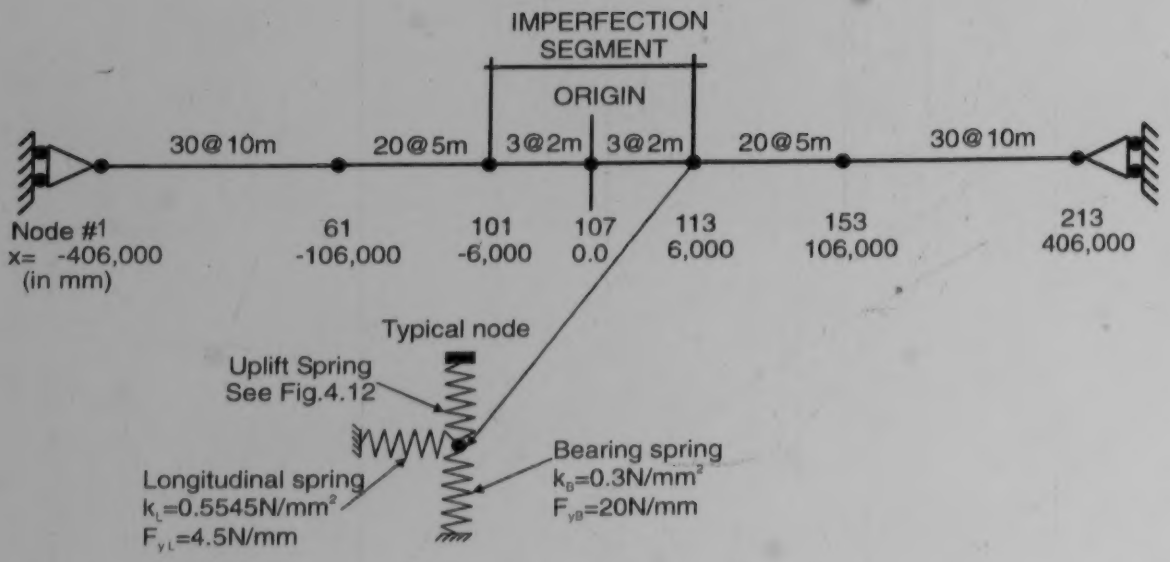

Figure 4.15 Schematic Model Used in ABP Program for Site #5

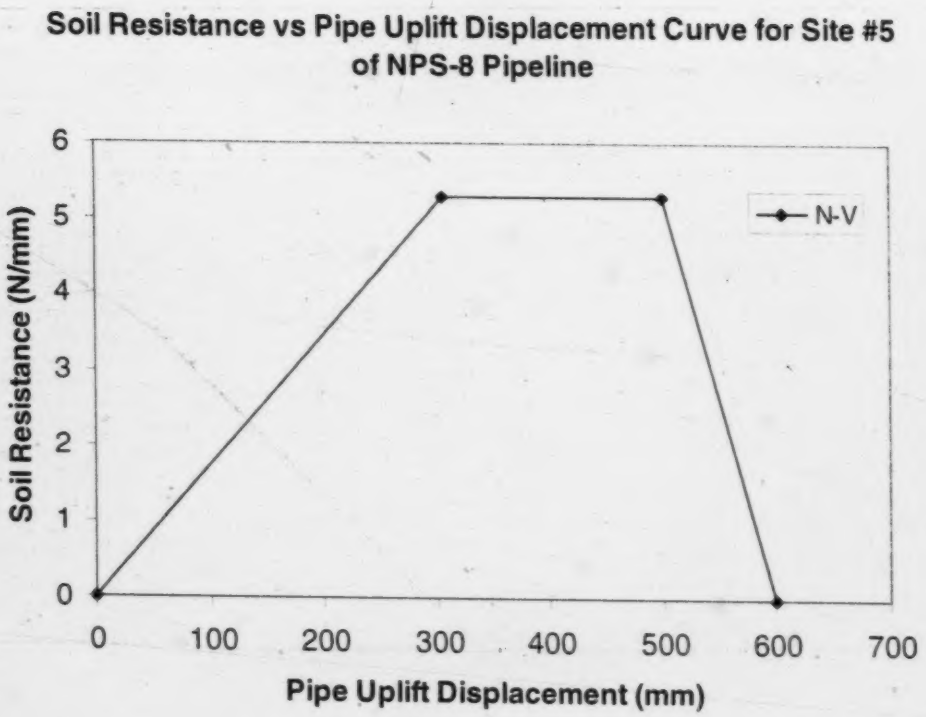

Figure 4.16 Soil Resistance vs. Pipe Uplift Displacement Curve for Site #5

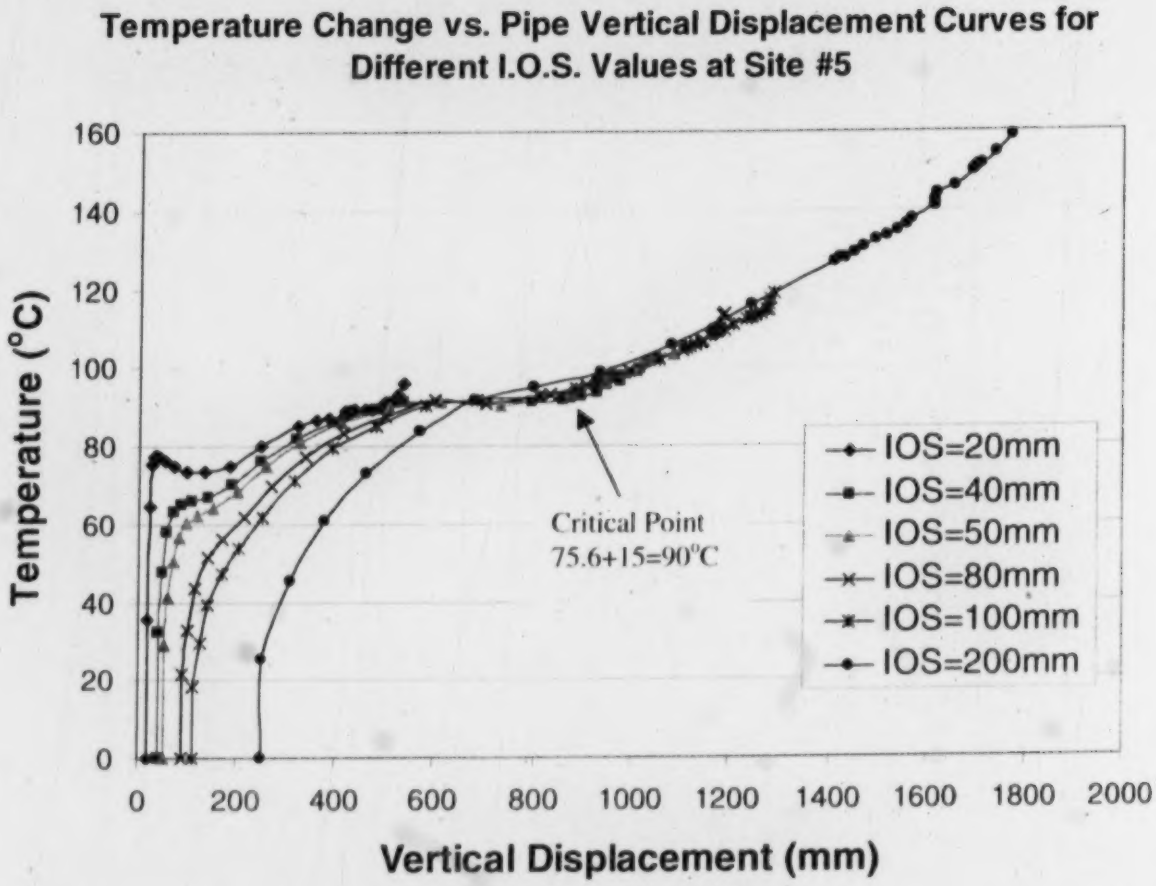

Figure 4.17 Temperature Increase vs. Pipe vertical Displacement Curves from ABP Analyses (Site #5)

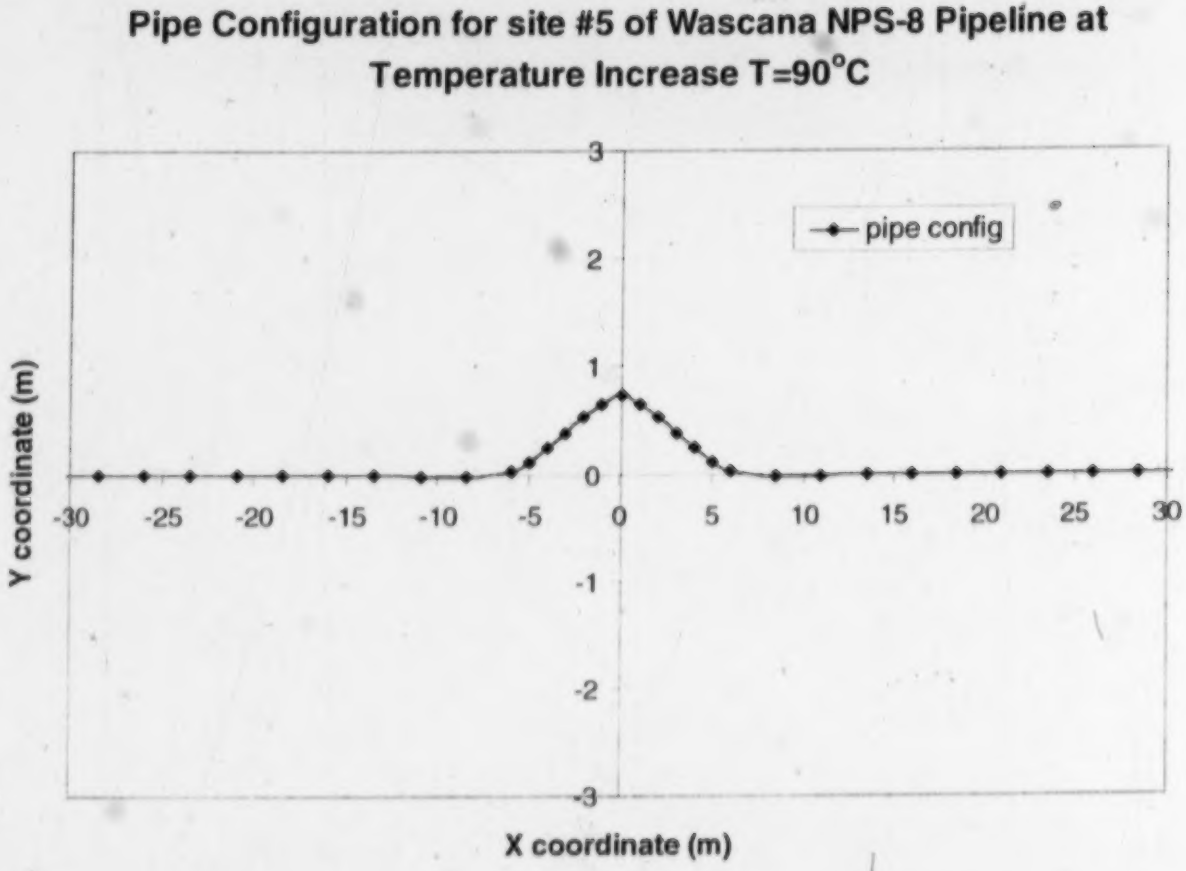

Figure 4.18 Pipe Deformed Configuration at Temperature Increase of 90°C from ABP Analyses (Site #5)

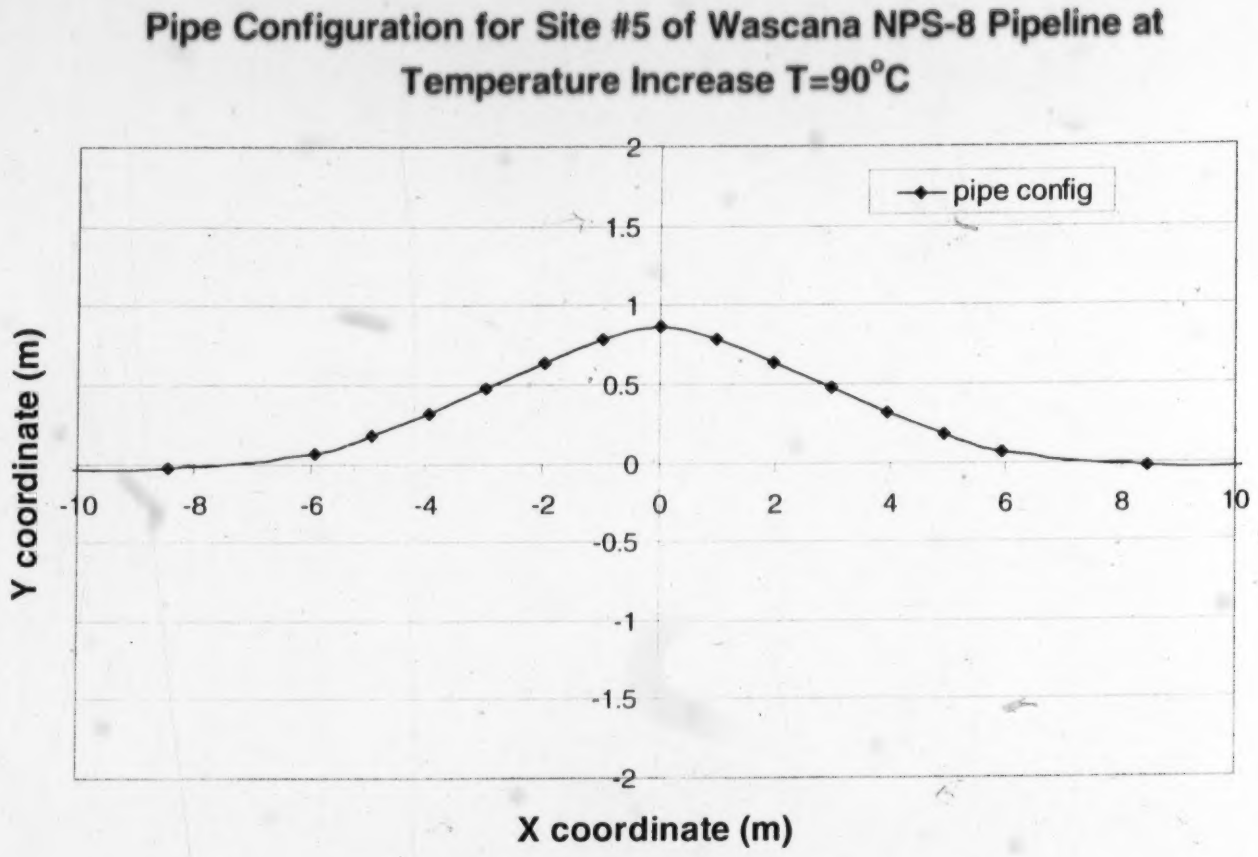

Figure 4.19 Pipe Deformed Configuration at Temperature Increase of 90°C from ABP Analyses with Smaller Scale (Site #5)

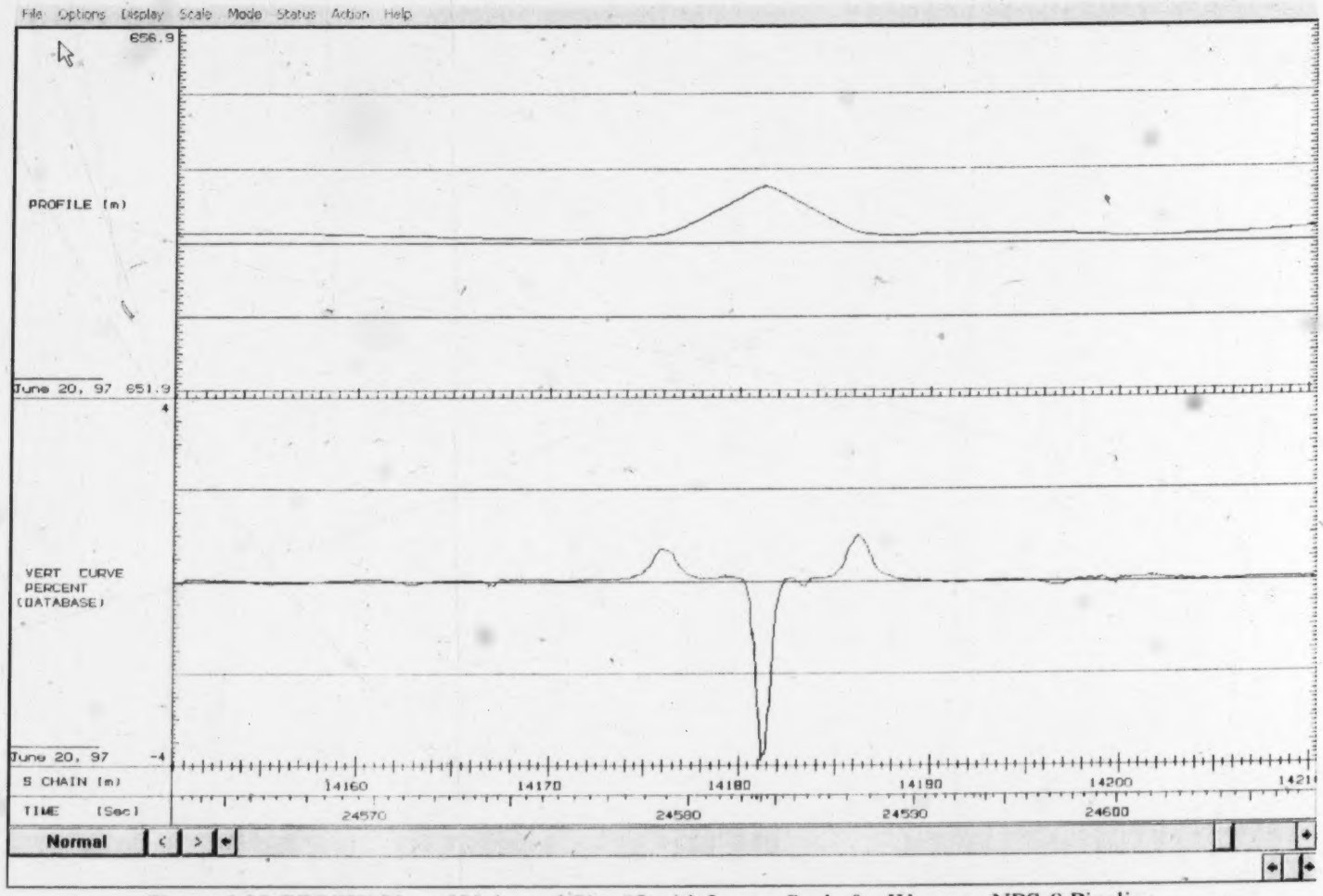

Figure 4.20 GEOPIG Plot of Upheaval Site #5 with Larger Scale for Wascana NPS-8 Pipeline

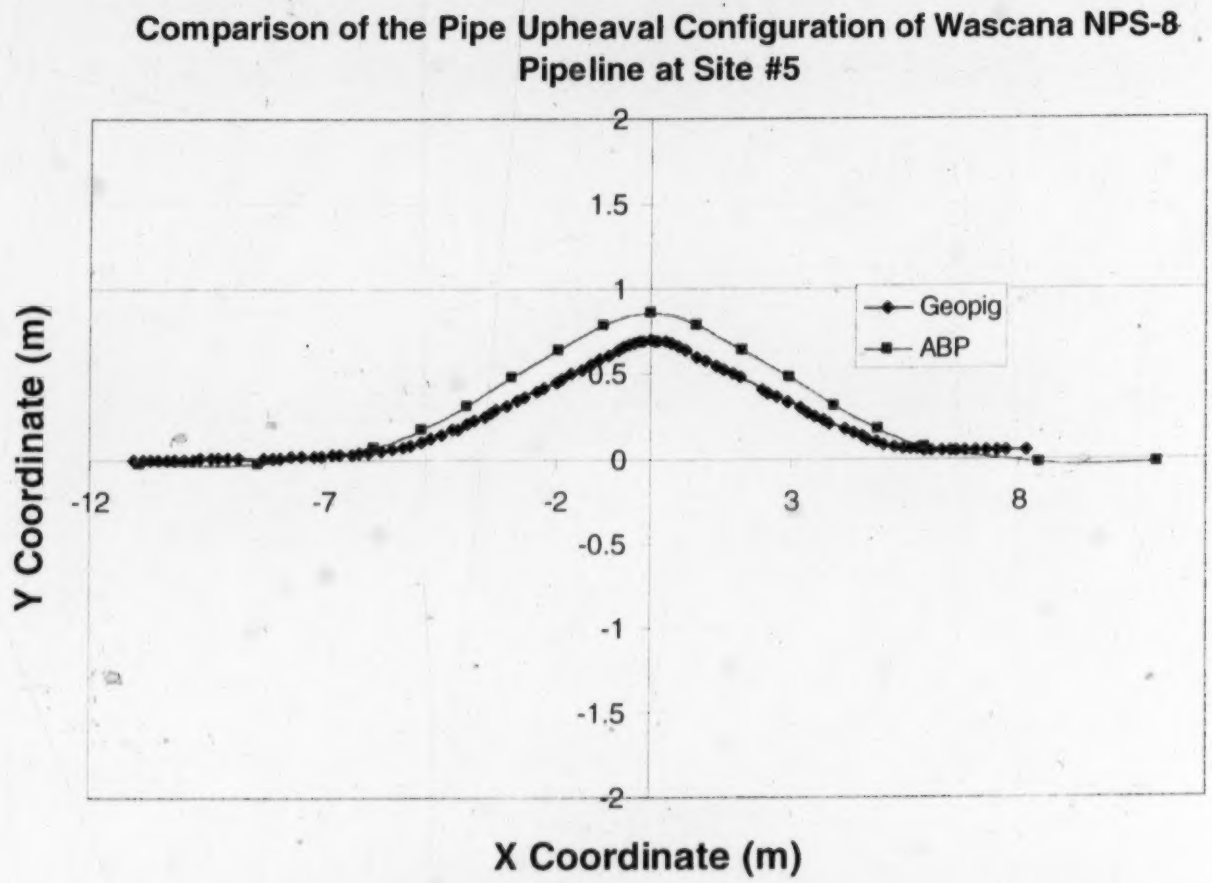

Figure 4.21 Comparison of the Pipe Configuration Between the GEOPIG Plot and ABP Result

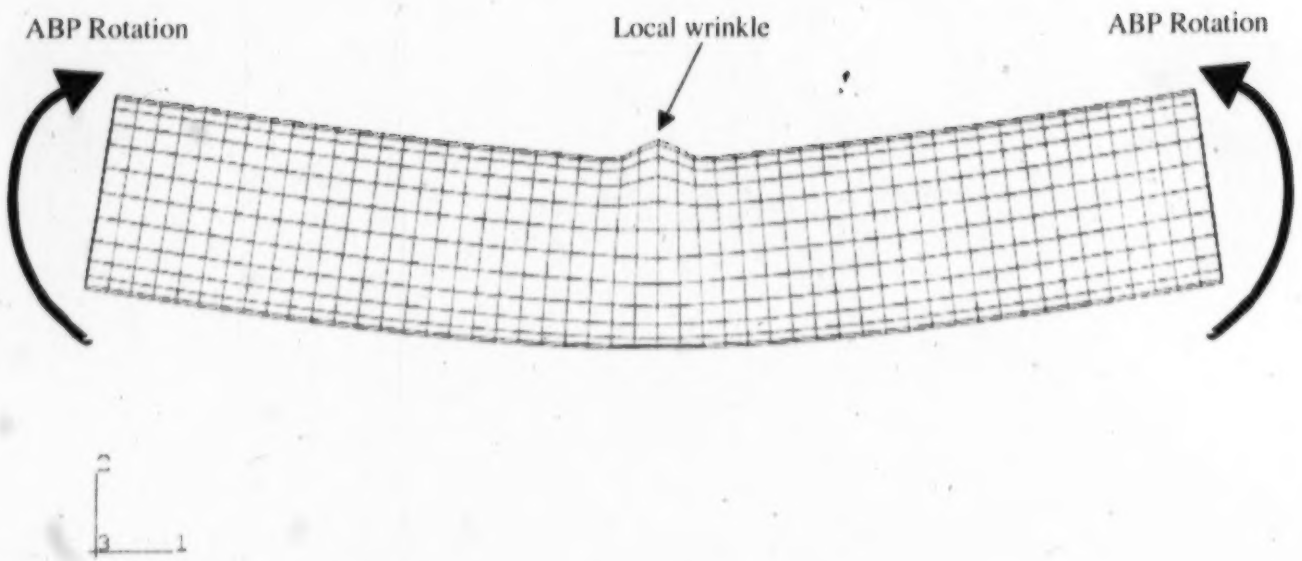

Figure 4.22 Pipe Deformed Shape for Critical Segment of Site #5 (ABAQUS)

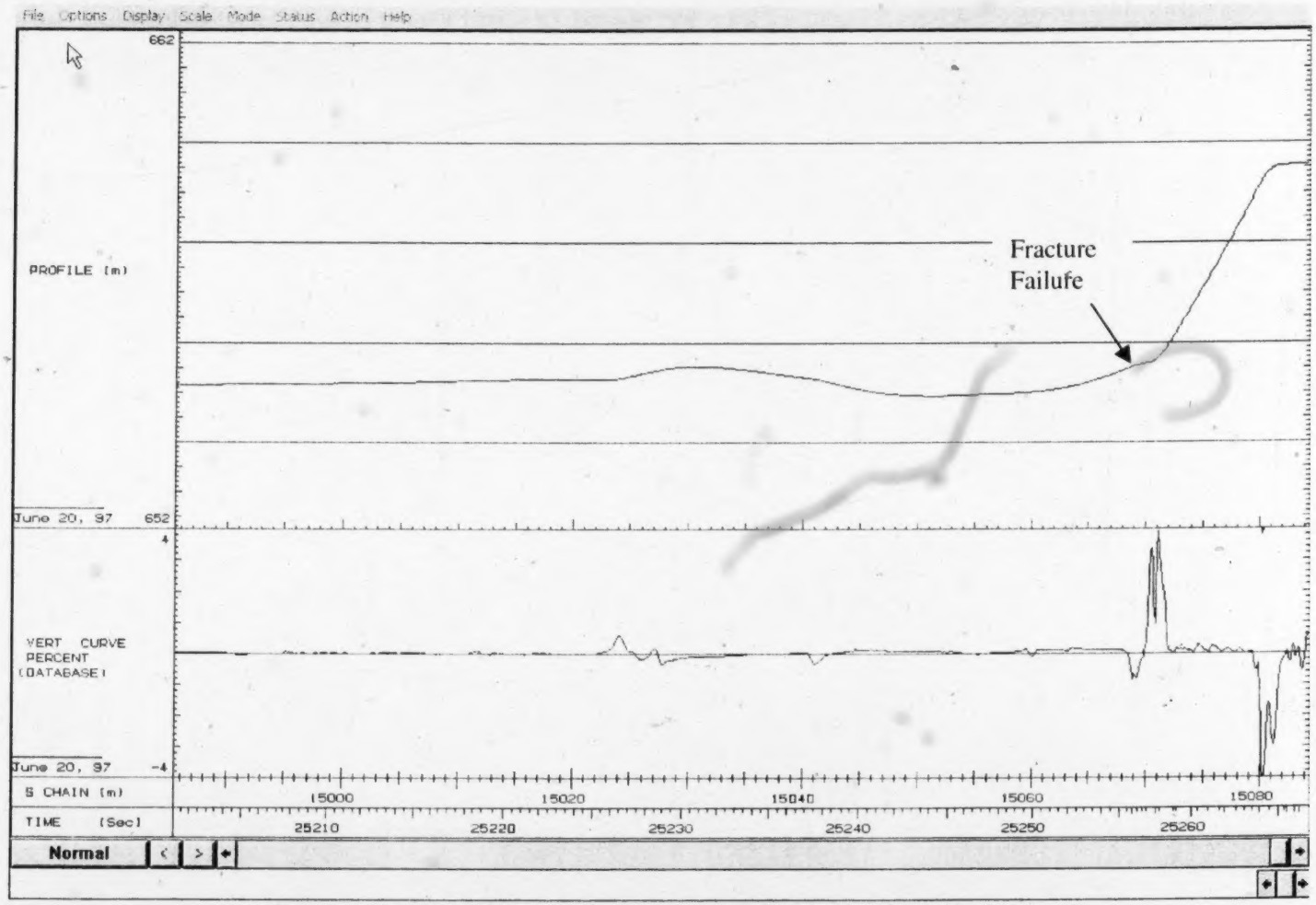

Figure 4.23 GEOPIG Plot of Fracture Site for Wascana NPS-8 Pipeline

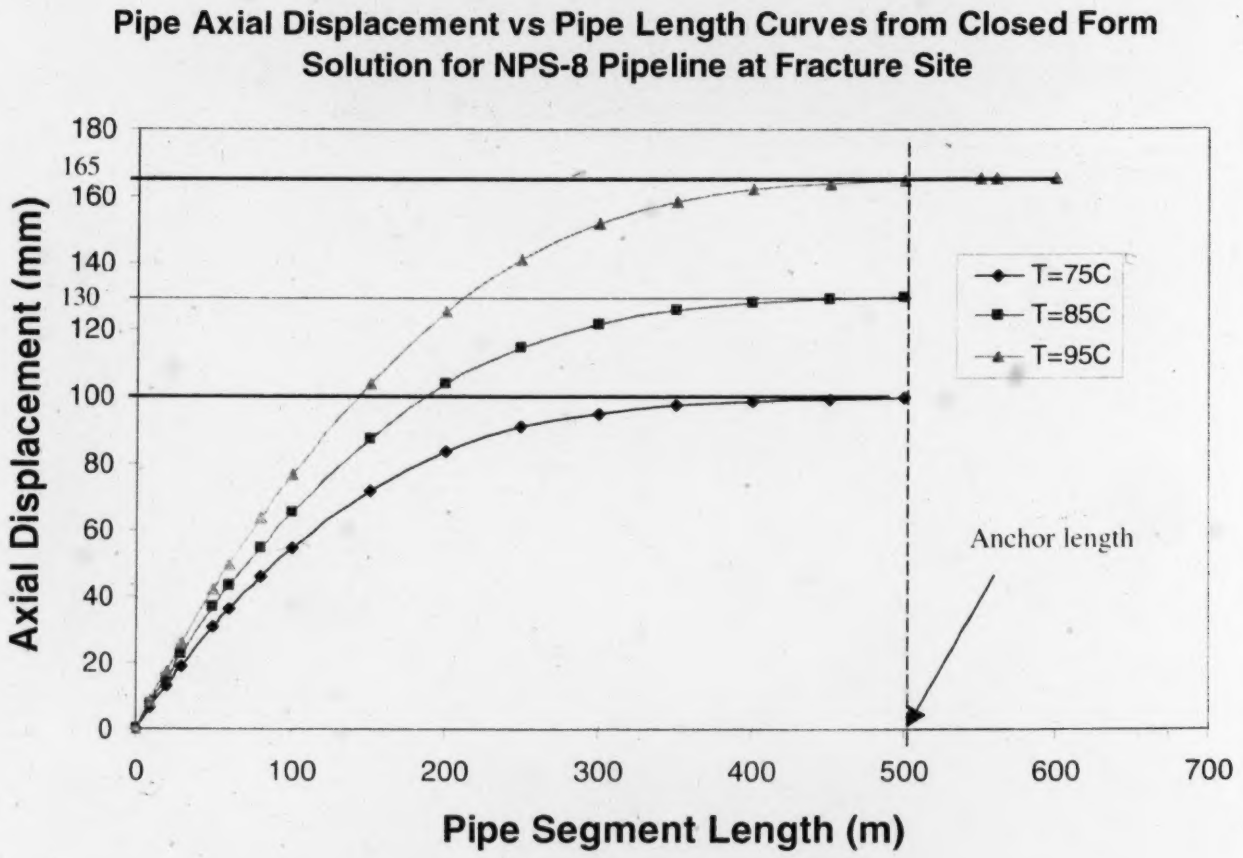

Figure 4.24 Computed Anchor Length by Closed Form Solution for Fracture Site

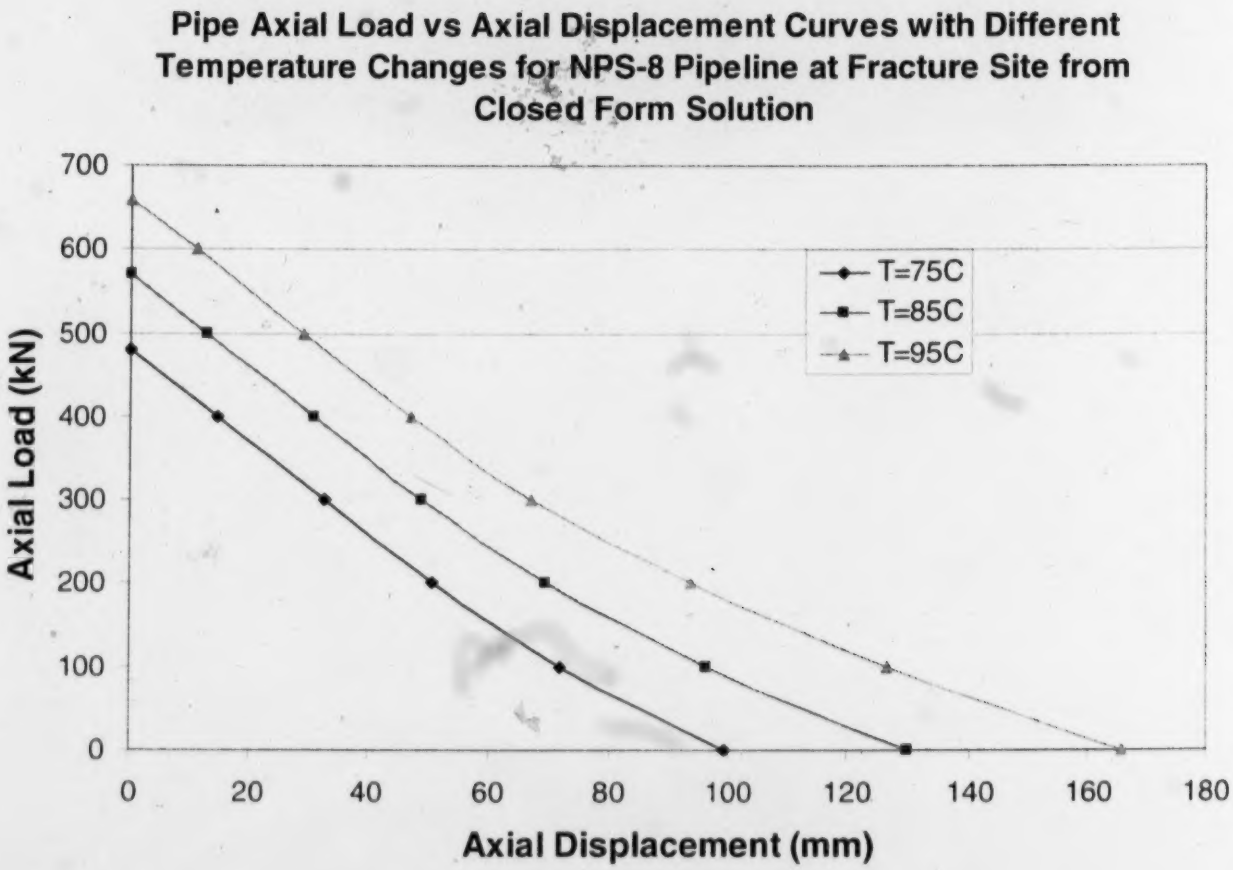

Figure 4.25 Axial Load vs. Axial Displacement Curve from Closed Form Solution

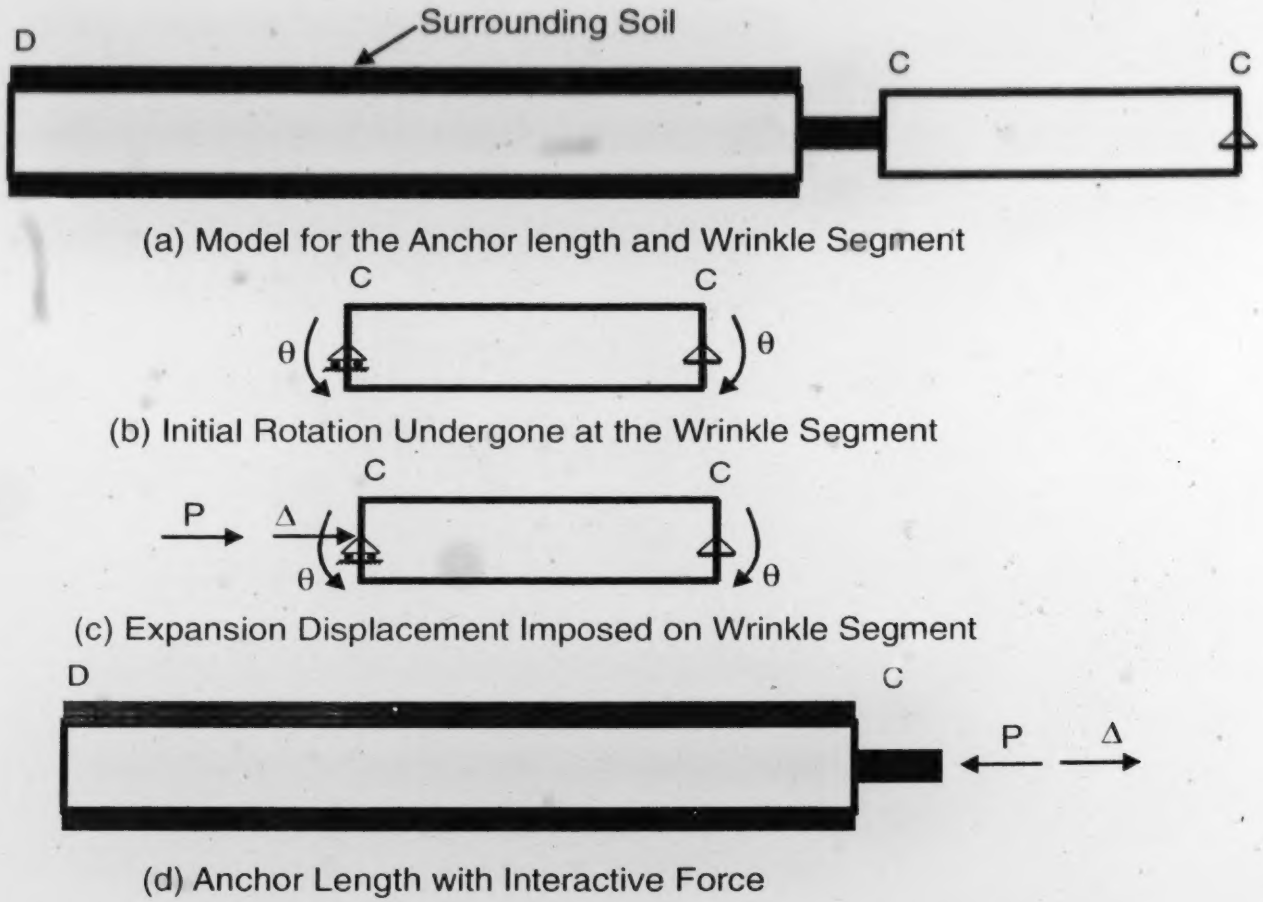

Figure 4.26 Expansion Interaction of Anchor Length and FE Model Segment

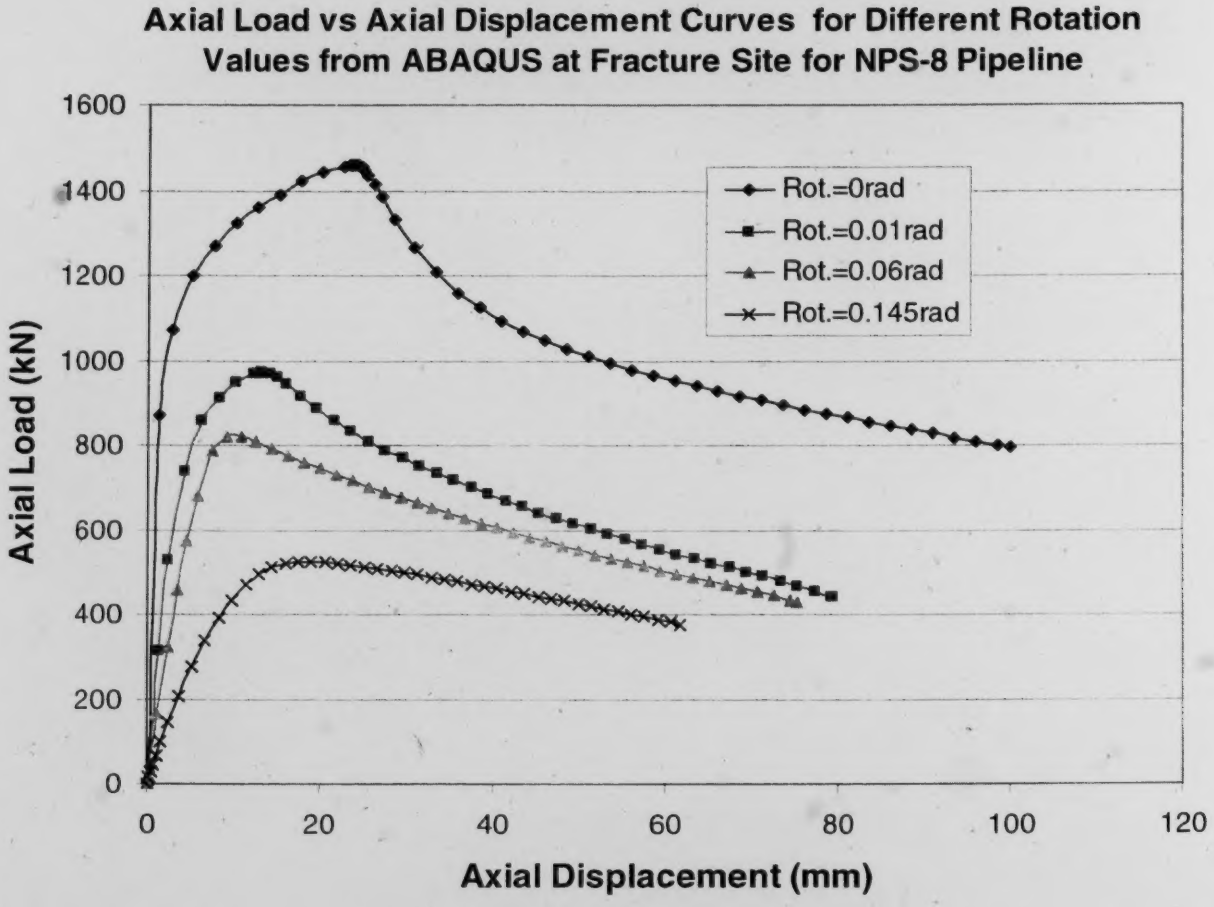

Figure 4.27 Axial Load vs. Axial Displacement Curves for Different Rotation Values of a 6D Segment from ABAQUS

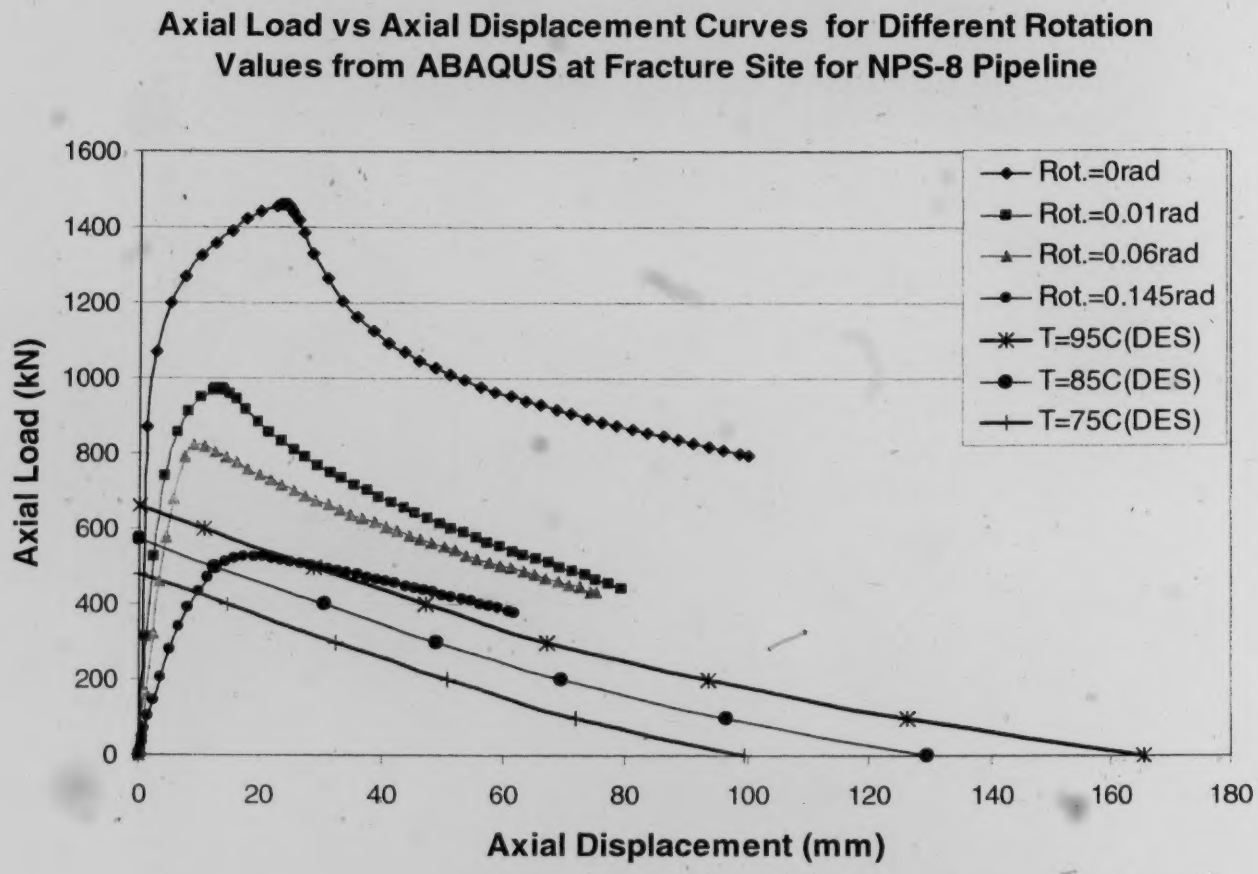

Figure 4.28 Axial Load vs. Axial Displacement Curve from DES and ABAQUS

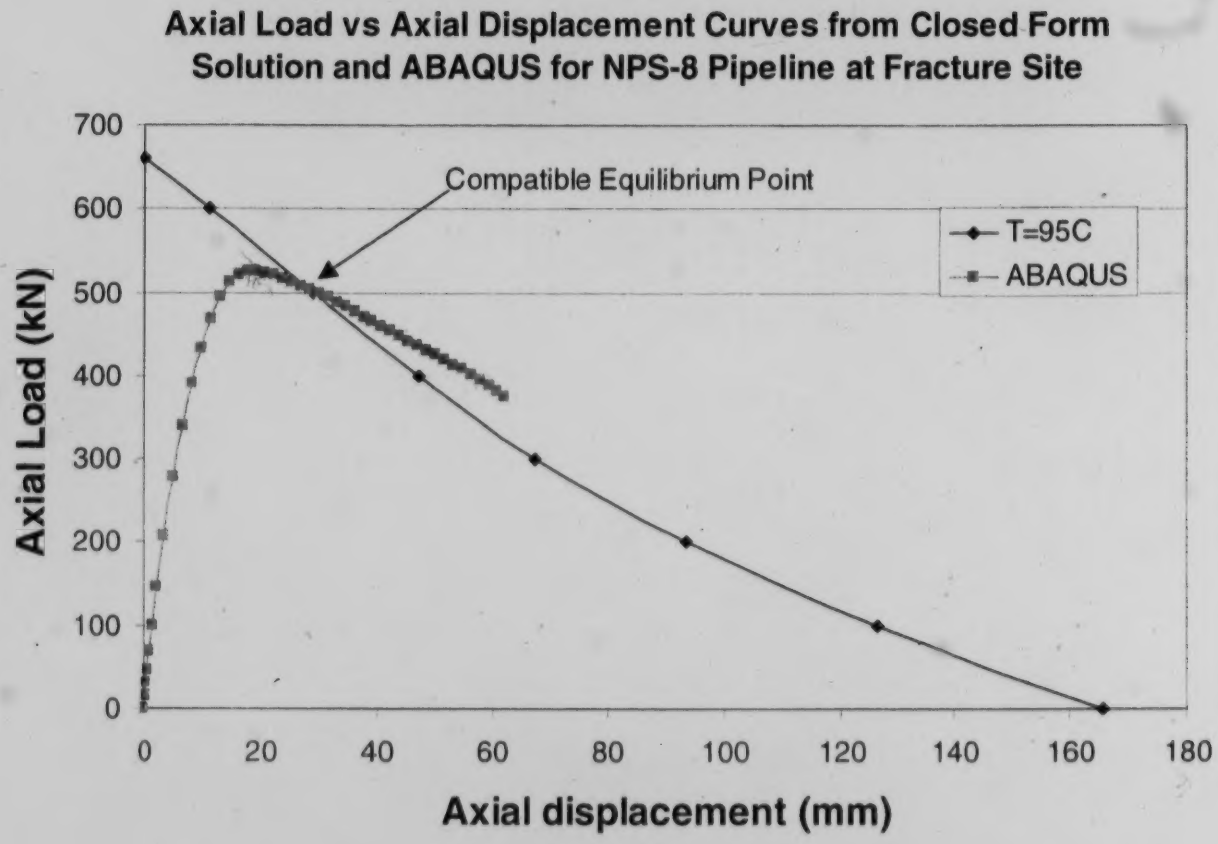

Figure 4.29 Axial Load vs. Axial Displacement Curves from Closed Form Solution and ABAQUS

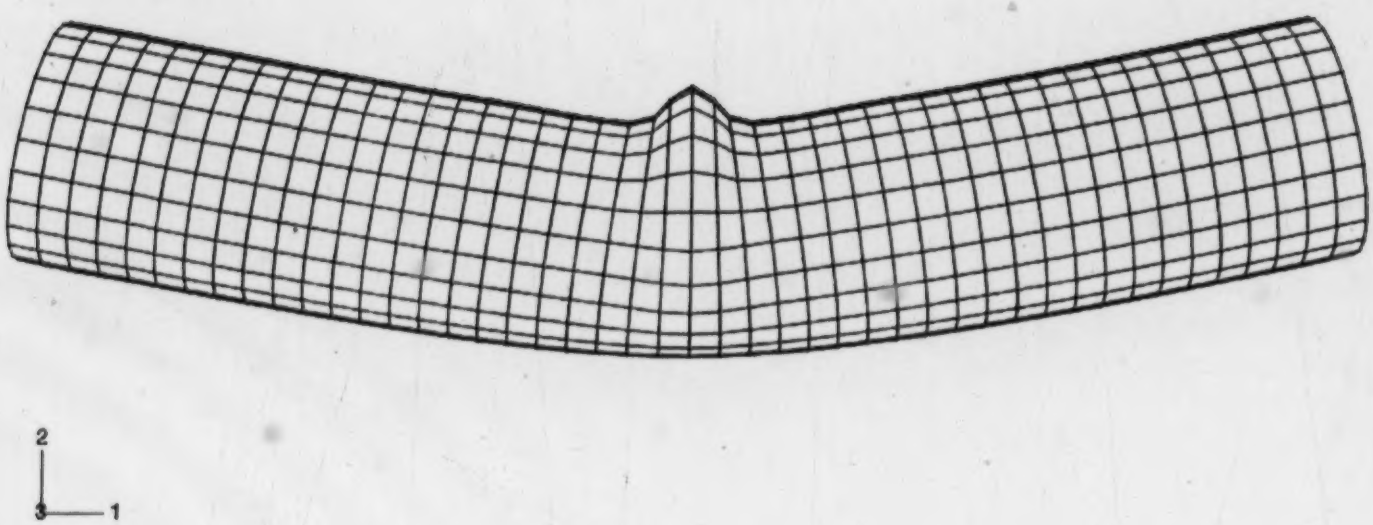

Figure 4.30 Pipe Deformed Shape for NPS-8 Pipeline at Fracture Site

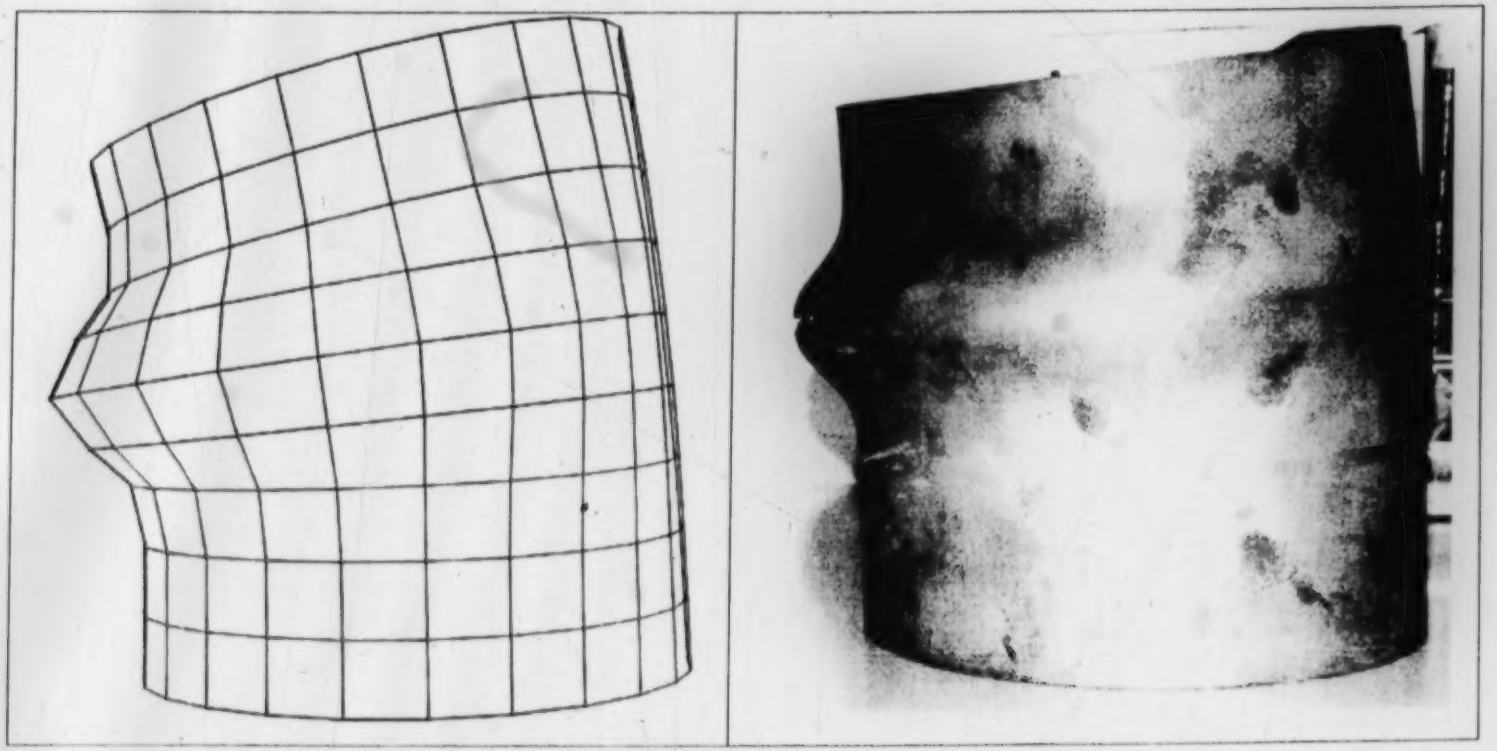

Figure 4.31 Comparison of the Wrinkles from the Field and ABAQUS

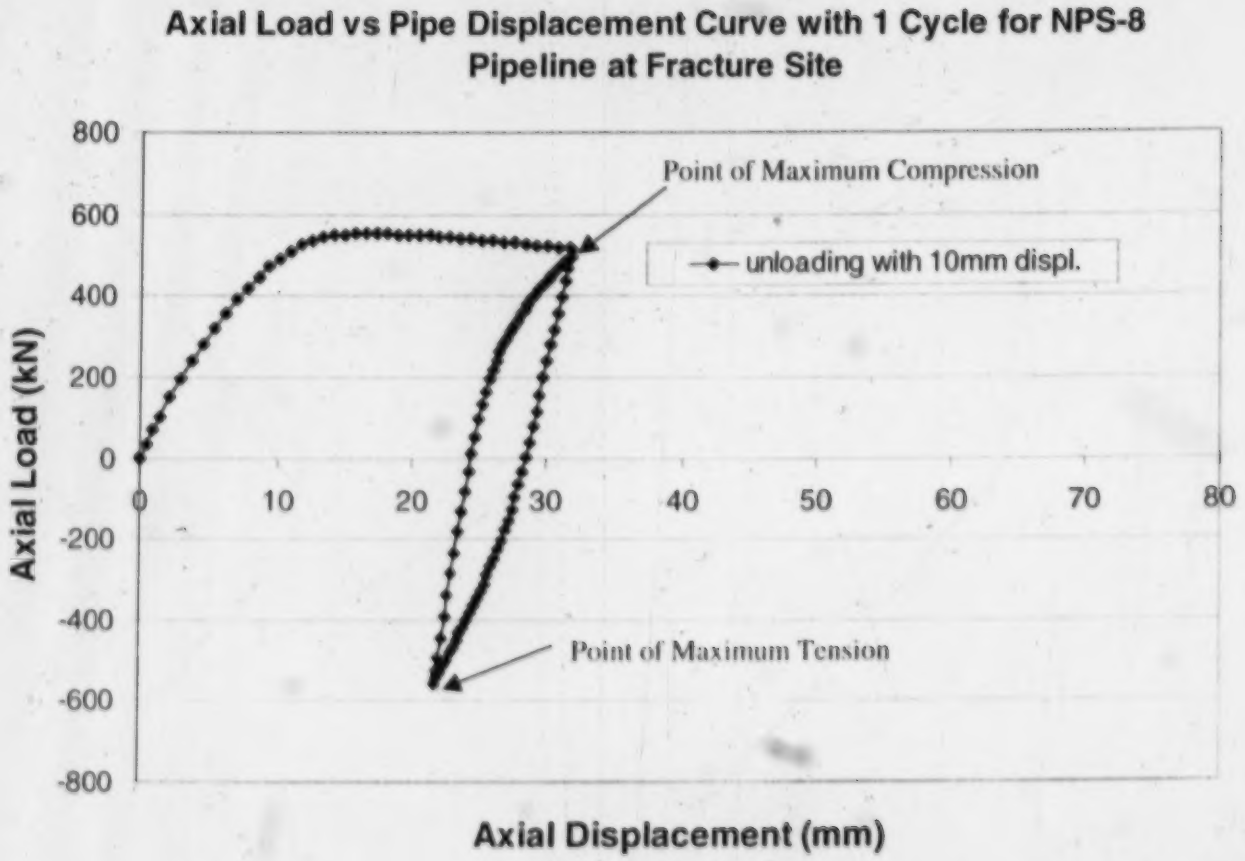

Figure 4.32 Axial Load vs. Axial Displacement Curve for Unloading with 10mm End Movement

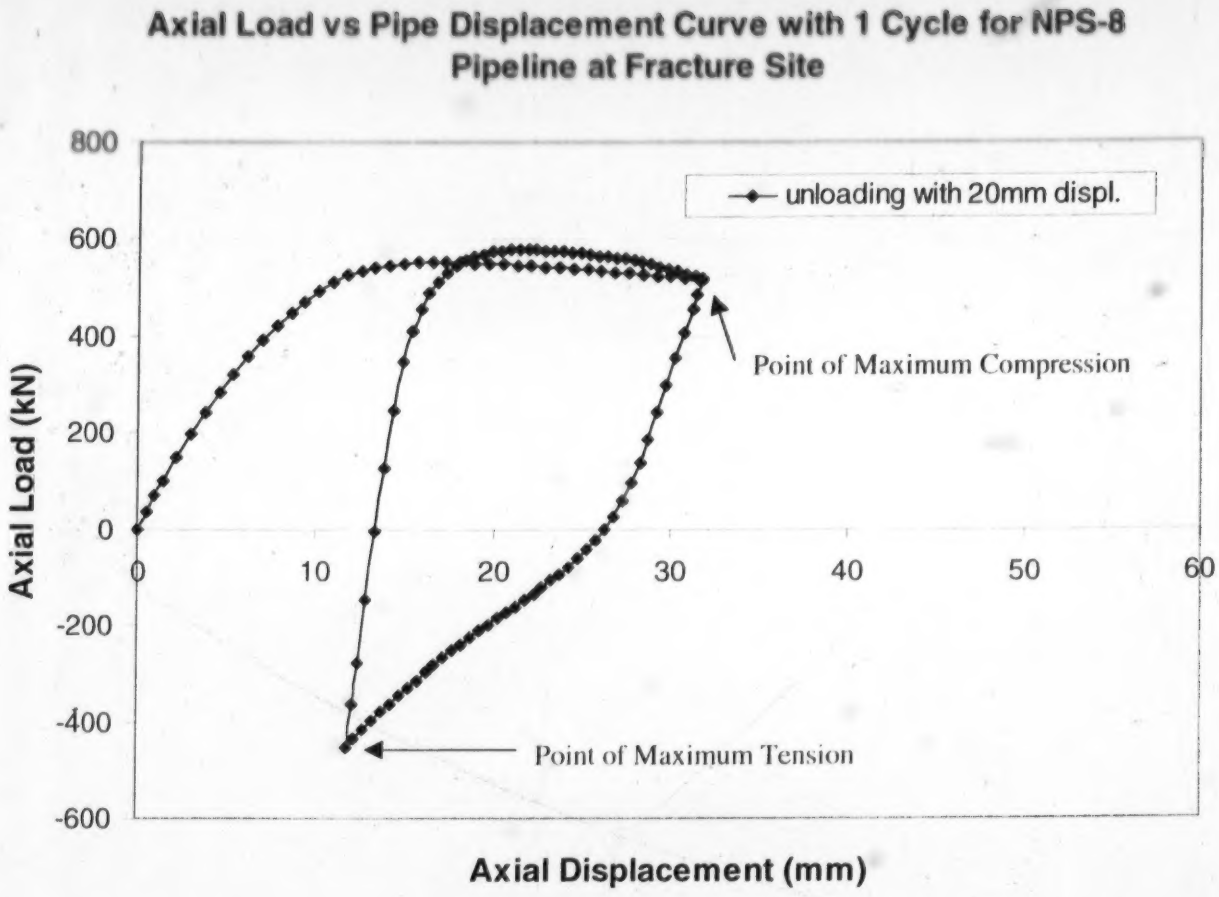

Figure 4.33 Axial Load vs. Axial Displacement Curve for Unloading with 20mm End Movement

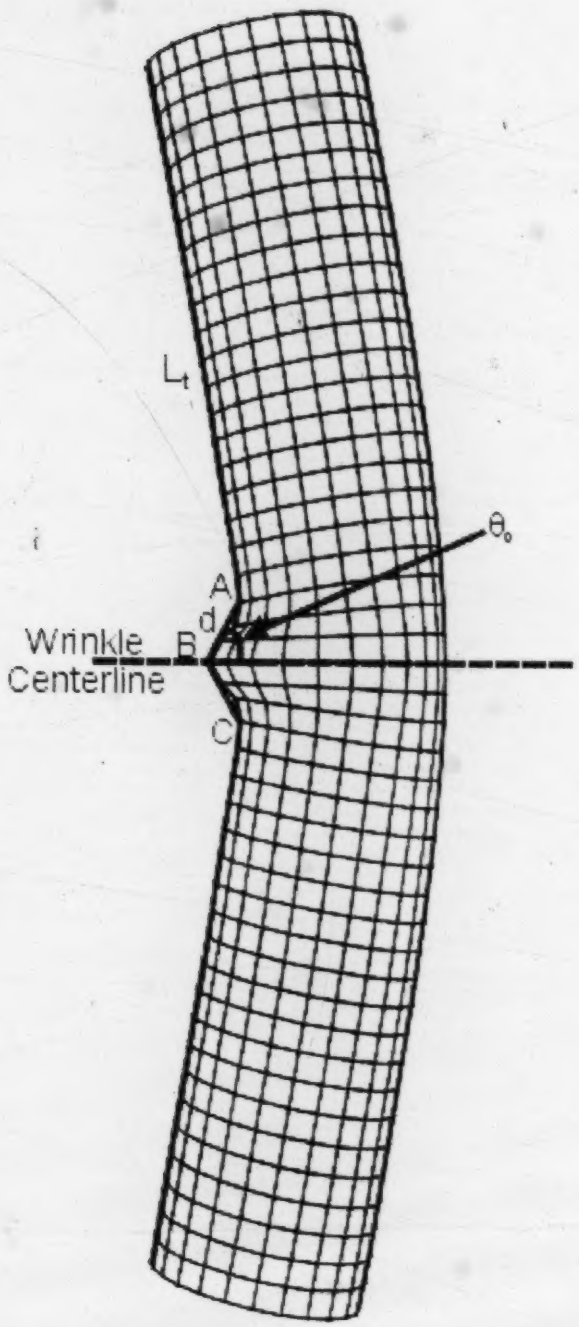

Figure 4.34 Pipe Deformed Configuration at Maximum Tension

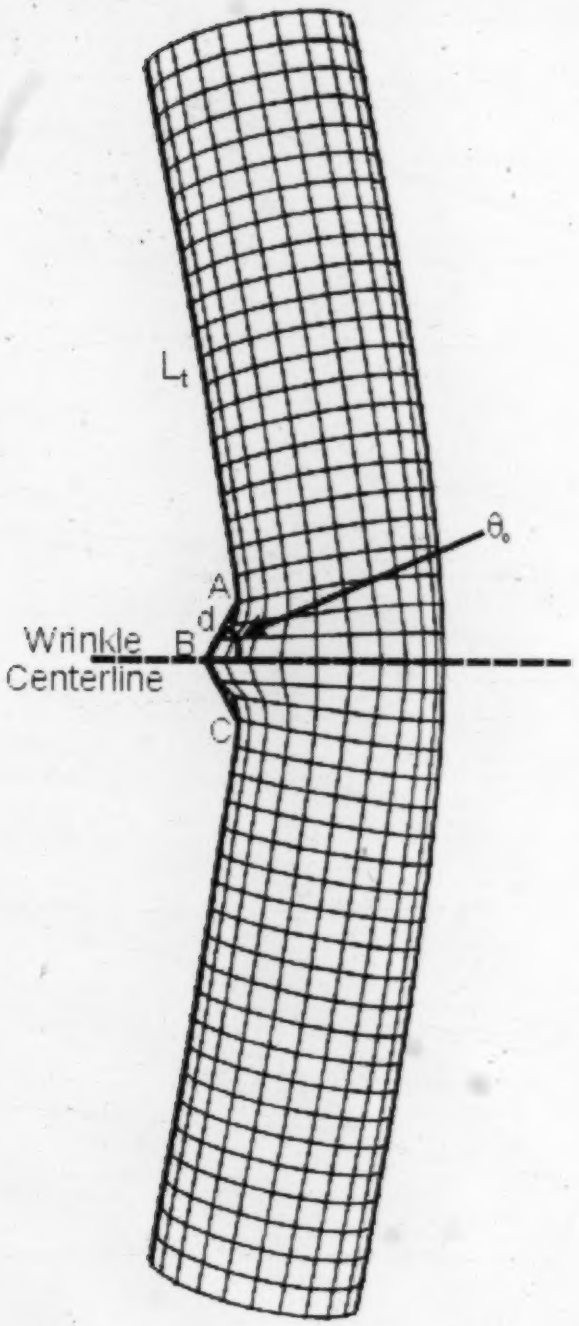

Figure 4.35 Pipe Deformed Configuration at Maximum Compression

CHAPTER 5 CONCLUSIONS

The main objectives of this project are to analyze the upheaval and fracture phenomena of the Gold Creek NPS-8 Pipeline and attempt to predict field failures and observations for wrinkled line pipe that developed during its operation. In addition, comparison between the ABP solutions and Hobbs' DESs for pipeline global buckling and comparison between ABP results and DESs for soil-pipe slip mechanisms are made. Based on the comparisons as stated in Chapter 3 and the analytical results as stated in Chapter 4, the following conclusions are obtained:

1.) By using the new ABP program (ABP-V2002), the upheaval phenomena that occurred in the Gold Creek NPS-8 Pipeline are successfully predicted from the field data, and the analytical results match well with the field observations, i.e., the GEOPIG plots.

2.) The computer program ABP is reliable for modeling large displacements and finite strains, particularly in handling upheaval (vertical) buckling if adequate field data are available.

3.) By combining the analytical results for global behavior from the ABP program with the finite element package ABAQUS results for local behavior, the localized pipe behavior can be obtained. This combination is helpful in understanding the true behavior of the pipeline in the field.

4.) Combining the closed form solutions for pipe-soil slip mechanism with ABAQUS, the local wrinkle that precedes the fracture is created. Cyclic thermal loading analysis that occurs subsequently is carried out thereafter and the numbers of cycles to cause the fracture in the Gold Creek NPS-8 Pipeline are estimated based on computed hysteresis loop and the equations provided by Das et al. (2002). The computed results appear to agree closely with the events that occurred at the fracture site.

5.) Comparing the ABP results with Hobbs's DESs for pipeline global buckling and with DESs for pipe- soil slip mechanisms shows good agreement. This validates the solutions of the computer program ABP-V2002.

6.) More applications of the ABP program need to be done in order to further verify its capability and powerfulness in handling thermal analysis of the pipelines.

REFERENCES

Anon, 1998, "Investigation Report KP318 – Slope 92 Norman Wells – Zama Pipeline", Internal Report of Enbridge Pipeline Ltd.

Crawford, Henry S., 1997, "WASCANA ENERGY INC. GOLD CREEK GAS LINE NEAR GRANDE PRAIRIE IN-SITU MEASUREMENTS OF PIPE CONFING PRESSURES", Internal Report of THURBER ENGINEERING LTD.

Das, Sreekanta, Cheng J.J.R. and Murray, D.W., 2002, "Fracture of Wrinkled Energy Pipelines", Structural Engineering Report No. 247, Department of Civil Engineering, University of Alberta, Edmonton, Canada

Dorey, A.B., Cheng, J.J.R., and Murray, D.W., 2001, "Critial Buckling Strains for Energy Pipelines", Structural Engineering Report No. 237, Department of Civil Engineering, University of Alberta, Edmonton, Canada

Dyck, W., 1998, "Wascana's NPS-8 Gold Creek Pipeline From 10-34 to Petro-Canada Plant Analysis of Pipeline with Upheavals Due to Thermal Expansion", Internal Report of STRESSTECH ENGINEERING INC..

Hibbitt et al., 2000, "ABAQUS/Standard User's Manual Version 6.1", Hibbitt, Karlsson, and Sorensen Inc., Pawtucket, USA

Hobbs, Roger E., 1984, "In-Service Buckling of Heated Pipelines", Journal of Transportation Engineering, ASCE, Vol. 110, pp175-189.

Ju, G.T. and Kyriakides, S., 1988, "Thermal Buckling of Offshore Pipelines", Journal of offshore Mechanics and Arctic Engineering, Vol. 110, pp. 355–364.

Kerr, A.D., 1978, "Analysis of Thermal Track Buckling in the Lateral Plane", Acta Mechanica, Vol. 30, pp. 17-50.

Marek, P. J., and Daniels, J. H., 1971, "Behavior of Continuous Crane Rails", Journal of the Structural Division, ASCE, Vol. 97, pp. 1081-1095.

Mohareb, M, Elwi, A.E., Kulak, G.L. and Murray, D.W., 1994, "Deformational Behavior of Line Pipe", Structural Engineering Report No. 202, Department of Civil Engineering, University of Alberta, Edmonton, Canada

Murray, D. W. and Yoosef-Ghodsi, Nader, 2001, "Swanson Creek Wrinkle Investigation", Report to Potomac Electric Power Company.

Yoosef-Ghodsi, Nader and Murray, D. W., 2000, "Thermal Analysis for Snap-Through Buckling of the January 2000 Pipeline Event at Guanabera Bay, Brazil", An Unsolicited Report to Petrobras

Yoosef-Ghodsi, N., Murray, D.W., Cheng, J.J.R., Doblanko, R.M. and Wilkie, S.A., 2000, "Analytical Simulation and Field Measurements for a Wrinkle on the Norman Well Pipeline", Proc. of Inter. Pipeline Confertence IPC 2000, ASME (OMAE Division), Calgary, Alberta. Oct. 1-5, 2000, pp 931-938

Yoosef-Ghodsi, Nader and Murray, D.W., 2002, "Analysis of Buried Pipelines with Thermal Application", Structural Engineering Report No. 246, Department of Civil Engineering, University of Alberta, Edmonton, Canada

Zhou, Z and Murray, D.W., 1993, "Numerical Analysis of Buried Pipelines", Structural Engineering Report No. 181, Department of Civil Engineering, University of Alberta, Edmonton, Canada

APPENDIX A

Fundamental Solutions for Mechanics of Pipe-Soil Slip

The following description is reproduced from Murray and Yoosef-Ghodsi (2001) for the differential equation solution of the soil-pipe slip mechanisms.

The variables required to formulate the slip problem are defined in Figure A1. The length of embedded pipe, L, is shown in Figure A1a, and it is assumed that both the soil and pipe are fixed at end D. When the temperature is changed by ΔT, the pipe expands and displaces a distance u(x) to the right while it is assumed that the soil does not move. The displacement u, therefore, becomes the relative movement between the pipe and the soil, i.e., the slip, δ. The frictional shear force per unit length, F, between the pipe and the soil, is assumed to be related to the slip according to the diagram in Figure A1b. The slip develops the shear force acting on the pipe shown in Figure A1a, such that the yield strength capacity of the shear friction force is mobilized at a distance x_1 from end D.

The axial tensile stress, σ, in a straight elastic pipe may be expressed in terms of the displacement gradient within the pipe and the effective thermal strain, ε_0, as

$$\sigma = E(\frac{du}{dx} - \varepsilon_o) \qquad (A1)$$

in which the effective thermal strain, ε_o, can be expressed as

$$\varepsilon_o = \alpha\Delta T - \frac{\nu\sigma_\theta}{E} \qquad (A2)$$

where ν is Poisson's ratio and σ_θ is the circumferential hoop stress produced by the internal pressure. The axial force in the pipe, N, can be evaluated for elastic response of the pipe, from Equation A1, as

$$N = AE(\frac{du}{dx} - \varepsilon_o) \qquad (A3)$$

Now, considering the region in Figure A1a for which $x \geq x_1$, the equilibrium equation for the free-body diagram of Figure A1c may be written as

$$N + F_y(L - x) + P = 0 \qquad \text{(A4)}$$

The displacement equation of equilibrium is obtained by substituting Equation A3 into Equation A4. Integrating and applying the boundary condition $u(x_1) = \delta_y$ results in

$$u(x) = \rho(x^2 - x_1^2)/2 - \beta(x - x_1) + \delta_y \qquad \text{(A5)}$$

in which

$$\rho = F_y / AE \qquad \text{(A6a)}$$

and

$$\beta = (P + F_y L)/AE - \varepsilon_o \qquad \text{(A6b)}$$

Consider now the region $x \le x_1$ for which the equilibrium condition can be expressed as

$$\frac{dN}{dx} = F = ku \qquad \text{(A7)}$$

in which k is the initial stiffness of the pipe-slip relationship (Figure A1b). Substituting for N from Equation A3 yields the displacement equation of equilibrium

$$\frac{d^2u}{d^2x} = \frac{k}{AE}u = \lambda^2 u \qquad \text{(A8)}$$

where λ is defined by identifying corresponding coefficients in Equation A8. Integrating Equation A8 results in

$$u = C_2 e^{-\lambda x} + C_3 e^{+\lambda x} \qquad \text{(A9)}$$

Evaluating C_2 and C_3 from the displacement boundary conditions on the region $x \le x_1$ and equating forces from each side of $x=x_1$, as evaluated by Equation A3 using Equations A5 and A9, requires that

$$(\rho x_1 - \beta)\tanh(\lambda x_1) - \lambda\delta_y = 0 \qquad \text{(A10)}$$

Equation A10 is a transcendental equation that can be solved by an iterative process to find its root, x_1. Once x_1 is established, the displacement at end C of Figure A1a may be evaluated from Equation A5. This displacement is

$$u_L = u(L) = \rho(L^2 - x_1^2)/2 - \beta(L - x_1) + \delta_y \qquad \text{(A11)}$$

A solution for the case when the soil does not yield (i.e. $x_1 > L$) can also be derived from Equation A8 and yields the following result

$$u_L = u(L) = \frac{\gamma}{\lambda}\tanh(\lambda L) \qquad \text{(A12)}$$

in which

$$\gamma = \varepsilon_o - P/EA \qquad \text{(A13)}$$

This solution is valid as long as $u_L < \delta_y$.

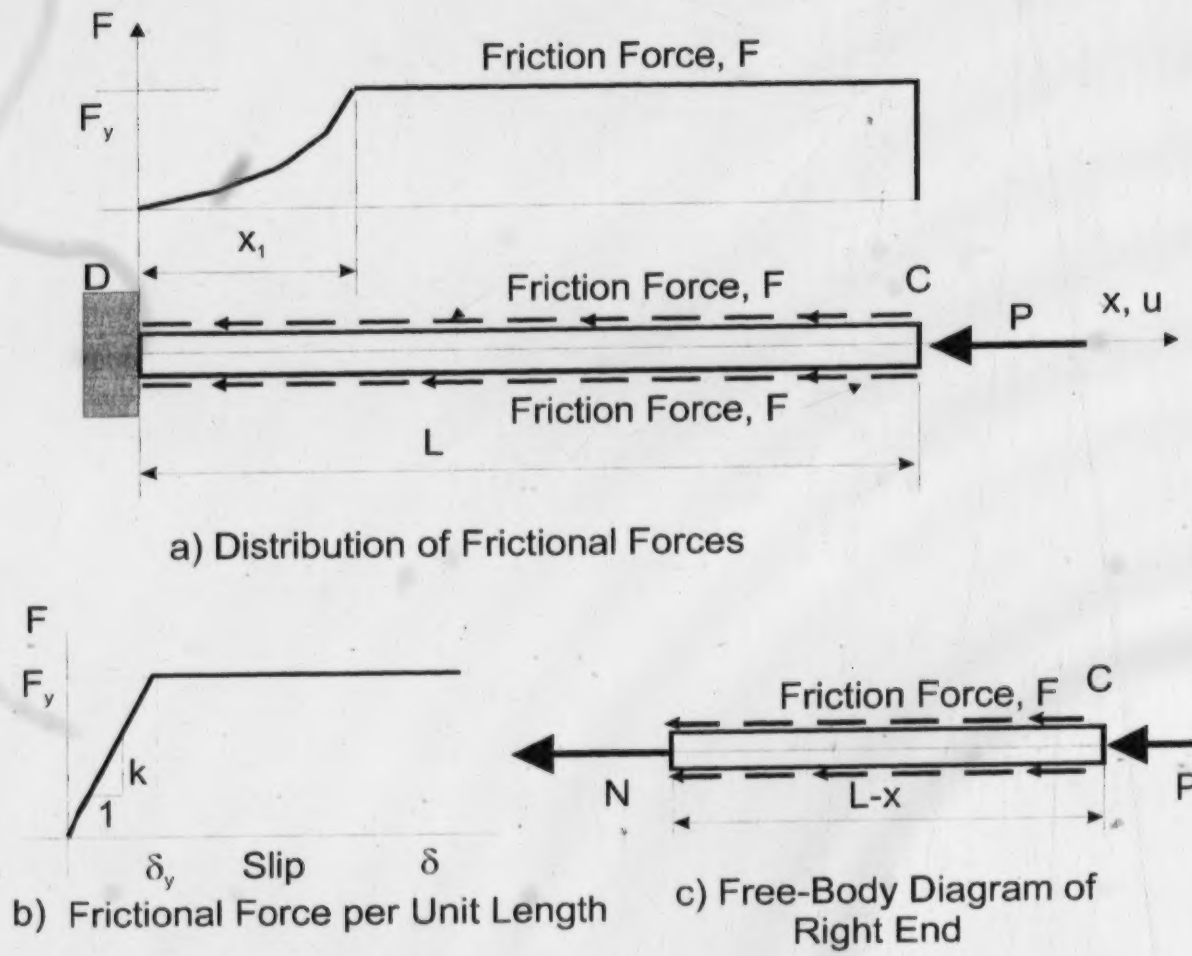

Figure A1 Model for Differential Equation Solution of Pipe-Soil Interactive Slip Problem

APPENDIX B FRACTURE MODEL OF PIPELINE UNDER CYCLIC LOADS

The following description is summarized from Das et al. (2002) for pipeline cyclic loading fracture analysis.

B1 Fracture Model

Based on the pipe test results done in the U of A, it is found that that the pipe specimens are highly ductile and do not normally fail in fracture when they are subjected to monotonically increasing axisymmetric compressive strain. If the pipe is subjected to strain reversals because of unloading and loading of primary loads, the fracture can occur in the wrinkle region in a few cycles, due to low cycle fatigue (Das et al., 2002).

As part of his project, Das used data of total 24 strip tests in order to develop a fracture model for wrinkled pipe subjected to cyclic loads (Das et al., 2002). A fracture failure criterion based on energy absorption behavior of a strip specimen was developed thereafter.

According to Das et al. (2002), a power relationship between the number of cycles to fracture a strip specimen at its crest (N_s) and the hysteresis loop energy (HLE), U_0, as shown in Figure B1, for a 6.84mm thick strip specimen, is:

$$N_s = A(U_0)^{-2.58} \qquad \text{(B1)}$$

where the value of coefficient (A) is 1.96.

Another expression of Equation B1 is to take natural log of each side. Equation B1 becomes

$$ln(N_s) = -ln(A_0) - 2.58ln(U_0/t) \qquad \text{(B2)}$$

where A_0 is a constant.

If U_0 is normalized by the thickness, t, and a linear relationship between $ln(A_0)$ and the thickness, t, is assumed, then

$$ln(A_0) = -0.1642t + 5.3654 \qquad \text{(B3)}$$

and the relationship between N_s, U_0 and t becomes

$$ln(N_s) = 0.1642t - 2.58ln(U_0/t) - 5.3654 \qquad \text{(B4)}$$

where the unit for U_0 is kNm, and the unit for b and t is mm.

Also according to Das et al. (2002), the HLE can be calculated for a slice through the pipe wrinkle in the same way as it is calculated for a strip specimen and a pipe wrinkle can be modeled in the same way as is done for the strip specimen or strip wrinkle. Hence, only a standard wrinkle width of 57mm at the highest wrinkle location of a wrinkled pipe specimen needs to be considered for prediction of the residual life. Consequently, this fracture model can be applied to both axial and bending specimens in the same way.

B2 Application to Axial Pipe Specimens

For an axial pipe specimen, the energy delivered to the pipe specimen may be considered absorbed by three plastic hinges: one at the crest and two at the feet of the wrinkle as shown in Figure B2. Consequently, the total energy, U_0, absorbed by a pipe wrinkle slice of 57mm width is computed as

$$U_0 = U_{0c} + U_{0f} \qquad \text{(B5)}$$

The values of U_{0c} and U_{0f} can be determined from the following relationships:

$$U_{0c} = 2M_u\phi \qquad \text{(B6)}$$

$$U_{0f} = \frac{U_{0c}}{2} \qquad \text{(B7)}$$

where M_u is the ultimate moment capacity of the wrinkle slice and ϕ is the maximum angle change at the crest of the wrinkle within one cycle. M_u can be determined as follows:

$$M_u = Z\sigma_u \qquad \text{(B8)}$$

in which Z is the plastic section modulus of the 57mm wide strip and is calculated as:

$$Z = \frac{bd^2}{4} = \frac{bt^2}{4} = \frac{57t^2}{4} = 14.25t^2 \qquad \text{(B9)}$$

and σ_u is the ultimate stress from the material coupon tests.

ϕ can be calculated as

$$\phi = 2(\theta_t - \theta_c) \qquad \text{(B10)}$$

where θ_t and θ_c are the half angle of the crest under tension and compression, respectively, as shown in Figure B2. One assumption made by Das (2002) is that the following relationship exists in Figure B2:

$$W_c = W_t - S_r \qquad \text{(B11)}$$

where S_r is the absolute value of stroke range, equal to half of the total stroke.

B3. Application to Pipe Bending Specimens

For pipe bending specimen, the total HLE absorbed by the three plastic hinges in a bending specimen had two components: (i) HLE due to variation in

axisymmetric axial stroke (S_{as}) as it was for axial specimens and (ii) HLE due to variation in end rotation.

Figure B3 is a sketch of a bending pipe specimen and a blow up of the end part. As shown in Figure B3, the total global stroke (S_{at}) at any time is composed of two stroke components: (i) stroke due to axisymmetric axial deformation (S_{as}) and (ii) stroke due to rotational or bending component (S_{ar}). The component S_{as} is the same as the axisymmetric axial stroke of axial pipe specimens. From the FEA of pipe bending tests, it was found that the neutral axis (NA) of these pipes moves toward the tension side of the pipe specimen, as the wrinkle on the compression side gets bigger. Average NA distance from the extreme compression edge (a) is usually $0.75D_c$ to $0.8D_c$ where D_c is diameter at the centerline of the pipe cross section. For calculation purpose, the value of a can be taken as $0.8D_c$. The following relationship can be obtained:

$$S_{as} = S_{at} - S_{ar} \tag{B12}$$

where, $$S_{ar} = \left(a - \frac{D_c}{2} \right) \tan \alpha_a \tag{B13}$$

Figure B4 shows an idealized model for the deformed shape at any stage of load cycling in a pipe bending specimen. Like axial pipe specimens, in this model of a bending pipe specimen, it is assumed that three plastic hinges are formed during the monotonic loading stage and these are: one at the crest of the wrinkle (Point B in Figure B4) and two others at the feet (Points A and C of Figure B4) of the wrinkle. It is assumed that the angle P-Q-A is a right angle. It is also assumed that this angle and the distance between Points Q and A (L_t) remain constant during the load cycling process. Consequently, from the compatibility of geometry, it can be said that the angle at Point A, that is, the angle T-A-Q, is the same as the rotation (α_a) that occurred at the top end of the pipe (see Figure B4). As a result, at any stage of load cycling, the change in angle T-A-Q at Point A, denoted by β_a, will be the same

as change in the angle at the top end, denoted by κ_a, for the bending pipe specimen. Hence, Equation B14 can be written.

$$\beta_a = \kappa_a \tag{B14}$$

However, the angle *A-B-O* at Point *B* (θ_a,) is different from α_a (applied rotation at the top end). Consequently, the change in angle *A-B-O* at Point *B* is also different from the change in angle that was applied at the top end (Point *P* in Figure B4) of a bending specimen. The angle *A-B-O* at Point *B* (θ_a), at any stage of the rotation cycle can be written as

$$\theta_a = Sin^{-1}\left(\frac{d - a\sin\alpha_a + L_t \sin\alpha_a \tan\alpha_a}{d}\right) \tag{B15}$$

where *d* is the arm-length of the wrinkle as it was for axial pipe specimens in Figure B2 and L_t is the distance between foot of wrinkle and the nearest end point of a pipe bending specimen. The values of 'd' and 'L_t' are found only from FEA results. Consequently, the change in rotation at Point B (τ_a) that occurs due to the change in end rotation (κ_a) that was applied to the pipe bending specimen is written as

$$\tau_a = \theta_a - \theta_o \tag{B16}$$

The total change in angle at the crest of the wrinkle due to the end rotation change (κ_a) is $2(\theta_a-\theta_o)$ or $2\tau_a$. Consequently, the components of HLE due to bending can be calculated as:

$$U_{0cr} = 2M_u(\phi)_r \tag{B17}$$

$$U_{0fi} = 2M_u\beta \tag{B18}$$

where U_{0cr} and U_{0fr} are the HLE absorbed by the crest hinge and by each of the two foot hinges, respectively. M_u can be computed using Equation B8. $(\phi)_r$ is the maximum change in total angle at the crest hinge and β is the maximum change in angle at each foot, due to one cycle of rotation that was applied to the ends of a bending specimen. And $(\phi)_r$ can be calculated in the same way as that in Equation B10, which is for axial deformation component.

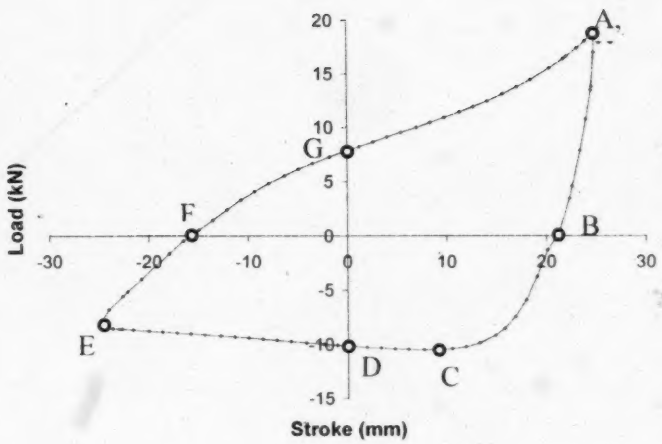

Figure B1 A Single Load Hysteresis Cycle for a Strip Specimen

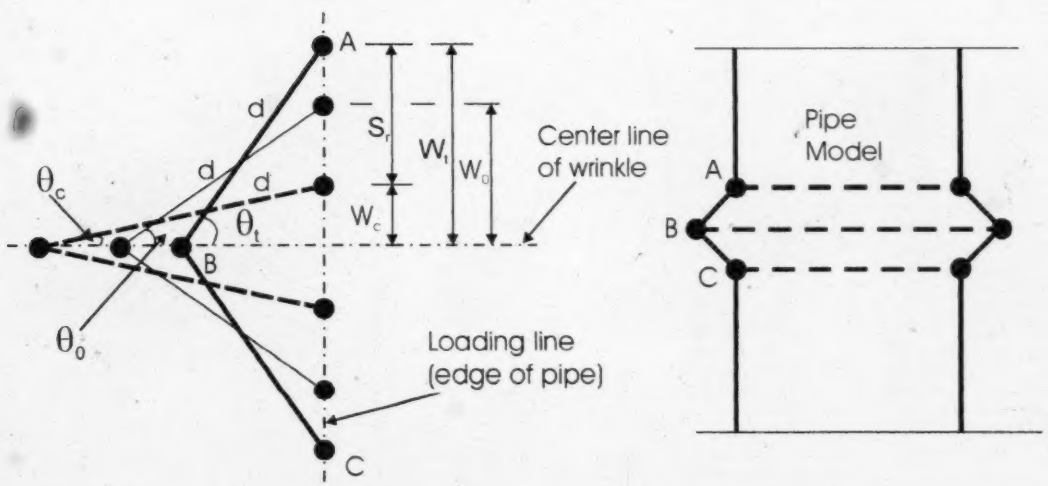

Figure B2 Model for the Axial Loaded Pipe Specimen

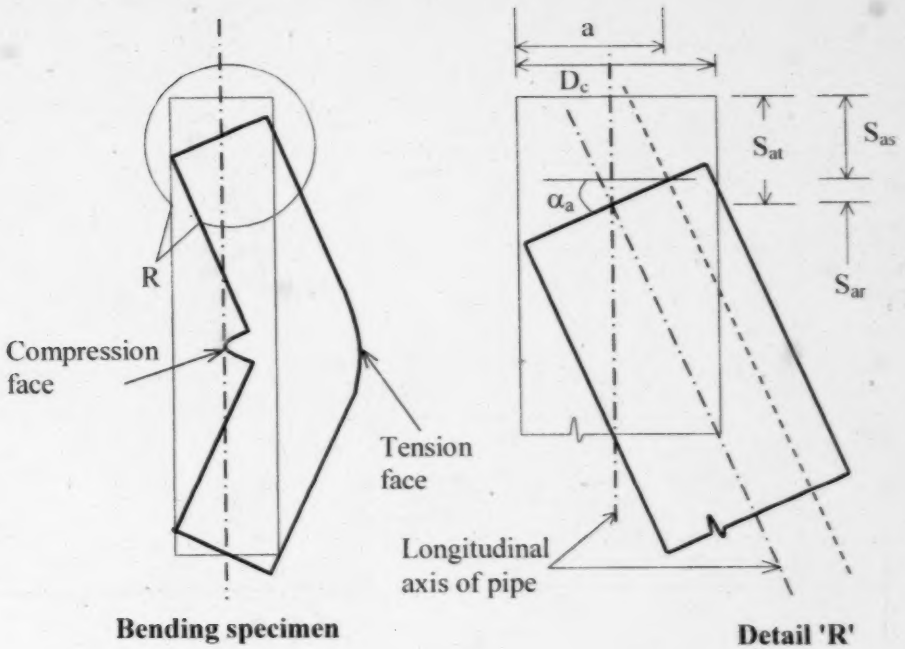

Figure B3 Bending Pipe Specimen and Its Detail 'R'

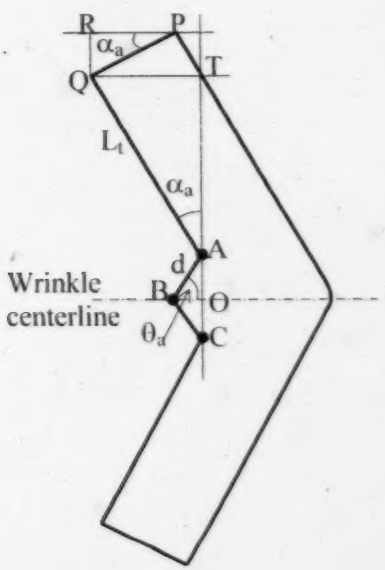

Figure B4 Model for Deformed Shape of a Bending Pipe Specimen